Study on Single Crystal Growth of Group IVa and Group Va Transition Metal Carbides by Floating Zone Technique

Shigeki OTANI

CONTENTS

1. INTRODUCTION

Floating zone technique is well suitable for preparing large single crystals with high melting points. Most of large single crystals with melting points above 2000°C are prepared by this method. Recently, there has been an increasing need for materials which can be used in severe conditions, and much intrest is paid to refractory materials. Their reliable physical and chemical data have been required in order to develope the suitable material design. Therefore, the necessity of single crystal has increased as a sample to determine the physical and chemical properties of materials, and as a standard sample even in the field of thin film and sintered body(ceramic materials).

A floating zone technique was at first applied to the preparation of Si single crystal in 1953 by Keck et al.[1]. Afterward, because a crucible is not needed in this method, the preparation of crystals of refractory metals, such as Mo[2] and W[3], were attempted. The heating method was electron bombardment. This is the most efficient method of heating, but must be opperated in vacuum condition(less than 1×10^{-2} Pa)[4]. This method can not be applied to refractory compounds because of their preferential evaporation under vacuum conditions. Therefore, Johnson[5] applied an RF induction heating technique using an eddy current concentrator to the preparation of single crystals of YB_4 and YB_6 under argon gas at atmospheric pressure.

Afterward, in order to reduce the evaporation rate further, attempts to prepare the crystals of carbides(VC, ZrC, HfC and TaC) and borides(ZrB_2 and HfB_2) were made under an ambient inert gas of high pressure(about 10^6 Pa) using an RF induction heating technique[6,7], but only a large single crystal of VC, which has a melting point lower than 3000°C, could be prepared. Since then, most of the crystals of refractory materials came to be grown by this method[8-11]. Using this floating zone method, the present author has attempted to prepare the single crystals of IVa and Va transition metal carbides.

The carbides have the highest melting points(2648-3983°C) among materials, great hardness(16000 and 29000 MN/m^2) and typically metallic properties, as shown in Table 1. They have an NaCl-type crystal structure and wide nonstoichiometric composition ranges(up to 50 at%) which comes from only carbon defects[12].

At present, the carbides are mainly used as cemented carbide cutting tools and wear-resistant parts in a super-hard tool field. Recently much attention is paid to their other properties, except the mechanical properties. For example, it is being examined to utilize the carbide single crystals, mainly TiC and TaC, as a stable field electron emitter[13,14] because of their low work function, low sputtering yield and the inertness of the surface for gas-absorption[15]. TiC may be used as a first wall of a fusion reactor[16,17], because it is one of low-Z materials and the sputtering yield is low[18]. NbC-NbN system

Table 1 Characteristics of transition metal carbides[1)]

	TiC	ZrC	HfC	VC	NbC	TaC
Melting point[2)] (°C)	3067	3420	3928	2648	3600	3983
Hardness[3)] (MN/m^2)	28000	26000	23000	29000	24000	16000
Electrical resistivity[3)] ($10^{-8}\Omega$ m)	130	40	34	46	32	18
Work function (eV)	3.8[4)]	3.5[4)]	3.4	3.8	3.8	3.8
Compositional range (Carbon/Metal ratio)	0.55-0.97	0.60-0.99	0.6-0.98	0.72-0.89	0.72-0.98	0.75-0.99

1) with the least carbon defect

2) the highest melting point

3) at room temperature

4) on (100) plane of the single crystal

The other work functions are obtained from polycrystals.

can be a superconductor which is tough for neutron irradiation[19].

In these carbide studies, there ia a big problem that the reported values of physical properties vary widely from sample to sample[12,20,21]. The main cause at the beginning of the stage for these studies were that all the measurements were performed on hot-pressed or sintered specimens with 5-50 % residual porosity. After that, an attempt was made to prepare the single crystals of carbides by applying several crystal-growth techniques, and measurements of physical properties were carried out using the single crystals. Nevertheless, the values were often different from sample to sample, because the properties of carbides are dependent on the composition(carbon to metal ratio, free and combined carbon), impurity concentration, especially oxygen, sample homogeneity and so on. These factors which influence the properties also depends on the crystal growing methods, as described below. Therefore, although many studies on the carbides have been carried out, the reliable data are little.

Single crystals of the carbides have been prepared so far by (1) chemical vapor deposition(CVD), (2) flux method, (3) recrystallization and (4) floating zone technique. These methods have the following merits and demerits.

(1) The crystal prepared by CVD has a needle or polyhedron shape. This method does not supply a large crystal. The prepared crystal contains many carbon vacancies and much oxygen impurity[22-24]. Further, the crystal is reported to contain

elements form the substrate and halogen impurities because the metal halide is used as a metal source. Therefore, for example, the microhardness of crystals varies strongly from sample to sample[25]. Therefore, the CVD method is not suitable to prepare the crystals with high quality for measurements of physical properties. However, this method has been developed to prepare the thin film of carbides, and at present widely used to make a coated cutting tools.

(2) The flux method is one of well-known single crystal growth techniques. The crystals were prepared using a metal, such as Fe, Co and Al, as a flux in a Al_2O_3 or graphite crucible[26,27]. The size of grown crystal is small, at most, 1-2 mm. The flux metal is included in the crystal as inclusions. The larger the crystal is, the higher the metal content is. As a method to prepare larger crystals, there is a method of pulling a crystal from a flux. By this method, the crystals of WC[28] and TaC[29] with the size of about 1 cm were prepared. However, in this method, it takes a long growth time and needs much experience for investigators to prepare good quality crystals. Therefore, this method should be used in the case when it is impossible to prepare a crystal by the floating zone method, which supplies a large crystal.

(3) Using a recrystallization method, large single crystals of VC[30] and HfC were prepared[31]. The former was obtained by the reaction of liquid vanadium metal with graphite thimble. The latter was obtained by a strain-anneal method. These crystals

have the least amount of carbon defects. However, it is difficult to control the composition of the crystal.

(4) A floating zone technique supplies a large and pure single crystal, although there is a difficulty that a sample must be heated up to its melting point. The large crystals prepared by this method were only those of VC and TiC[10,16,32]. They have melting points lower than 3000°C. The large crystals with melting points higher than 3000°C have not been yet prepared. This came from the fact that a zone pass could not be carried out stably at higher temperatures above 3000°C. In other materials with melting points higher than 3000°C, a molten zone could not be passed stably. In addition, since the carbides have wide nonstoichiometric composition ranges, the crystal rod prepared by a usual floating zone method has a compositional gradient along a growth direction, as discussed in detail later. Further, the chemical composition of the crystal was deviated from that of the feed rod by preferential evaporation of metal or carbon depending on a molten zone composition. Therefore, the crystal rods with desired chemical compositions were not prepared yet.

Thus, a floating zone technique is the best to prepare the carbide crystals, if the following problems are solved:

(1) Establishment of the technique to keep a molten zone stably at temperatures higher than 3000°C.

(2) Preparation of large single crystals of carbides with homogeneous desired compositions over the entire chemical composition range.

(3) Examination of the factors which influence the preparation of high quality crystals.
(4) Characterization of a single crystal with respect to chemical composition, purity, quality and so on.

From this point of view, large and pure single crystals of the IVa and Va transition metal carbides with desired chemical composition were prepared by a floating zone technique in the present study. The contents of this thesis are as follows:
(1) Preparation and characterization of the carbide crystals are studied. The floating zone technique in preparing carbide crystals is improved to keep a molten zone stably at higher temperature conditions above 3000°C. A new method to prepare a crystal with a desired composition is studied in detail. The principle is that, on the basis of a phase diagram, the chemical composition of a molten zone is kept at the liquidus composition which coexists with a desired crystal composition during a zone pass. Using an improved floaitng zone technique under investigation, single crystal of each carbide is prepared and characterized. Total discussion on preparation of carbide crystals is given, comparing with one another and paying attention to the growth temperature and the difference between the IVa and Va transition metel carbides. Further, an impurity refining, a growth mechanism and a crystal quality are studied.
(2) The temperature distribution in a growing crystal rod is calculated. Since the carbide crystals are prepared under a steep temperature gradient, the temperature distribution in

growing crystal is important to prepare the high quality crystals. The factors which determine the distribution are examined by calculating a proposed model. In order to verify the model, the temperature along the crystal rod and the crystal-molten zone interface shape are experimentally examined and compared with the calculational results. In addition, selecting TiC as an representative example, the change in the temperature distribution due to modifying a model is examined. The best growing method to prepare the high quality crystal is surveyed.

2. PREPARATION AND CHARACTERIZATION OF CARBIDE CRYSTALS

2-1 Apparatus

Figure 1 shows the conceptional figure of the apparatus for sintering and crystal growth. The RF generator whose frequency is 200 kHz is used as a common power source. The maximum output power is 40 kW. Sintering is carried out under vacuum in a graphite-susceptor which is wounded with graphite wool as an insulator. The clearances among the turns of a work coil are arranged so as to heat the susceptor uniformly. The susceptor can be heated up to about 2300°C. The temperature is measured through the top view port using a pyrometer. In order to sinter a sample under high vacuum condition, a rotary vacuum pump with high evacuation rate(500 l/min) is used to make a diffusion pump work during a sintering because a large amount of gas generates from the sample.

A furnace for preparing a crystal is a radio-frequency induction heating furnace(Athur D. Little Inc., High pressure type). The body of the furnace chamber is made of stainless steel. The view port is made of strengthened pylex glass(77ϕ x 32 mm). The chamber with 14 liter volume can be pressurized with the innert gas with the magnitude up to 10 MPa. The pressure is shielded by O rings. The pressurized gas is introduced from the gas bomb(max. 150 kg/cm^2) directly into the chamber evacuated by a diffusion pump through the regulator.

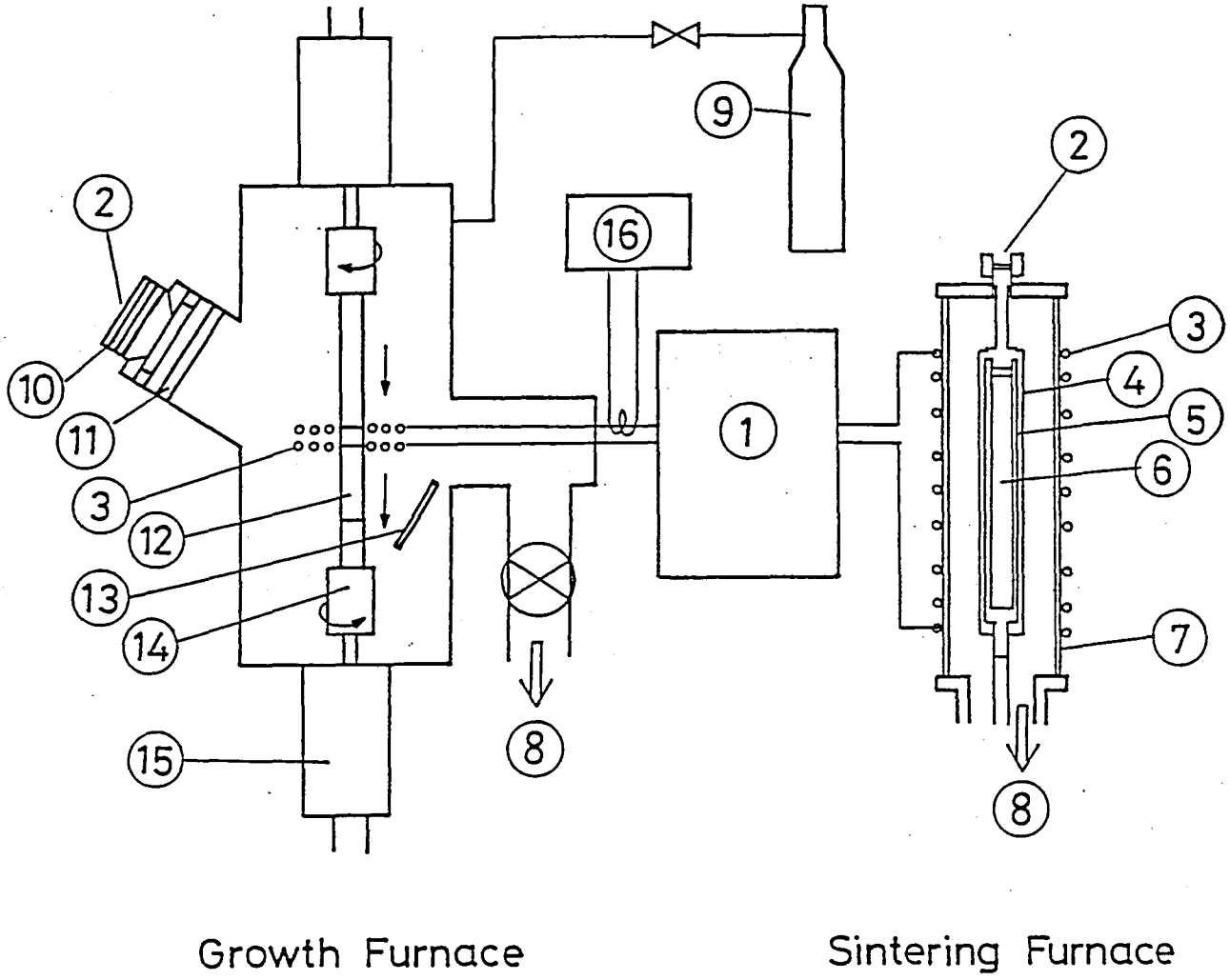

Fig. 1 Conceptional figure of furnaces for sintering and growth:(1) RF generator(200 kHz, 40 kW), (2) View port, (3) RF coil, (4) Graphite wool, (5) Graphite susceptor, (6) Sample for sintering, (7) Qurtz tube, (8) Vacuum system, (9) Gas bomb(He), (10) Shading filter, (11) IR-absorption filter, (12) Crystal rod, (13) Mirror, (14) BN holder, (15) Part for derive and rotation of shaft and (16) Recorder.

A large mouth with 180 mm diameter is fixed up so as to set up the sample and clean the inside of the chamber easily. In order to protect the view port and mouth, which are mechanically weak at elevated temperatures out of radiation from a molten zone(2700-4000°C), a IR-absorption filter and a metal shield plate are fixed up at the inside of them, respectively. Further, the body of the furnace is wounded at the close intervals with a water cooled pipe.

The shading filters(polarized and ND filters) are set up at the outside of the view port to observe the molten zone during a zone pass with the naked eye.

2-2 Experimentals

2-2-1 Raw materials

It is very important to choose raw materials in order to prepare single crystals with high purity and quality. As raw materials, commercial powders of the carbides, carbon and metal were used.

The carbide powders are required to be highly pure and fine grained(less than an average partical size of several μm).

The commercial powders are prepared mainly using three kinds of preparation methods: a menstruum method, an oxide method and a metal method. The powders prepared by a menstruum method are contains much menstruum metal impurities(less than 1 wt%) because the carbides are synthesized from the metal(or oxide) and carbon in the molten metal(menstruum), such as Fe, Co, Ni

and Al. When a large amount of these metals are contained, an initial molten zone can not be formed because only the impurity metal melts at the low temperature(< 1500°C) and runs away into the feed rod, and then the feed rod swells up. Therefore, this kind of powder is not suitable for a crystal growth by a floating zone method. The powder prepared from the reaction of oxide and carbon(an oxide method) has much oxygen and nitrogen impurities. This kind of powder is also not good because their content in the crystal depend on those in the feed rod, as described in section 2-4. The powder prepared by a metal method($M + C \rightarrow MC_x$) is the best one for crystal growth because this powder is the purest. However, the commercial powder genelally contains W as impurity(max. 0.5 wt%), especially, in the fourth group carbides. The IVa carbides are synthsized at the temperature condition of 1700-2300 °C higher than that for the Va carbides(1100-1500°C). The products of the IVa carbides are obtained in a form of hard solid. In the process of powdering by a WC ball mill, the sample is contaminated with W. The fine powder tends to have a large amount of W content. Therefore, the relatively coarse powders with low W content were used in the present study.

The metal and carbon powders are used to control the chemical composition of the starting materials. The metal powders with high purity and less than 100 mesh are used to form the pure sintered rod and react well with the carbide powder. A spectroscopic graphite powder was used as a carbon powder. When the carbon black was used, the feed rod was not so hard and the

evaporation product was bulky during a zone pass, compared with the case of graphite powder.

2-2-2 Sintering

The quality of a sintering rod strongly influences the success in a preparation of the single crystal by a floating zone technique. The ideal sintered rod is a hard cylindrical rod with uniform high density and purity. It is desirable that the density of the rod is, at least, 60 % of the theoretical value. In order to prepare the straight sintered rod, a little experience is needed especially in the process of a powder compacting.

A sintered rod was prepared according to the experimental procedure shown in Fig. 2. The raw materials used were the carbide, metal and graphite powders. The starting materials with various kinds of chemical compositions were prepared by mixing the carbide powder with the metal or graphite powder in the desired ratio by agate mortar. A small amount of camphor ethanol solution was added as a binder. The mixture was compacted in the mold and uniaxially pressed into a bar of 1 x 1 x 20 cm^3, and then isostatically pressed(100 MPa) in a rubber bag to obtain a uniform density within the bar. After shaping it cylindrically, the pressed rod was sintered under vacuum condition until the outgassing stops from the rod in order to remove the impurities, especially oxygen and nitrogen impurities. The sintering time was generally 0.5-2.0 hours, which is long enough to react the

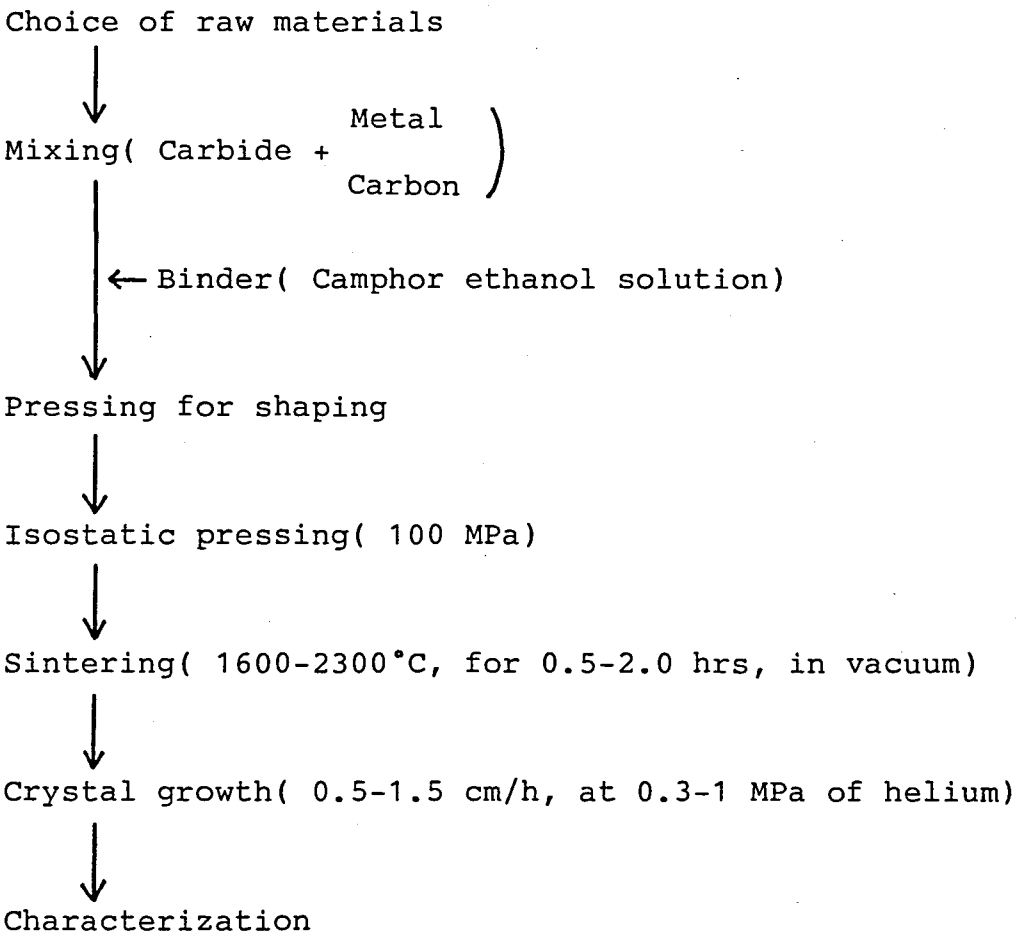

Fig.2 Experimental procedures.

carbide with the added metal. The sintering temperature was 1700-2300 °C, which was selected depending on the melting point of the sample. The densities of the sintered rods were 45-80 % of the theoretical values. The sintered rod to which the metal was addd was hard and had high density(about 80 %). On the other hand, the sintered rod to which the graphite was added hardly contracted in the sintering process. In the case of preparation of HfC and TaC crystals, it was required to add much carbon because of their high melting points.

2-2-3 Preparation of crystals by RF floating zone technique

The single crystal was prepared by a floating zone technique as follows. The sample is heated by the current which is induced in itself by a RF current through the work coil and the molten zone is formed by melting the part of the sintered rod and passed to prepare the crystal. The high RF current(200-350 A) must be flown through the coil because of their high melting points. Therefore, strong repulsion works between the coil and the zone. The zone form, which is a little contracted at the middle part, is determined by the coil form. Also, because of the repulsion between the coil and the zone, the molten zone is moved to the center of the coil. If the sintered rod is not set up at the center of the coil, the molten zone drops down and/or blows up. In addition, the crystal is prepared under the violent heat flow because of their high growth temperature condition above 2500 °C. Therefore, the growing crystal rod must have a cylindrical

symmetry. Otherwise, in the case when the zone width becomes non-uniform, the crystal can not be prepared smoothly.

The sintered rod prepared by the above method is fixed in the BN holder with Mo wire(0.5 mm ϕ), as shown in Fig. 1, and set up at the center of the work coil. The BN holder is used to electrically insulate the sample from the earth. After it takes enough time to evacuate the chamber, it is filled up with 3-15 x 10^5 Pa of helium gas. An initial molten zone is formed after about 20 minutes from the start of heating. The molten zone is passed by moving the feed rod and crystal rod through the work coil. The crystals were prepared at a rate of 5-25 mm/h and the feed rods were melted into the zone at higher rate of the crystal growth in order to obtain the crystal rod with the same diameter as the feed rod because of the low density feed. During a zone pass, the upper and lower shafts are counter-rotated or only the growing crystal rod is rotated at a rate of 5-20 rpm. A stable zone pass is indispensable to preparation of the high quality single crystal. The stability during a zone pass is determined mainly from a zone shape. Therefore, the zone is observed from the upper and lower directions using a mirror through the view port during a zone pass. Further, by the combined-use of monitoring the change in the RF current using a recorder as shown in Fig.1, the stability after several minutes can be predicted. Generally, if the heating power is too high, the zone becomes long and the middle part of the zone is contracted. Consequently, the coil current increases because the mutual

impedance between the coil and the zone becomes small. In the case when the power is lack, the current, in the opposite, decreases. Therefore, by monitoring the coil current , we can see a sign that a zone becomes unstable after several minutes, and the zone can be stabilized by a small power control. In addition, the power control should be minimized during a zone pass because the trace is left in the crystal. The crystal rod controlls by itself by changing the zone length in the allowed region. Therefore, the power should be controlled only when the power is not in the allowed region.

Several important points which must be considered on preparation of crystal are described below.

Several of 10^5 Pa of an ambient innert gas contributes to suppressing the arc discharge between the turns of the work coil and reducing an evaporation from the zone. The gas was helium because only helium, which has the highest ionization potential, can suppress the arc discharge perfectly for preparing the carbide crystals. On the other hand, the high pressure of helium gas tends to decrease the crystal quality, as described in section 2-5. Therefore, the carbide crystals are prepared at the lowest pressure in the range where the trouble of arc discharge do not occur. The crystals with low melting points(lower than 3000°C), such as TiC and VC, are prepared at the low pressure condition(3-5 x 10^5 Pa). The crysral with high melting points(3300°C), such as TaC,HfC and NbC, are prepared at the high pressure condition(about 10 x 10^5 Pa).

The coil configuration is an important factor. When the molten zone can be effectively heated by the work coil ideally arranged, the molten zone with short length(60 % of the rod diameter) can be formed and the evaporation product does not adhere to the coil. In order to heat a sample effectively, the inside diameter of th coil must be small. However, in the case when the inside diameter of the work coil is small, many evaporation products adhere to the coil and a zone pass is impossible because the evaporation product on the coil touches the zone. Therefore, the best inside diameter of the work coil must be selected depending on the diameter of the sintered rod, the melting point of a sample, the degree of evaporation and the helium gas pressure. In order to form the zone with 60 % of the rod diameter, the two step coil is adoped in the present study. The heated width(= the coil thickness) must be almost the same as the zone length because of achievement of effective heating, as described in section 3-2. Furthermore, the coil consisting of many turns has good efficiency to heat the zone in the range of a few of turns. However, the coil must be made of a limited length of copper pipe(3 mmϕ(2 mmϕinside diameter)) in order to prevent the cooling water from boiling. Therefore, a 3 turn-2 step coil with 15-20 mm inside diameter is made from the copper pipe with shorter than 70 cm. In the case of preparing the TaC and HfC crystals, which have the highest melting points, the coil is made from the ordered copper pipe with 2.3 mm inside diameter in order to increase the efficiency of cooling by water.

The crystals prepared at the lower growth rate generally have a good quality. Therefore, the crystals are prepared at the slowest growth rate in the range where the troubles do not occur. The crystals of TiC and VC, which have relatively low melting points, are prepared at a rate of 5 mm/h. The growth rate of ZrC crystal is 10 mm/h. The crystals with high melting points, such as TaC, HfC and NbC, are prepared at a relatively high growth rate(1.25-1.5 cm/h).

The rotation of the shafts has an effect to homogenize the temperature and composition in the zone. Therefore, a zone can be passed more stably due to rotation. Especially, it becomes smooth to melt the feed rod with low density into the zone. The single crystals with high melting points, such as TaC and HfC, can not be prepared without rotation because the composition at the zone surface becomes unhomogeneous due to violent preferential evaporation and the part of the zone is solidified.

In order to pass the zone smoothly, it is important to form the initial molten zone with the same shape as that during a zone pass.

When the zone is finished, the heating power must be decreased slowly. Otherwise, cracks are often formed at the final part of the crystal rod.

2-2-4 Characterization

The total carbon analysis was carried out by the following method. The sample was fired in O_2 gas flow at around 1400 °C.

The generated CO_2 gas was determined by a gas chromatographic method. The free carbon which was not dissolved in hot HNO_3 or $HF-HNO_3$ solution, was filtered and analyzed by the same method as the amount of total carbon. The combined carbon contents were obtained by the subtraction of the free carbon from the total carbon. The accuracy in analyzing for total and free carbon was about 0.05 %.

Oxygen impurity in the carbide was analyzed by the vacuum-fusion technique. The samples were fused in a graphite crucible under vacuum with the aid of a flux of molten Ni metal. Oxygen within the sample changes to CO_2 and determined by infrared absorption. The limit of detection was about 10-20 ppm.

Nitrogen impurity in the sample was analyzed by the fusion in innert gas chromatography technique. The sample was heated in a helium gas flow, and the generating N_2 gas was determined by gas chromatography.

Impurities of metal, which are heavier than Ti, were analyzed by X-ray fluorescence spectroscopy(Rh, 50 kV, 40 mA, LiF analyzing crystal). Impurities in the crystals were analyzed by spark mass spectroscopy.

The lattice constants were measured by X-ray powder diffraction method using Si powder(a=0.54301 nm) as an internal standard.

The densities were measured by a hydrostatic method using hexachloro-1,3-butadiene as a solvent and Si single crystal($d=2.3303 \times 10^3$ kg/m^3) was used as a standard. The accuracy was

about 0.02 %.

The back-reflection Laue technique was used to determine the growth direction of the crystal rods and to check the crystal quality. An X-ray transmission topograph of TiC was taken with (400) reflection using $NbK\alpha_1$.

The (100) cleavage plane of the crystals was chemically etched in a $HF-HNO_3-H_2O$=1:1:2 solution at room temperature for about one minute. As another method, the sample was electrically etched at several voltage in a $HF-HNO_3-H_2O$ solution at room temperature for several seconds. The etch patterns were observed by a optical microscope and a scanning electron microscope.

2-3 Principle to prepare crystals with homogeneous and desired chemical compositions

The IVa and Va groups of the carbides have wide nonstoichiometric composition ranges. Therefore, the crystal rod with a desired chemical composition can not be prepared by a usual floating zone technique because the crystal rod has a composition gradient along the growth direction, as shown in Fig. 3. When the crystal is prepared using a sintered rod with x_1 composition by a usual floating zone technique, the initial molten zone is formed at the temperature of T_2 and deposits the crystal with x_4 composition. As the zone shifts, the chemical compositions of the crystal and zone change along the solidus and liquidus lines, respectively, as shown in Fig. 3. When the zone composition reaches x_2 composition, the zone continues to deposit a crystal with x_1 composition. This is a zone leveling condition. However, the zone pass was often finished in the state on the way, for example, the chemical compositions of the molten zone and the final part of the crystal rod are x_6 and x_5, respectively, because the zone pass distance is limited. Therefore, the grown crystal rod has a composition gradient ranged from x_4 to x_5 (or x_1).

In order to prepare a crystal rod with a constant chemical composition, the zone composition must be kept constant during a zone pass. For example, in the preparation of a crystal with x_1 composition, a zone composition must be kept to be x_2, as shown in Fig. 4. The zone composition is changed by carbon

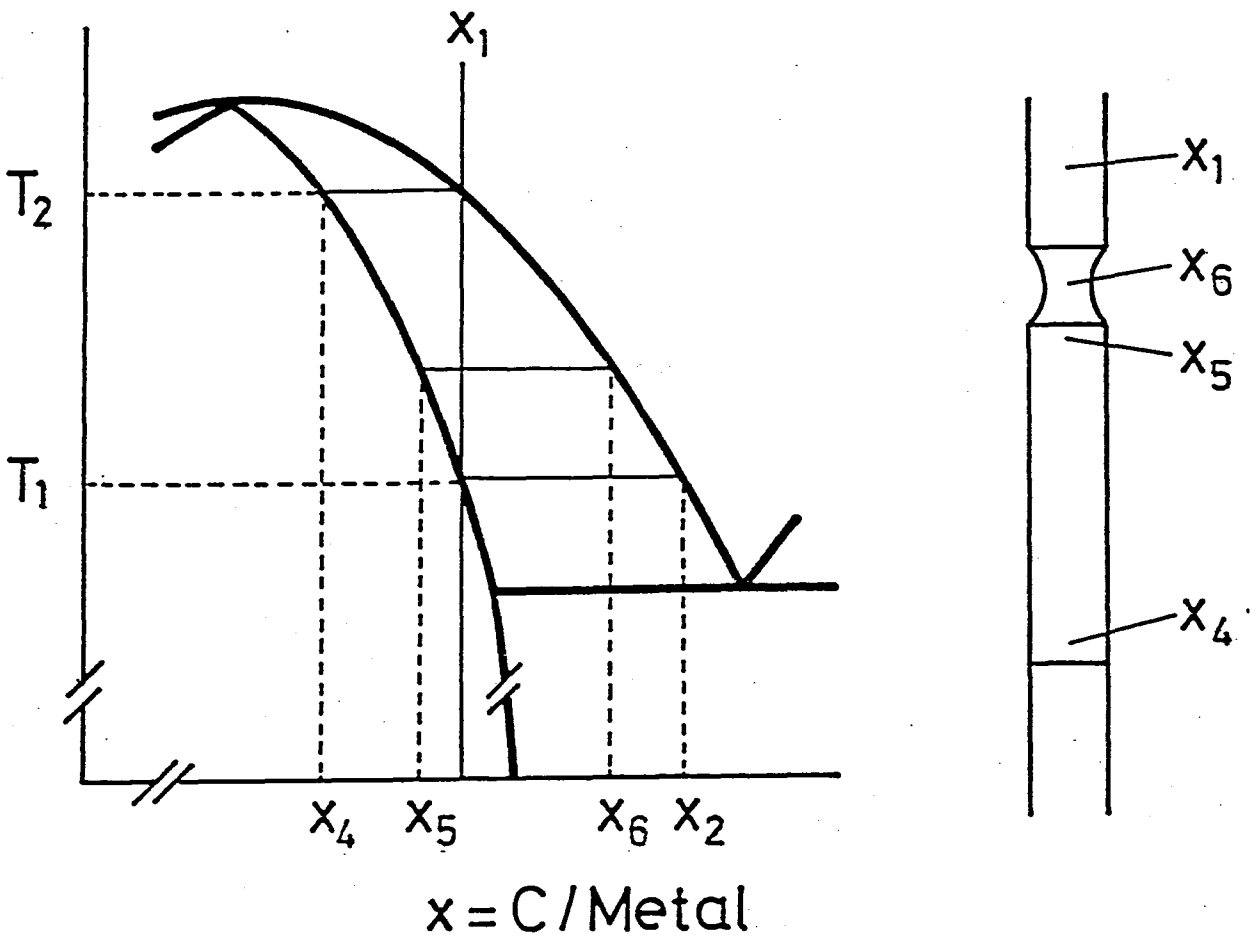

Fig. 3 Compositional change of the crystal rod prepared by a usual floating zone method.

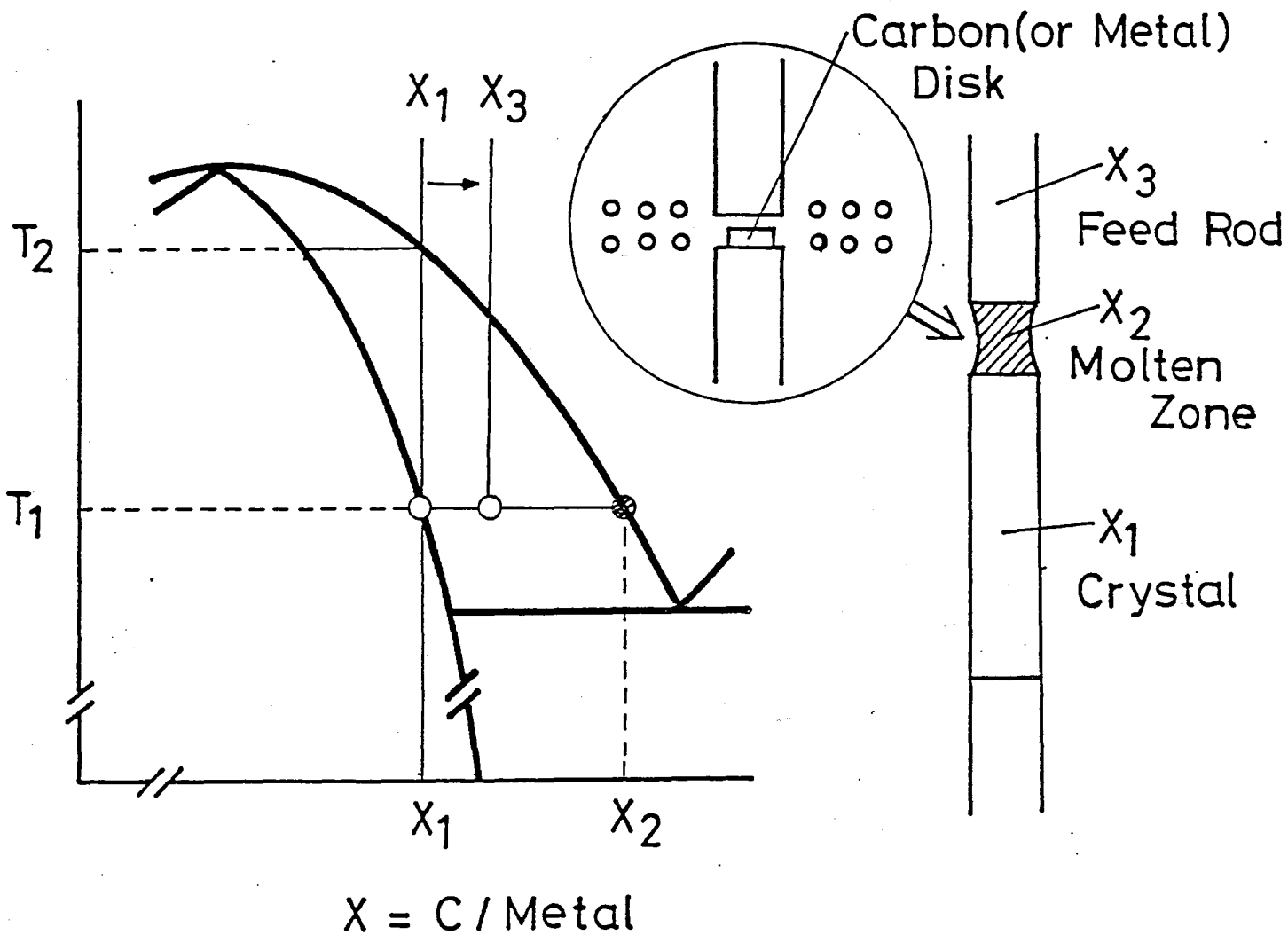

Fig. 4 Principle to prepare a crystal with homogeneous chemical composition. a modified zone leveling method

redistribution at the zone-crystal interface and further by evaporation. Therefore, the chemical compositions of initial molten zone and feed rod must be controlled so as to keep the zone composition constant. This is called "a modified zone leveling method". The former is controlled to be the liquidus composition(x_2) on initial melting so as to prepare the crystal under a zone leveling condition. The latter is controlled to be x_3 so as to compensate for the chemical composition change of the zone due to evaporation.

In principle, the crystal rod with constant chemical composition can be prepared by the above mentioned method. However, in actual, without a stable zone pass, the crystal rod with constant chemical composition can not be prepared. For example, if the zone volume changes during a zone pass, the zone composition changes and the chemical composition of the grown crystal changes, too. Therefore, even if the present method would be applied, the crystal with a homogeneous desired chemical composition can be prepared only when a molten zone can be passed stably.

The present method supplies not only highly homogeneous crystals, but also additional advantages as mentioned below. (1) The zone can be passed at a constant temperature(T_1) because the zone composition is kept constant. Therefore, it needs hardly to control the heating power during a zone pass. A zone can be passed stably. On the other hand, in a usual floating zone technique, the power must be controlled because of the

change in the zone composition.

(2) In a usual floating zone method, it was often pointed out[12,14] that it was difficult to form an initial molten zone because of a low density sintered rod. When the initial zone is formed, any longitudinal deep cracks and a big cavity are formed and reduced the RF coupling to the conditions where melting is impossible. However, using the present method "a modified zone leveling mehtod", it is easy to form an initial molten zone because it can be formed at a lower temperature(T_1), compared with the temperature(T_2) in the case when a usual floating zone method was used. In addition, a molten carbide can not melt down into the sintered rod because the sintered rod with a higher melting point is set below the initial molten zone.

(3) In the present method, the feed rod is not melted, but soluted into the zone because the zone has the liquidus composition. Therefore, the zone can be passed stably even if the feed rod has a low density. If the present method was not used, the feed rod must be melted into the zone only by heating and can not be melted smoothly.

2-4 Preparation and characterization of single crystal of each carbide

The IVa and Va transition metal monocarbides have the similar physical properties one another, as already described in Chapter 1. All of these single crystals are prepared by a modified zone leveling method. However, the preparing conditions, such as growth temperature, growth rate and gas pressure, in these single crystals, are different from sample to sample because of the different characteristic properties in the IVa and Va group carbides, that is, depending on the growth temperature, the vapor pressure and the chemical composition of the grown crystal. In this section, preparation and characterization of the single crystals of the IVa and Va transition metal carbides are concretely described.

2-4-1 TiC_x

TiC crystals were already prepared mainly in a carbon rich composition region by several workers[9,10,32,33]. The large crystals were obtained, but crystals contained some cracks[10,32]. The large single crystal with a desired chemical composition is not prepared yet. The fact that the chemical composition of the grown crystal is influenced by evaporation, was not pointed out in the previous works. Therefore, the present author closely examined the change of chemical composition along the growth direction of the crystal rod prepared by a usual floating zone method. The compositional

gradient in single crystal was confirmed to be due to both zone refining and evaporation by the present experimental results. On the basis of this results, the crystal rod with the maximum carbon content(C/Ti=0.96), which is the same chemical composition as the industrially used TiC, was prepared by a modified zone leveling method[34]. Also, by applying this method, the single crystals with low carbon content were prepared.

1) Growth of TiC_x single crystals with maximum carbon content

1-1) Confirmation of carbon evaporation during a zone pass

In order to grow TiC_x crystals with maximum carbon content, the present author examined the change in chemical composition along the growth direction of crystal rod prepared by a ususal floating zone method, and experimental results were compared with the calculated curve. The compositional change along the growth direction was calculated according to the theory of zone refining[35] under the same assumptions as reported by Pfann; constant zone length(L), uniform concentration(C_L) in the zone, uniform composition(C_0) throughout the feed rod, and so on. However, for the present calculation, a new distribution coefficient(k') was introduced because the distribution coefficient(k) was not constant during a zone pass.

In order to simplify the calculation, the new constant coefficient(k') was introduced as follows. The relationship between the solidus and liquidus compositions was already

reported in ref.[32], According to the relationship, by making the vertical(temperature) axis arbitrary, it is expected that the solidus and liquidus lines can be shown as straight lines in the regions of C/Ti=0.89 to 0.97 and C/Ti=0.95 to 1.41, respectively, as shown in Fig. 5. The ratio of C/Ti in the TiC-C eutectic point, the carbon maximum composition of the crystal, and the composition at the point of intersection of the solidus and extrapolated liquidus lines are determined to be C/Ti=1.41, 0.97 and 0.88, respectively. By regarding the point of intersection of the solidus and extrapolated liquidus lines as the origin of the X axis in Fig. 5, the new distribution coefficient(k') can be written as

$$k' = C_S'/C_L' = (C_s-0.88)/(C_L-0.88), \quad (1)$$

where $C_S' = C_S-0.88$, and $C_L' = C_L-0.88$. (2)

Substituting $C_S=0.97$ and $C_L=1.41$ in (1), we obtain

$$k' = (0.97 - 0.88)/(1.41- 0.88) = 0.17. \quad (3)$$

The new distribution coefficient(k') is found to be constant.

Now, we can obtain the concentration in the crystal rod according to the equation of zone refining[35], i.e.,

$$C_S'/C_0' = 1 - (1 - k')\exp(-k' x/L)$$
$$= 1 - 0.83 \exp(-0.17x/L), \quad (4)$$

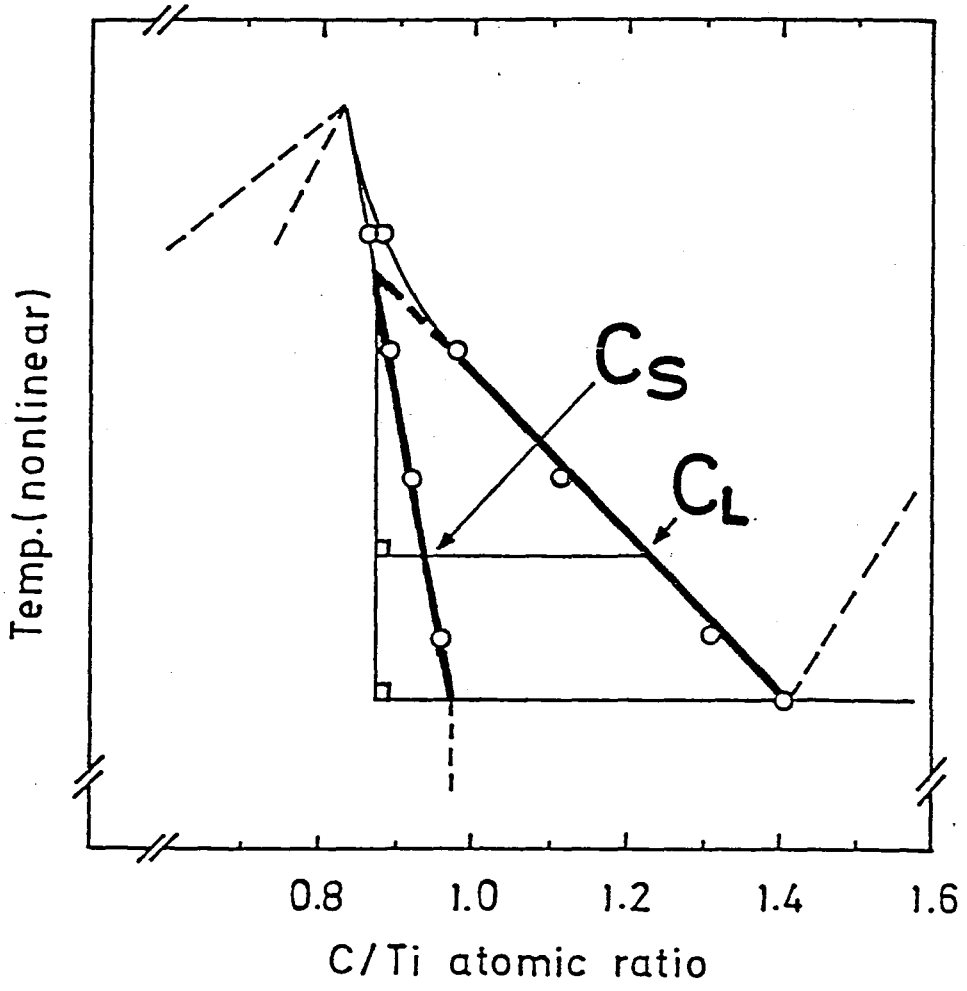

Fig. 5 Relationship between the solidus and liquidus lines which are shown as straight lines by making the vertical (temperature) axis arbitrary.

where x is the distance in the zone lengths,

$$C_0' = C_0 - 0.88, \qquad (5)$$

Substituting (2) and (5) in (4), we arrive at

$$\frac{C_S - 0.88}{C_0 - 0.88} = 1 - 0.83 \exp(-0.17x/L),$$

or

$$C_S(x) = C_0 + (-0.83C_0 + 0.73) \exp(-0.17x/L), \qquad (6) .$$

where $C_S(x)$ is the concentration in the crystal rod at the zone pass distance x. A curve of C_S versus x/L, calculated from eq.(6) for C_0=0.988, is shown as a dashed line in Fig. 6.

The experimental data shown in fig.6 indicate the change of chemical composition of crystal rod along the growth direction, which is prepared from the feed rod with C/Ti=0.988. The effective zone length(L) was estimated to be 4 mm from its weight, which corresponds to that of the crystal rod with 4 mm length. The final molten zone composition was C/Ti=1.31. The crystal rod had the compositional change from C/Ti= 0.91 to 0.956. The chemical composition of crystal was not asymptotic to that of the feed rod (C/Ti=0.988), but to C/Ti=0.956. Most of

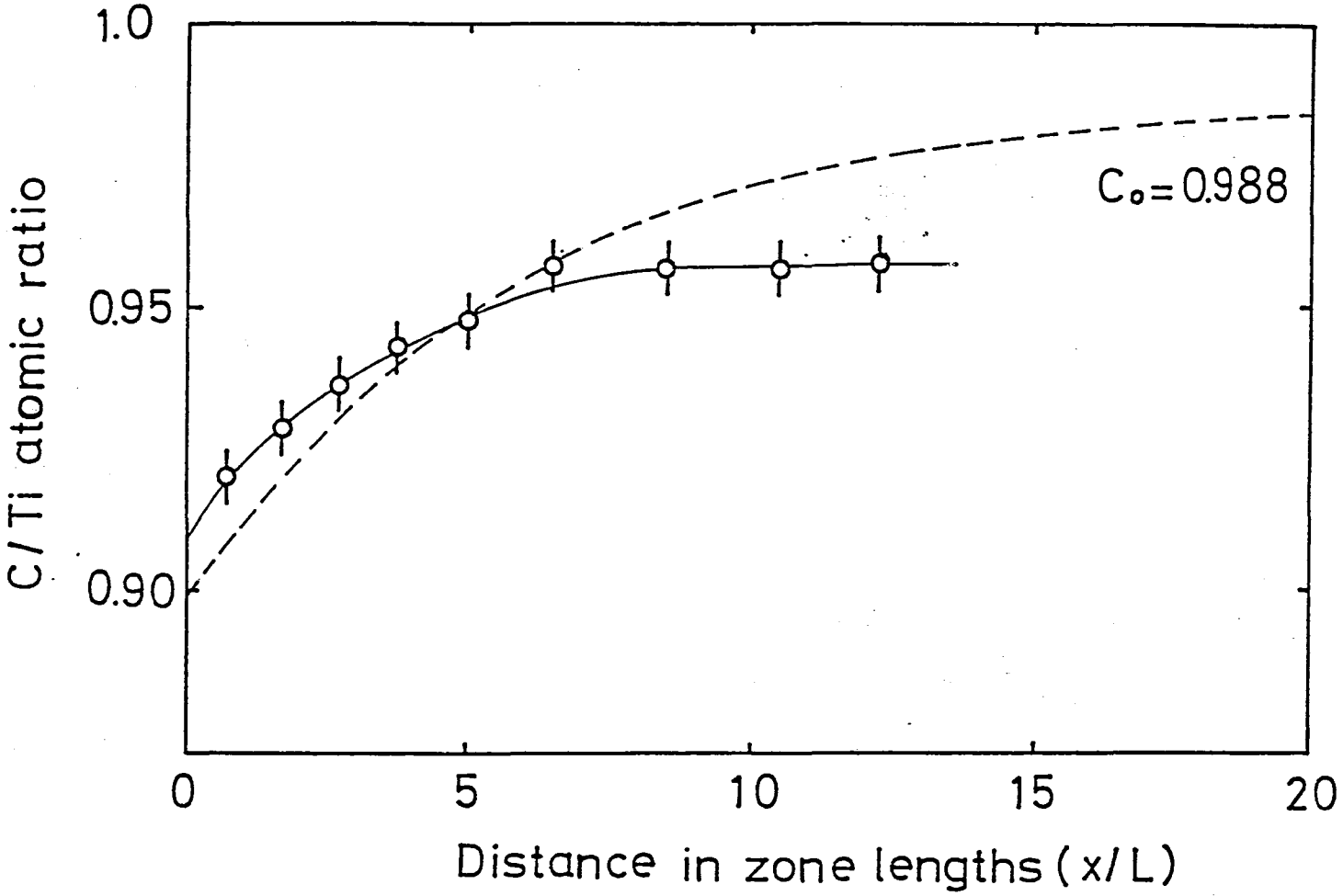

Fig. 6 Compositional change calculated from formula(6) in the case of C_0=0.988. Analytical values(o) of the crystal rod prepared from the feed rod having a chemical composition of C/Ti=0.988 by the usual floating zone technique. L is the effective zone length(4 mm), which is estimated from the zone weight.

this 3 at % difference(= 0.988 - 0.956) was attributed to the carbon evaporation from the molten zone. The present result could not be explained from the carbon extraction by oxygen solely, because the feed rod contained only 910 ppm oxygen.

In addition, the evidence of carbon evaporation was confirmed by another experimental method. In the case when a $TiC_{0.96}$ crystal was prepared, the zone pass stopped and the zone temperature was kept constant. Then the molten zone was solidified within a few minutes. That is to say, the melting temperature of the zone became higher. The phase diagram[12] shows that the carbon content in the molten zone decreased. The evaporation product was found to have a higher carbon content than the molten zone(C/Ti=1.3). Since the maximum carbon content of TiC is less than C/Ti=1.0, it is considered that the evaporation product consisted of TiC and carbon. Consequently, the fact that carbon evaporated from the zone during a zone pass was confirmed, although the carbon is amorphous and could not be detected by X-ray powder diffraction method.

1-2) Growth of TiC_x single crystals with maximum carbon content

On the basis of the present experimental result shown in Fig. 6, a $TiC_{0.96}$ crystal rod with no change of chemical composition is found to be prepared by using the feed rod with C/Ti=0.99 and by controlling the molten zone composition to be C/Ti=1.3 on initial melting(a modified zone leveling method). The way to prepare the crystal is shown in Fig. 7. The crystal

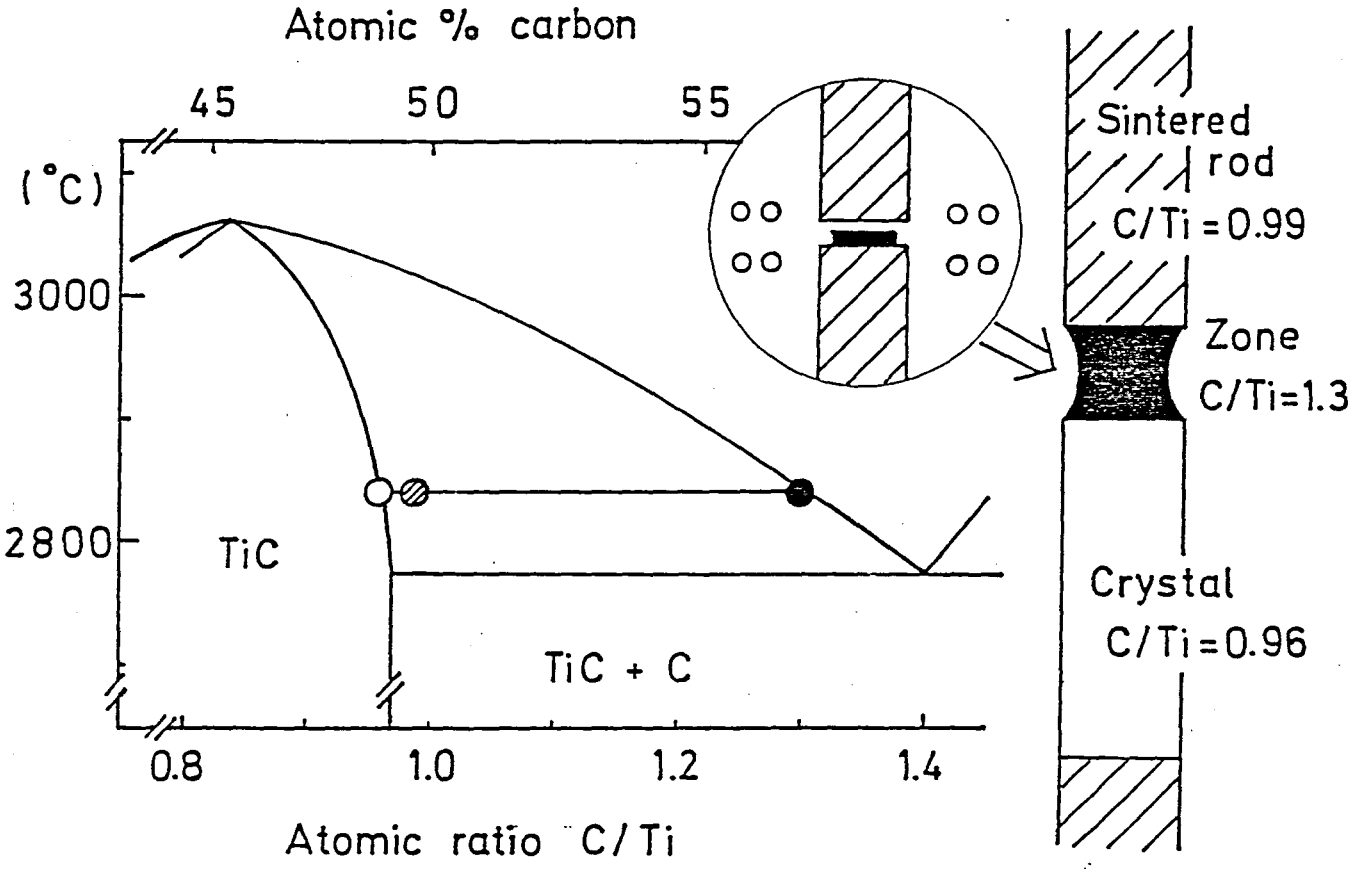

Fig. 7 Preparation of $TiC_{0.96}$ crystal rod.

rod obtained in this way had a constant chemical composition along the growth direction, such as C/Ti = 0.962, 0.959 and 0.959, as shown in Table 2. In addition, in order to examine the compositional change along the radial direction, a 5 x 5 x 15 mm^3 block was cut out of the central part of the crystal rod. The both block and residual crystal were analyzed. The result is listed in Table 2. The chemical compositions of both central and peripheral parts were C/Ti=0.957 and 0.964, respectively. The crystal rod prepared by the modified zone leveling method was found to be a homogeneous composition within 1 at%.

In order to prepare TiC crystal with a higher carbon content, a feed rod with C/Ti=1.006 was used, which was about 2 at% richer in carbon than that of the preceding feed rod(C/Ti=0.988). The results are tabulated in Table 3. The final molten zone composition was C/Ti=1.41. The chemical compositions of crystal rod were Cry-I, -M and -F = 0.962, 0.960 and 0.960, respectively. A little free carbon was contained in the Cry-I and -M. The free carbon mainly came from a small fluctiation during a zone pass because the chemical composition of the molten zone is almost identical with that of the TiC-C eutectic composition.

When a feed rod with C/Ti=1.017 was used, it was difficult to pass the molten zone smoothly because the chemical composition of the molten zone reached the eutectic composition. Inside the crystal rod obtained, parts where free carbon was deposited periodically along the growth direction were found. The chemical

Table 2 Carbon content and chemical compositions of the crystal rod prepared from the feed rod with C/Ti=0.988;
TC, FC and CC are total, free and combined carbon, respectively; Cry-I, -M and -F are the initial, middle and final parts of the crystal rod; M is molten zone; S is sintered feed rod.

	TC (wt%)	FC (wt%)	CC (wt%)	Composition(C/Ti) from TC	from CC
Cry-I	19.44	0.00	19.44	0.962	0.962
Cry-M	19.39	0.00	19.39	0.959	0.959
Cry-F	19.38	0.00	19.38	0.959	0.959
M	24.29			1.28	
S	19.86			0.988	
Center	19.35	0.00	19.35	0.957	0.957
Periphery	19.47	0.00	19.35	0.964	0.964

Table 3 Carbon content and chemical compositions of the crystal rod prepared from the feed rod with C/Ti=1.006

	TC (wt%)	FC (wt%)	CC (wt%)	Composition(C/Ti) from TC	from CC
Cry-I	19.46	0.04	19.42	0.964	0.962
Cry-M	19.41	0.02	19.39	0.961	0.960
Cry-F	19.40	0.00	19.40	0.960	0.960
M	26.14			1.41	
S	20.14			1.006	

composition of single phase part in the crystal was C/Ti=0.967, judging from combined carbon(CC). The free carbon content was 0.03 wt%.

It is found that a modified zone leveling method is the useful method to prepare TiC crystal rods with a maximum carbon content.

2)Growth of the single crystals with poor content of carbon

The crystals with poor content of carbon were prepared by the same method as mentioned above. The different points from the preparation of $TiC_{0.96}$ crystal are as follows. The melting temperature of TiC_x increases with decreasing the carbon content of x in the molten zone. In addition, Ti metal violently evaporates from the molten zone. Fig.8 shows the relationship between the evaporation rate and the chemical composition of molten zone(and prepared crystal). The evaporation rate was calculated from the measured results of the weight loss, the growth time and the surface area of a molten zone. When the zone composition is less than C/Ti=1.1, in which the chemical composition of the crystal is less than C/Ti=0.9, both TiC and Ti evaporate from the molten zone. The Ti metal violently evaporates with decreasing the carbon content in the molten zone. The evaporated Ti make the zone pass impossible because the Ti adhered to the work coil and touch the molten zone. The evaporated Ti metal burns by shock, when the furnace is opened after a zone pass.

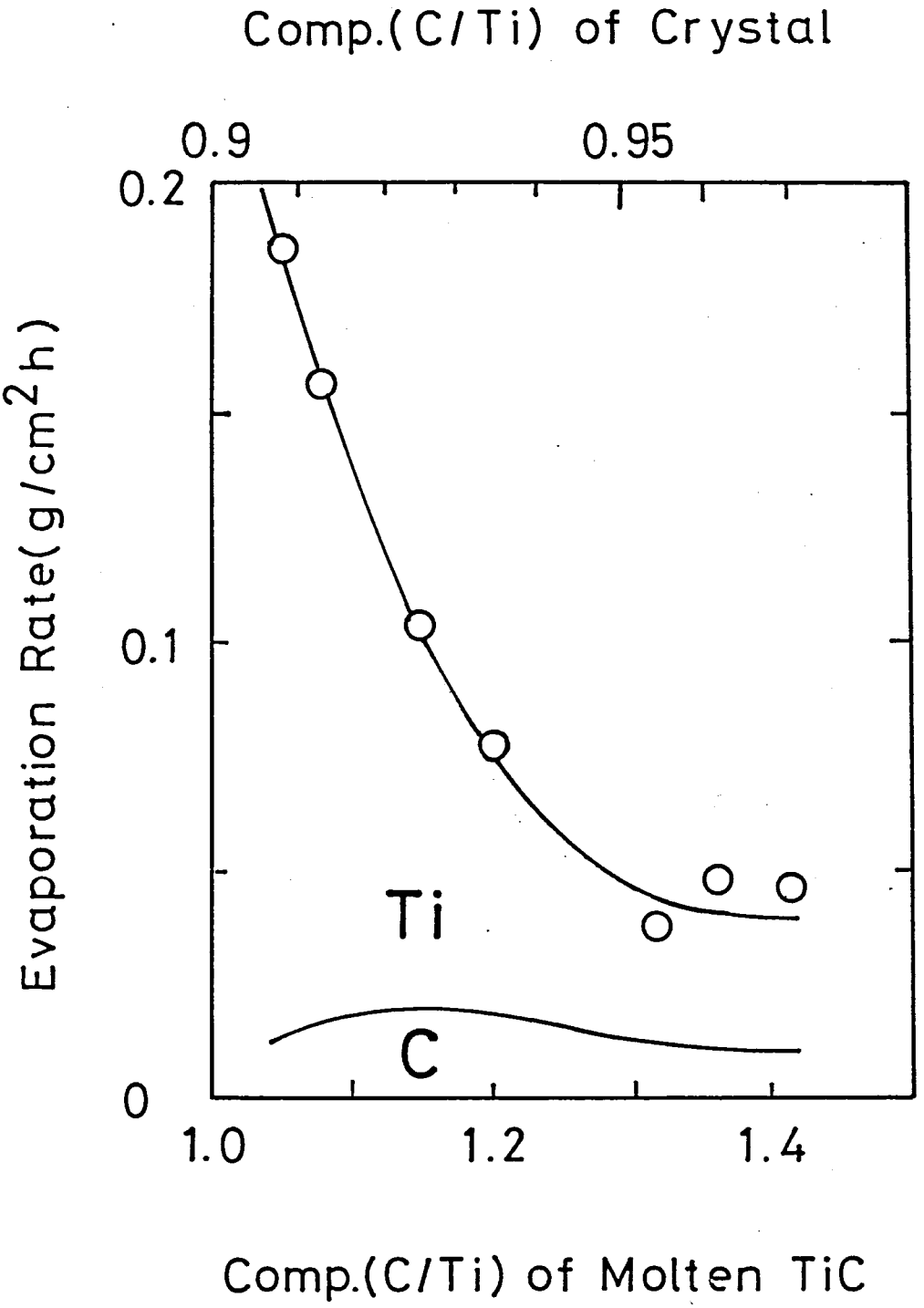

Fig. 8 Relationship between the chemical composition of molten zone(crystal) and the evaporation rate.

Table 4 Carbon content and chemincal compositions of the crystal rods of $TiC_{0.90}$ and $TiC_{0.85}$; S' is sintered feed rod just above the zone.

	(a)		(b)	
	$TiC_{0.90}$		$TiC_{0.85}$	
	TC (wt%)	Composition (C/Ti)	TC (wt%)	Composition (C/Ti)
Cry-I	18.28	0.892	17.50	0.846
Cry-M	18.38	0.898		
Cry-F	18.37	0.897	17.60	0.852
M	21.33	1.08	18.12	0.883
S	17.86	0.867	14.28	0.664
S'			15.59	0.737

Table 4(a) and (b) show the analytical results of the $TiC_{0.90}$ and $TiC_{0.85}$ crystal rods. The middle part(Cry-M) of the $TiC_{0.85}$ crystal rod was not analyzed because it was short(about 4 cm long) to analyze. The compositional change due to Ti evaporation were 3 at%(= 0.897-0.867) and 20 at%(= 0.852-0.664) in the $TiC_{0.90}$ and $TiC_{0.85}$ crystals, respectively. It is found that Ti violently evaporates from the molten zone with low carbon content. Therefore, the crystal can not be prepared in the chemical compositional region of lower than C/Ti=0.8.

3) Impurity

The oxygen and nitrogen impurity content in the crystal and feed rod are listed in Table 5. The $TiC_{0.96}$ crystal contained less than 10 ppm oxygen and 360 ppm nitrogen. The crystal of $TiC_{0.85}$ contained 570 ppm oxygen and 340 ppm nitrogen impurities. Oxygen impurity in the crystal decreased higher than one order by a zone pass. The impurity content tends to increase with increasing the carbon defect content. On the the other hand, the content of the nitrogen impurity did not change by a zone pass. Therefore, a feed rod having a low oxygen and nitrogen content is necessary in order to prepare a pure crystal.

Metal impurities in the crystal(final part), starting material, feed rod and evaporation product were examined by X-ray fluorescence spectroscopy. All detectable impurities are tabulated in Table 6. Each impurity content in the starting material was less than 500 ppm. Each peak height was normalized

Table 5 Oxygen and nitrogen impurities in the $TiC_{0.96}$ and $TiC_{0.85}$ crystals and in the feed rod from which the crystals were prepared(wt%).

		$TiC_{0.96}$	$TiC_{0.85}$
Oxygen	S	0.15	0.32
	Cry	<0.0001	0.057
Nitrogen	S	0.030	0.059
	Cry	0.036	0.034

by the Ti K_β peak. Comparing the impurities in the starting material with those of the feed rod, it was found that Fe and Co were partially refined during sintering, but the content of W, which is always contained in the IVa group carbide commercial powders, did not change by sintering.

Each impurity peak height in the feed rod(Feed) was compared with the peak height in the evaporation product(Evap.). The ratio(Evap./Feed) of each impurity peak is listed in Table 6. The impurity peak height ratio means the evaporation rate ratio of impurity to TiC. When an impurity is entirely refined by evaporation, the ratio becomes maximum. In the case of the present preparation condition, about 5 wt% of TiC is lost due to evaporation from the molten zone. The maximum value of the ratio is about 20(= 1/0.05). The refining effect is presented by the following expression:

$$\text{Refining effect(\%)= ratio value(Evap./feed) } X\frac{W_{evp}}{W_{cry}} \times 100$$

where $W_{evp}/W_{cry} = 1/20$.

The value of the ratio indicated that Fe was entirely refined by evaporation. Other impurities, such as Cr, Co and Ni, were thought to be entirely refined by evaporation because the melting points of chromium, cobalt and nickel carbides were not so high as TiC. On the other hand, W could not be observed in the evaporation product. From other experimental results, it was known that the ratio of W was less than 0.01. Tungusten carbide

Table 6 Impurities in the crystal($TiC_{0.96}$), starting material, feed rod and evaporation product(peak heights normalized by Ti Kβ)

	Crystal	Starting material	Feed rod	Evaporation product	Ratio (Evap./Feed)
Cr Kα	-	-	-	0.6	>6
Fe Kα	-	3.0	1.5	35	23
Co Kα	-	0.1	-	0.5	>5
Ni Kα	-	-	-	0.2	>2
W Lα_1	0.6	0.6	0.6	-	<0.2

does not evaporate from the molten zone. Therefore, the content of W has a tendency to increase in the crystal due to the evaporation of the host TiC.

These impurity evaporation rates are well consistent with the data on their vapor pressures described in ref.[36]. Impurities, such as Cr, Fe, Co and Ni, were refined partially by sintering and entirely during a zone pass. On the other hand, W metal, whose carbide has a very low vapor pressure, is not refined by both processes of sintering and zone refining. Therefore, the detectable impurity in the crystal was only W, as seen in Table 6. In order to prepare high purity crystals, the starting material should not contain impurities with low vapor pressures.

4) Relationship among the compositions, lattice constants and densities

The lattice constants and densities of these crystals were measured. The lattice defects at the Ti and C sites were calculated from the experimental results of the carbon content, the lattice constant and the density. The results are shown in Table 7. The values of Ti is about 0.2 % higher than unity because of the content of 500 ppm of W impurity. Therefore, it was concluded that no defects exist at the Ti sites, and then the nonstoichiometry comes from only carbon defects. Among the first three examples, the lattice constants are same within the limits of error in this narrow chemical composition(C/Ti=0.96-0.97),

Table 7 Chemical compositions calculated from the atomic ratios, lattice constants and densities; c is atomic ratio, which is obtained from carbon analysis; a is lattice constant; d is density.

c (C/Ti) ±0.005	a (nm) ±0.00004	d (kg/m^3) ±0.1	Crystal composition
0.967	0.43286	4878.4	$Ti_{1.001}C_{0.968}$
0.960	0.43282	4877.1	$Ti_{1.002}C_{0.962}$
0.959	0.43286	4870.9	$Ti_{1.001}C_{0.960}$
0.908	0.43295	4829.8	$Ti_{1.003}C_{0.911}$
0.807	0.43300	4714.5	$Ti_{1.001}C_{0.807}$

while the densities reflect the small difference in the chemical composition of crystal. The first sample (C/Ti=0.967) contained 0.03 wt% free carbon, as described before, but 0.03 wt% of free carbon does not influence the density within the limits of error. The last sample has the lowest carbon content among the TiC_x crystal prepared in the present study. This sample also shows a nonstoichiometry comes from only carbon defect.

5) Appearance and cross section of the crystal rod

The obtained crystal rod was about 6 cm long and 0.9 cm in diameter, as shown in Fig. 9. The fact that outward appearance of the crystal rod was smooth, indicated that the zone was passed smoothly by a modified zone leveling method.

The growth directions of the $TiC_{0.96}$ crystal rods were examined by a back-reflection Laue method. Figure 10 shows the grown directions on a part of a Wulff-net. It is apparent that $TiC_{0.96}$ has no prefered growth direction. Using a seed crystal, the crystal can be made to grow to any direction. However, the subgrains(a few degree disorientation) are introduced in the initial part. After all, the grown crystal is not different from that prepared without a seed crystal.

The longitudinal cross section of the crystal rod is shown in Fig.11. The initial part consists of many grains. However, when the zone is passed, the central grain gets larger and the central part becomes single crystal after a 2 cm zone pass. The single crystal is surrunded by a polycrystalline rim. As being

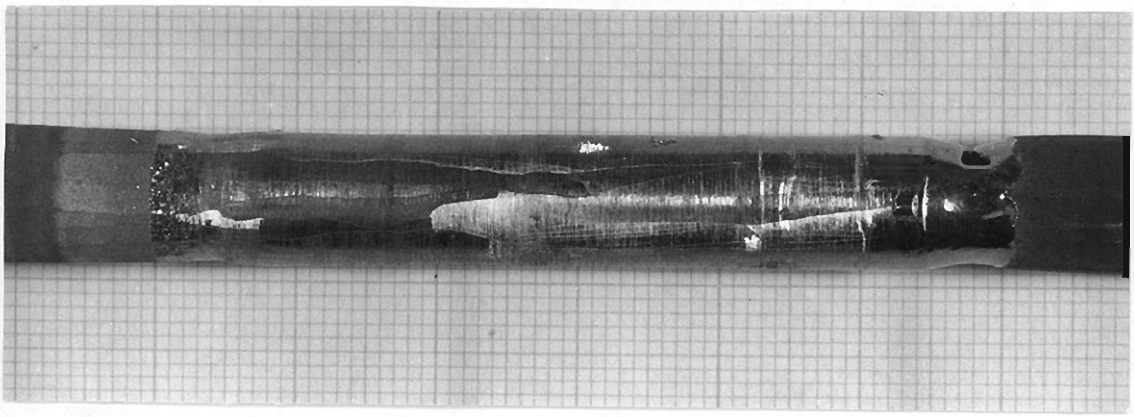

Fig. 9 As-grown $TiC_{0.96}$ crystal rod.

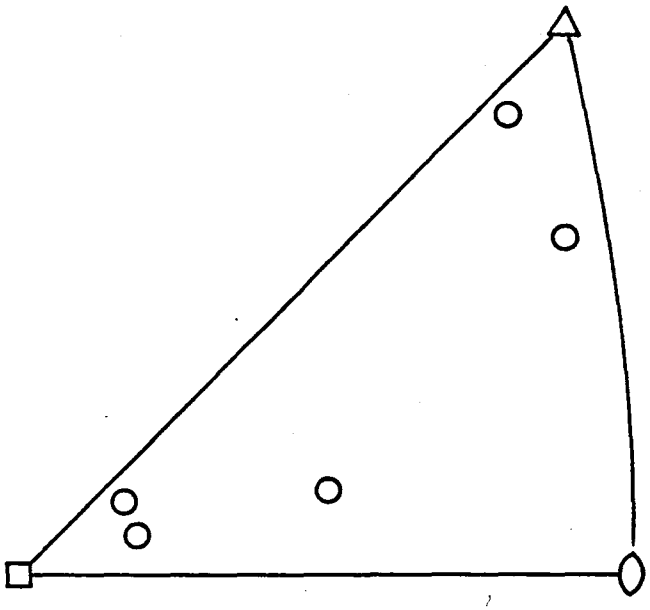

Fig. 10 Cyclographic projections onto a Wulff net of the growth directions of $TiC_{0.96}$ single crystals.

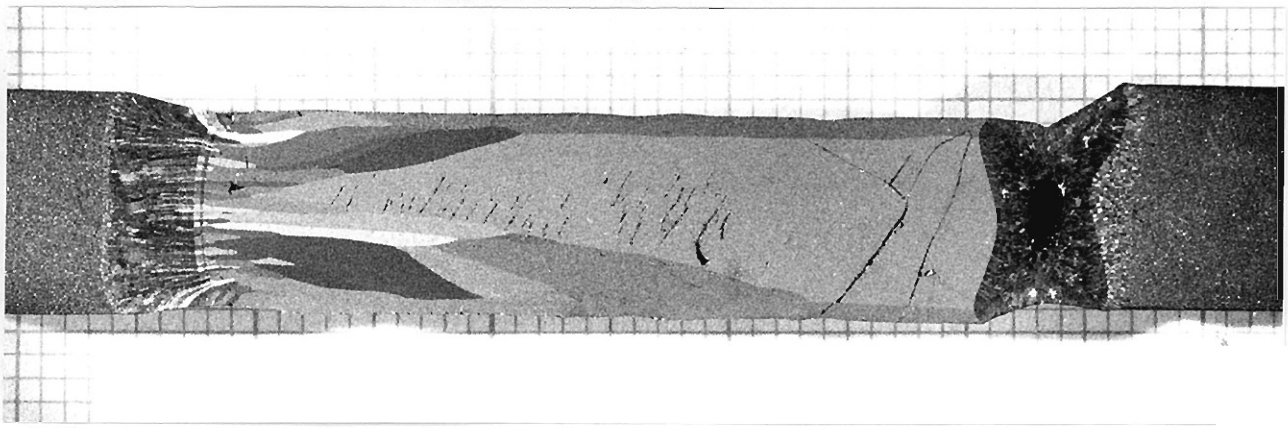

Fig. 11 Longitudinal cross section of $TiC_{0.94}$ crystal rod.

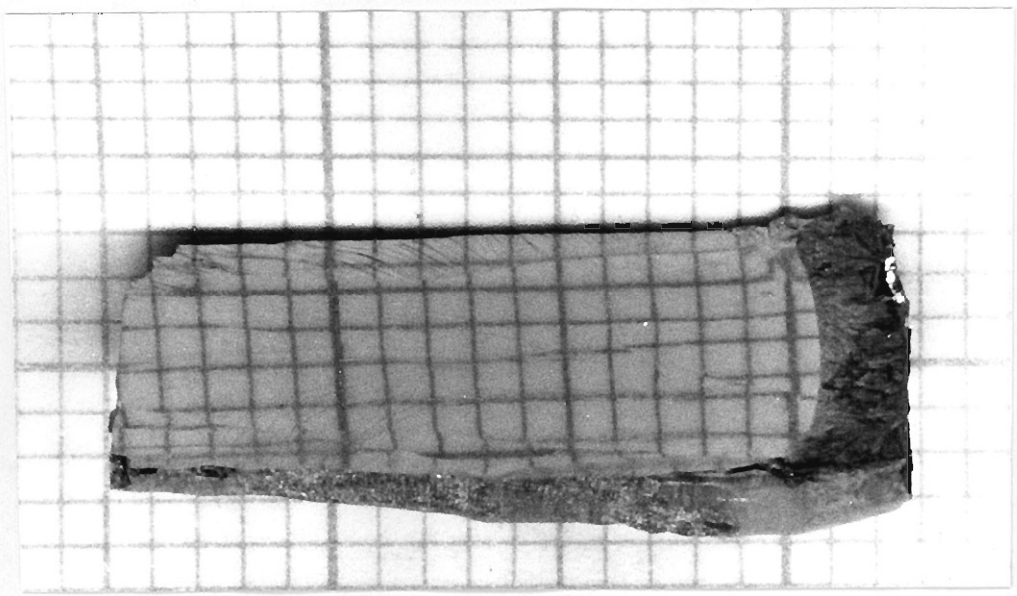

Fig. 12 Cleavage plane of $TiC_{0.96}$ crystal.

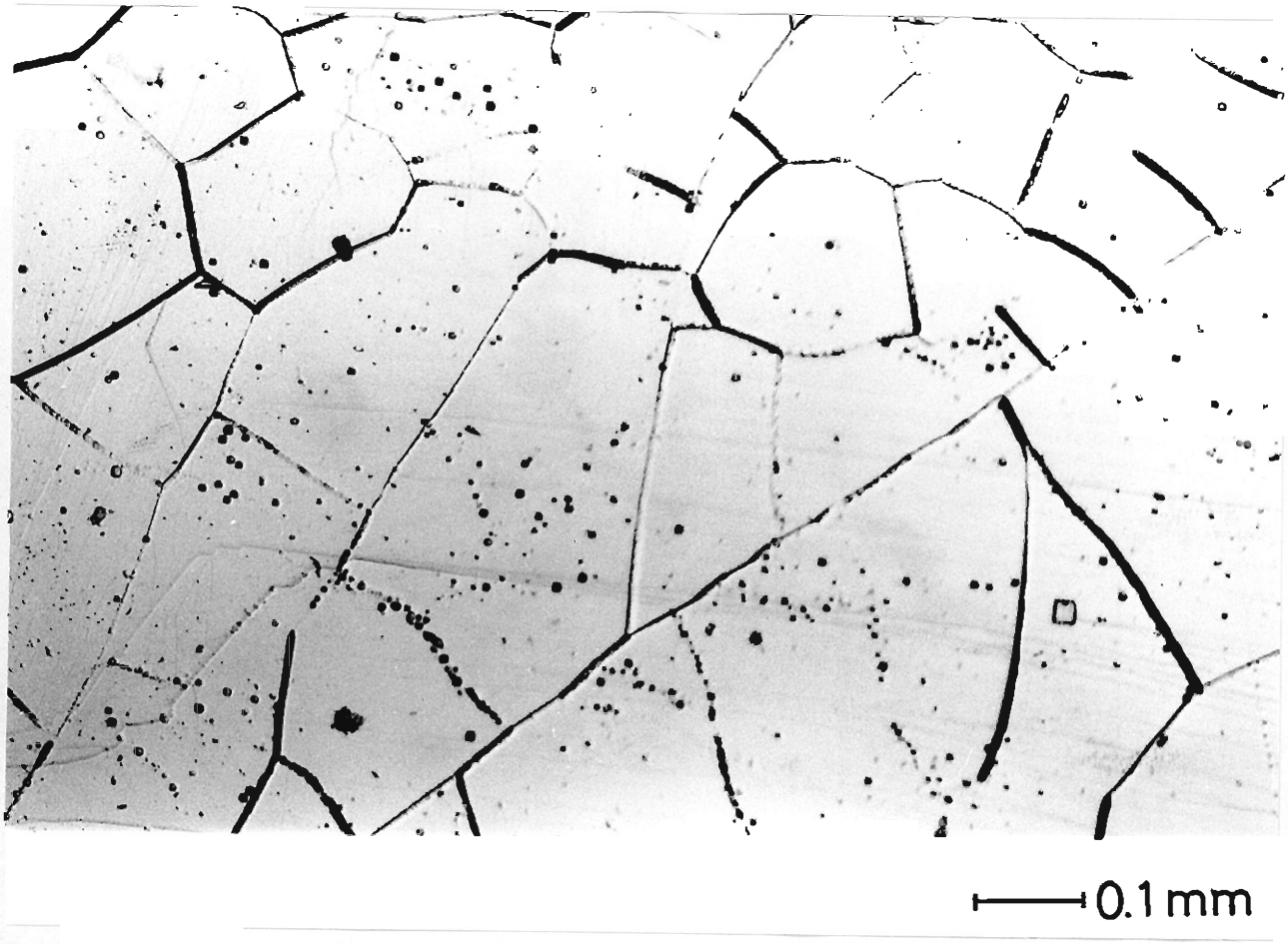

Fig. 13 Etch pit pattern in the (100) cleavage plane of $TiC_{0.96}$ crystal.

described later, the present experimental results are explained by the shape of crystal-zone interface, which is convex to the zone at the central part and concave at the peripheral part. The grains grow to the normal direction of the interface. Therefore, at the peripheral part, the new grains grow from the surface to the concave point and form a polycrystalline rim with 1 mm thickness.

Figure 12 shows the cleavage (100) plane. The crystal is found to be a good crystal.

The etch pit pattern is shown in Fig. 13. There are two kinds of pits: large one and small one. The large one is said to be caused by inclusion(free carbon)[37]. The small one is caused by dislocation.

(7) Conclusion

TiC crystals with the chemical composition of C/Ti being higher than 0.85 were prepared by a modified zone leveling method. TiC single crystals having a homogeneous near-stoichiometric composition(C/Ti=0.96-0.97) can be prepared by a modified zone leveling method.

As for the crystal with low carbon content, when the TiC crystal with C/Ti<0.9 is prepared, the TiC and Ti metal evaporate from the molten zone. The evaporated Ti metal disturbed the zone pass. Therefore, the crystal with C/Ti>0.80 were prepared. Most impurities are refined and eliminated by evaporation during the process of sintering and zone refining. However, impurities

having a low vapor pressure, such as W, could not be refined at all. On the basis of these results, crystals whose analytical chemical compositions corresponded to those calculated from their lattice constants and densities could be prepared.

2-4-2 ZrC_x

Preparation of ZrC crystal had been performed by several workers[17,33], but the large crystals are not prepared yet because of the reasons why the molten ZrC has a very low viscousity and easily drop down or blow up during a zone pass, and why it is difficult to form the initial molten zone because of a higher melting point than TiC. By applying a modified zone leveling method, these problems were sloved and the large single crystals with homogeneous chemical compositions were prepared[38].

1) Preparation of ZrC_x single crystals with constant chemical compositions

1-1) Determination of the composition diagram

It is necessary to obtain the relationship between the solidus and liquidus compositions under the growth condition, because the crystal growth does not occur under equilibrium condition.

The ZrC_x crystal rods were prepared using the sintered rods with various chemical compositions(C/Zr=1.12, 1.07, 0.98, 0.8 and 0.69) by a usual floating zone method. The thin work coil was used in order to form a molten zone with short length because of low viscousity. As the zone was passed, the heating power had to be decreased. The chemical compositions of several parts of the obtained crystal rods were determined from the results of carbon analysis, as listed in Table 8. When the zone was passed,

Table 8 Carbon content and chemical compositions of the crystal rod prepared by a usual floating zone method;
TC, FC and CC are total, free and combined carbon, respectively;
Cry-I and -F are the initial and final parts of the crystal rod;
M is molten zone; S is sintered feed rod.

	TC (wt%)	FC (wt%)	CC (wt%)	Composition(C/Zr) from TC	from CC
S	12.85			1.12	
Cry-I	11.12	0.04	11.08	0.950	0.947
Cry-F	11.52	0.05	11.45	0.987	0.983
M	19.52			1.84	
S	12.39			1.07	
Cry-I	10.98	0.07	10.91	0.937	0.931
Cry-F	11.30	0.05	11.25	0.968	0.963
M	17.68			1.631	
S	11.48			0.985	
Cry-I	10.54	0.05	10.49	0.895	0.891
Cry-F	10.82	0.05	10.77	0.921	0.917
M	12.80			1.115	
S	9.54			0.801	
Cry-I	9.98	0.40	9.58	0.842	0.808
Cry-F	9.66	0.58	9.08	0.817	0.763
M	7.60			0.625	
S	8.37			0.694	
Cry-I	8.02	0.35	7.67	0.662	0.633
Cry-F	6.88	0.19	6.69	0.560	0.546
M	3.22			0.253	

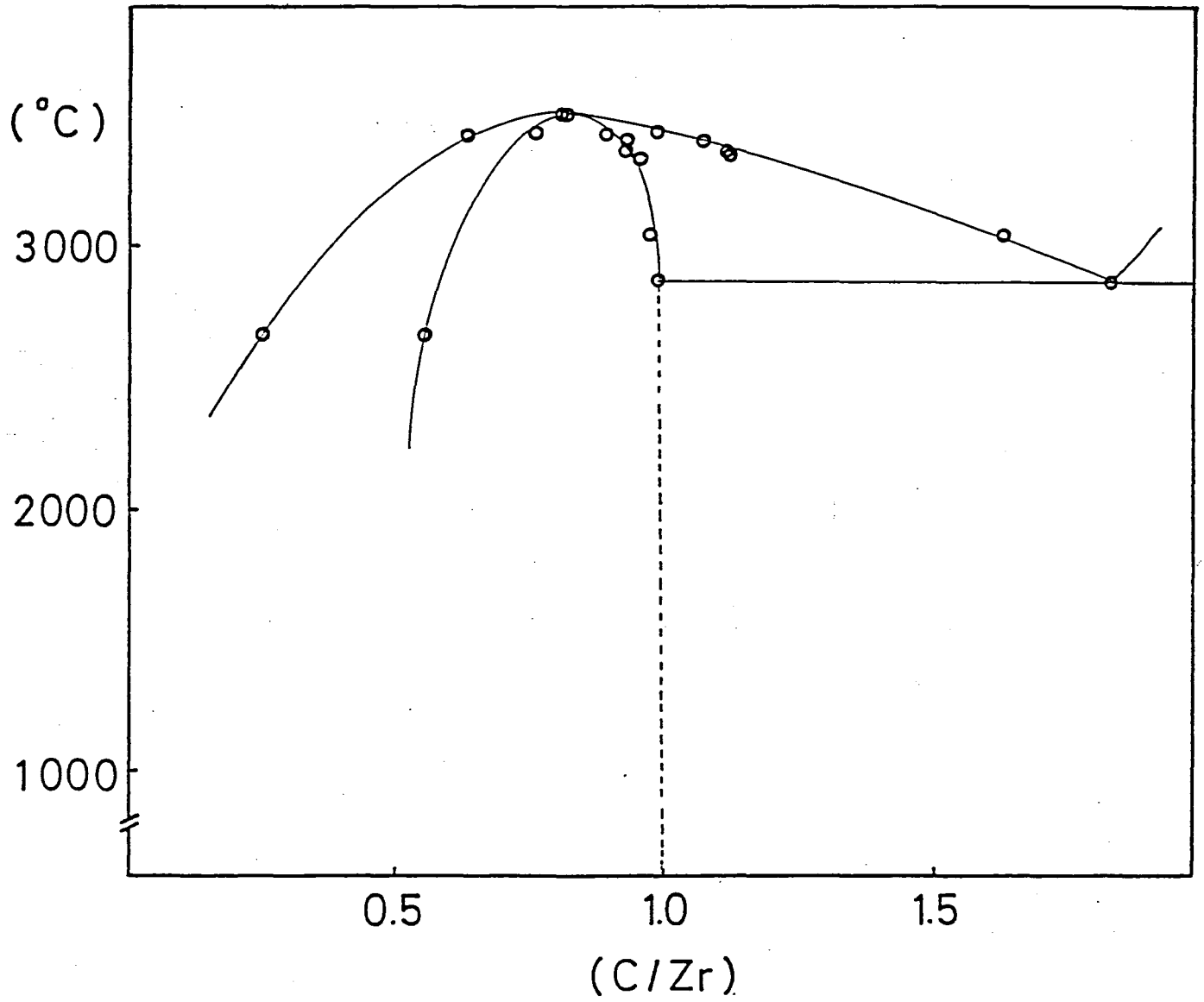

Fig. 14 A compositional diagram of ZrC_x estimated from a usual floating zone method.

the carbon content increased in the carbon rich region, and decreased in the carbon poor region. For example, when the zone was passed using a feed rod with C/Zr=0.985, the chemical compositon of the crystal rod changes from C/Zr=0.891 to 0.917, while the chemical composition of the molten zone changed from C/Zr=0.985 to 1.115. A pair of the chemical compositions of an initial part of the crystal rod and the feed rod, and another pair of the chemical compositions of the final part of the crystal rod and a final molten zone correspond to pairs of the solidus and liquidus compositions, as shown in Fig. 3. The relationship between the liquidus and solidus compositions determined using the experimental results listed in Table 8, is shown in Fig. 14. The ordinate is refered by that of the phase diagram of Storms[20]. The relationship of chemical composition between the sintered rod and the initial part of the crystal rod of the last example in Table 8, was not plotted. The effective carbon content in the feed rod was smaller than the analytical value because oxygen extracted carbon on melting.

1-2) Variation in chemical composition by evaporation from the molten zone

On the basis of the composition diagram obtained above, the preparation of $ZrC_{0.98}$ crystal was carried out, using a feed rod having a molar ratio of C/Zr=0.979, in which the compositional ratio of the initial molten zone was C/Zr=1.7, which is the liquidus composition coexisting with the desired crystal

Table 9 Variation in chemical composition along the growth direction due to preferential evaporation of carbon from the zone

	TC (wt%)	FC (wt%)	CC (wt%)	Composition(C/Zr) from TC	from CC
Cry-I	12.14	0.66	11.48	1.049	0.992
Cry-M	11.14	0.04	11.10	0.952	0.949
Cry-F	10.92	0.04	10.88	0.931	0.928
M	14.26			1.26	
S	11.42			0.979	

composition(C/Zr=0.98). However, the crystal with constant chemical composition could not be prepared. The results of the carbon analysis of several parts of the crystal rod were listed in Table 9. The chemical composition of crystal rod changed from C/Zr=0.992 to 0.928, as the zone was passed. The chemical composition of the molten zone changed from C/Zr=1.7 to 1.26.

Two reasons are pointed out to explain the variation in the C/Zr ratio: the carbon evaporation from the molten zone, and the carbon extraction by oxygen in the feed rod. However, the contribution of the latter case was little because the feed rod contained only 700-800 ppm oxygen, as seen in Table 11. Therefore, its compositional change mainly comes from the evaporation of carbon from the molten zone. When the zone composition was near the ZrC-C eutectic composition, the evaporation products were graphite and ZrC_x. On the other hand, ZrC_x and Zr metal evaporated from the molten zone whose carbon content was less than a ratio of C/Zr=1.0. The evaporated Zr metal was burned by shock, when the furnace was opened. The amount of evaporation loss during a 6-7 hour zone pass was 0.2-1.3 g. Increasing the amount of added Zr metal(in the carbon poor region), the amount of the evaporation products increased.

1-3) Preparation of ZrC_x single crystals with constant chemical compositions by a modified zone leveling method.

In order to prepare a crystal with constant chemical

composition, the molten zone composition must be kept constant. Therefore, the carbon or Zr metal content in the feed rod should increase in order to compensate for the amount of loss of the carbon, or Zr metal due to evaporation.

It was found, from the experimental results on the third example listed in Table 8(applying the usual floating zone method) and Table 9, that the chemical compositions of the obtained crystal rods changed from 0.891 to 0.917, and from 0.992 to 0.928, by using the same composition of the feed rod(C/Zr=0.98). As the molten zone is passed, the steady state condition is approached. Therefore, the crystal with constant chemical composition of C/Zr=0.92-0.93 can be prepared by using the feed rod of C/Zr=0.98 and the initial molten zone of C/Zr=1.15, which is the liquidus composition coexisting with the solidus composition of C/Zr=0.92-0.93, as shown in Fig. 14. The arrangements and procedures to prepare the crystal are shown in Fig. 15. The bottom of the upper rod whose chemical composition is C/Zr=1.15 was melted to make the initial molten zone(Fig. 15(a) and (b)), and then the rods were moved upwards(Fig. 15(c)). The obtained crystal rod is shown in Fig. 19. The chemical composition did not change from the initial to the final parts within the limits of errors, as listed in the second example of Table 10. That is to say, the feed rod of C/Zr=0.977 was supplied to the molten zone, and the molten zone which had a constant chemical composition of C/Zr=1.141-1.161, produced a crystal having a ratio of C/Zr=0.93 constantly. The difference

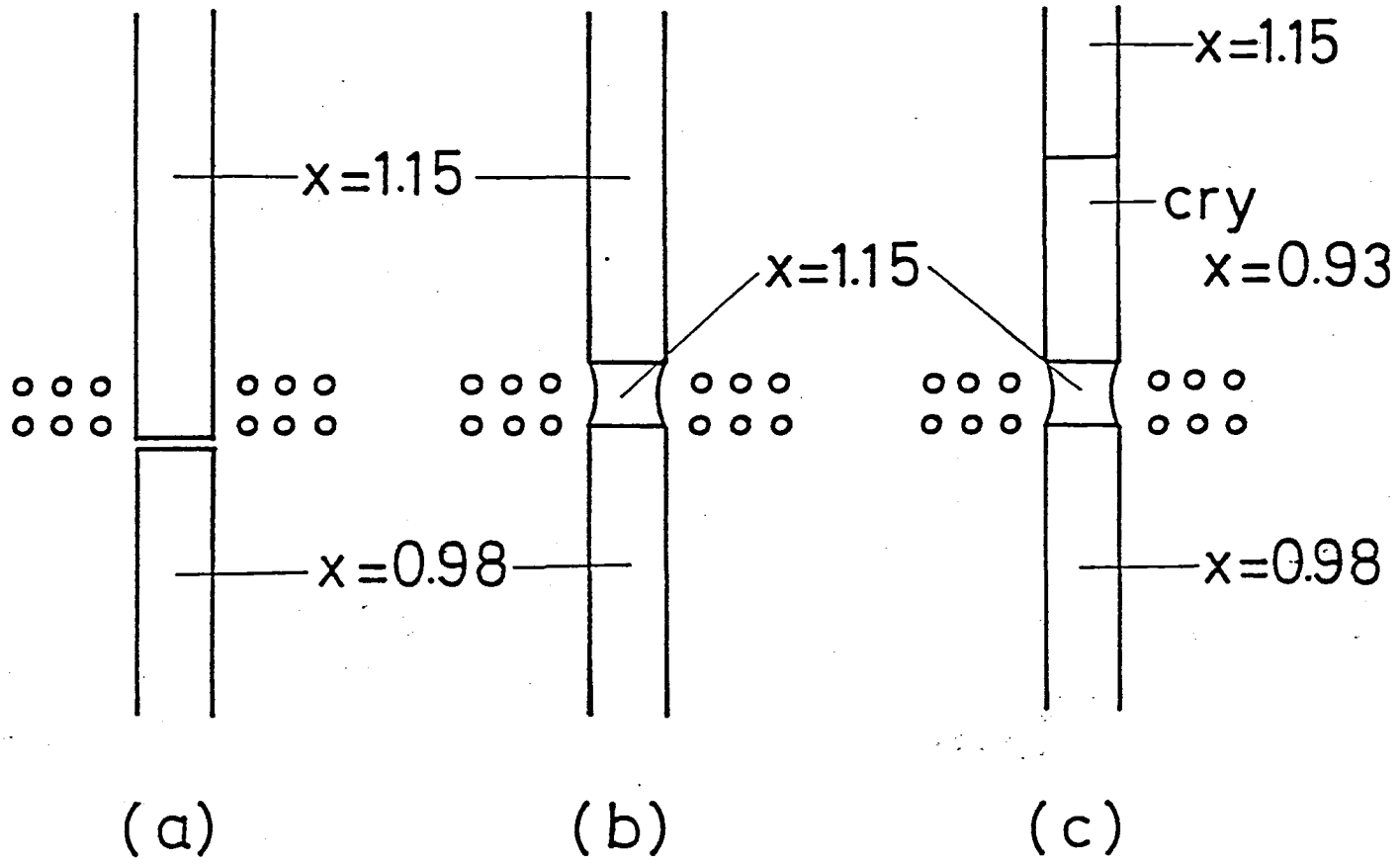

Fig. 15 Procedures of preparation of $ZrC_{0.93}$ by a modified zone leveling method. (a) A sintered rod for an initial molten zone is set at the upper shaft and a feed rod, whose chemical composition is controlled so as to compensate for the composition change of the zone due to evaporation, is set at the lower shaft. (b) The upper rod is melted to form the initial molten zone. (c) The rods are driven upwards. A crystal rod with a constant chemical composition is thus prepared.

Table 10 Carbon content and chemical compositions of the crystal rod prepared from a modified zone leveling method

	TC (wt%)	FC (wt%)	CC (wt%)	Composition(C/Zr) from TC	from CC
Cry-I	11.50	0.07	11.43	0.987	0.981
Cry-M	11.52	0.06	11.46	0.989	0.983
Cry-F	10.52	0.04	10.48	0.989	0.985
M	18.72			1.75	
S	12.38			1.07	
S'	13.26			1.16	
Cry-I	10.94	0.04	10.90	0.933	0.930
Cry-M	10.90	0.03	10.87	0.929	0.927
Cry-F	10.96	0.03	10.93	0.935	0.932
M	13.06			1.14	
S	11.40			0.977	
Cry-I	7.75	0.35	7.40	0.638	0.609
Cry-M	7.86	0.42	7.44	0.648	0.613
Cry-F	7.72	0.51	7.21	0.635	0.593
M	3.90			0.308	
S	7.86			0.648	

(S'=sintered rod for an initial molten zone)

in chemical composition between the feed rod(C/Zr=0.977) and the growing crystal(C/Zr=0.93) arose from the preferential evaporation of carbon.

As seen the first example in Table 10, the floating zone was carried out using a feed rod of C/Zr=1.08 and an initial molten zone of C/Zr=1.7 in order to obtain a $ZrC_{0.98}$ crystal. The chemical composition of the feed rod was estimated from the results of the first two examples in Table 8, and empirically determined to be C/Zr=1.08. The sintered rods with a ratio of C/Zr larger than 1.4 do not have enough high mechanical strength. Therefore, an estimated amount of a graphite disk was inserted between the upper and lower rods. The initial molten zone with C/Zr=1.7 was formed by melting the part around the disk. This method has the advantages that both the upward and downward zone pass can be easily carried out, and that the seeding process can be done. The several parts of the crystal rod prepared in this method had the same chemical composition, such as C/Zr=0.981, 0.983, and 0.985, as listed in Table 10.

As seen the third example of Table 10, the crystal with C/Zr=0.61 was prepared by the same method as the previous example. The chemical compositional change due to the preferential evaporation of Zr metal from the molten zone could not be observed clearly. This result stems from the carbon extraction caused by the excessive oxygen content(about 0.5 wt%), which was adsorbed by the added Zr metal during the sintering process. A curious problem is that this crystal(C/Zr=0.61)

contained much free carbon.

2) Impurities

The amounts of oxygen and nitrogen impurities in the crystals depend on the kinds of starting materials. Oxygen content decreased by zone pass, but nitrogen hardly, as seen in Table 11. Oxygen and nitrogen impurities were below the detection limits of 20 ppm, and 200-300 ppm, respectively, in the crystals(C/Zr=0.93) prepared from ZrC and carbon. The crystal(C/Zr=0.85) prepared from ZrC and Zr powders contained 280 ppm oxygen and 370 ppm nitrogen impurities. However, the crystal with less than C/Zr=0.8 can not be prepared because of violent evcaporation of Zr. In the case when the feed rod contained much oxygen, the crystal with carbon poor composition(C/Zr=0.60) can be prepared, as listed in Table 10, because Zr metal does not evaporate from the molten zone. Table 11 shows the result of $ZrC_{0.59}$ crystal prepared from ZrC and ZrO_2. It is found that much oxygen was contained. Figure 16 shows the relationship between the chemical composition of crystal and impurity content. These impurities are found to increase with increasing the amount of added Zr metal. In addition, these impurities were examined at the center and peripherary of $ZrC_{0.85}$ crystal rod, as seen in Table 12. Only the surface of the crystal rod do not contain them.

Impurities in the $ZrC_{0.98}$ crystal which was prepared from the starting material with high purity were analyzed by spark

Table 11 Oxygen and nitrogen impurities in the ZrC_x.

		$ZrC_{0.59}$	$ZrC_{0.85}$	$ZrC_{0.93}$
Starting Material		$ZrC + ZrO_2$	ZrC + Zr	ZrC + C
Oxygen	S	4.10	0.32	0.07
	Cry	1.7	0.028	<0.002
Nitrogen	S	0.12	0.08	0.03
	Cry	0.13	0.037	0.025

(wt%)

Table 12 Oxygen and nitrogen impurities in crystal rod(C/Zr= 0.85).

	Oxygen (wt%)	nitrogen (wt%)
Central part	0.055	0.040
Peripheral part	0.069	0.049

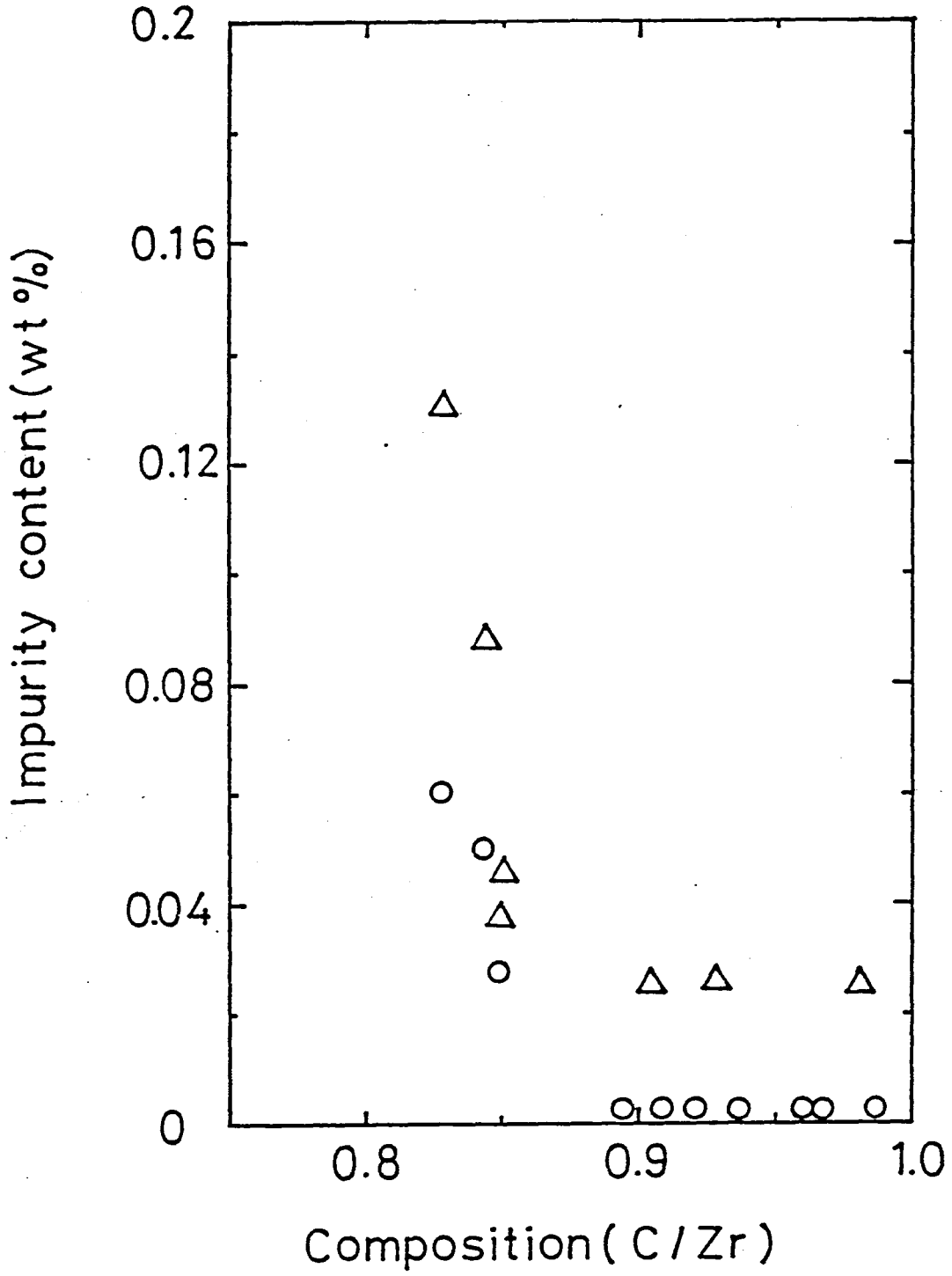

Fig. 16 Oxygen(o) and Nitrogen(Δ) content in ZrC_x crystal.

Table 13 Impurities in the crystals analyzed by spark mass-spectroscopy(ppm)

W	900	Mg, Cu, Zn	7
Hf	380	Na	5
Ti	130	Co	3
Ta	30	Cr	< 3
Fe	30-20	F	1
Al	20-10	V, Ni, Mn	< 1
B	20-10	Ga, P, As	
K, Cl, Ca	20		
Si	< 20		
Nb	10		
Mo	10-7		

mass spectroscopy. The results are listed in Table 13. The main impurities are W, Hf and Ti, which come from the ZrC starting material.

3) Relationship among the composition, lattice constant and density.

The lattice constant and density of the grown crystals in the composition region higher than C/Zr=0.8 were measured. The relationship between the composition and lattice constant is shown in Fig. 17. The dash-dotted line shows the result estimated from the reported values by Toth[12] because the reported ones varies widely due to the contents of oxygen and nitrogen. The present results are 0.002 nm shorter than the estimated ones. The relationship between the composition and density is tabulated in Table 18. A dash line is the result calculated from the lattice constant(Fig. 17) under the assumption that the lattice defect exist only at the carbon sites. A dash-dotted line is the estimated one. The measured densities is 20-30 kg/m^3 higher than the calculated ones in which a small amount of W(0.4 wt%) and Hf(0.2 wt%) contained. Table 14 lists the compositions of Zr and C which are calculated from the carbon content, lattice constant and density. The composition of Zr is about 0.3 % higher than unity because of the contents of W and Hf. Therefore, it is expected that no defects exist at Zr sites and the nonstoichiometry comes from only carbon defects.

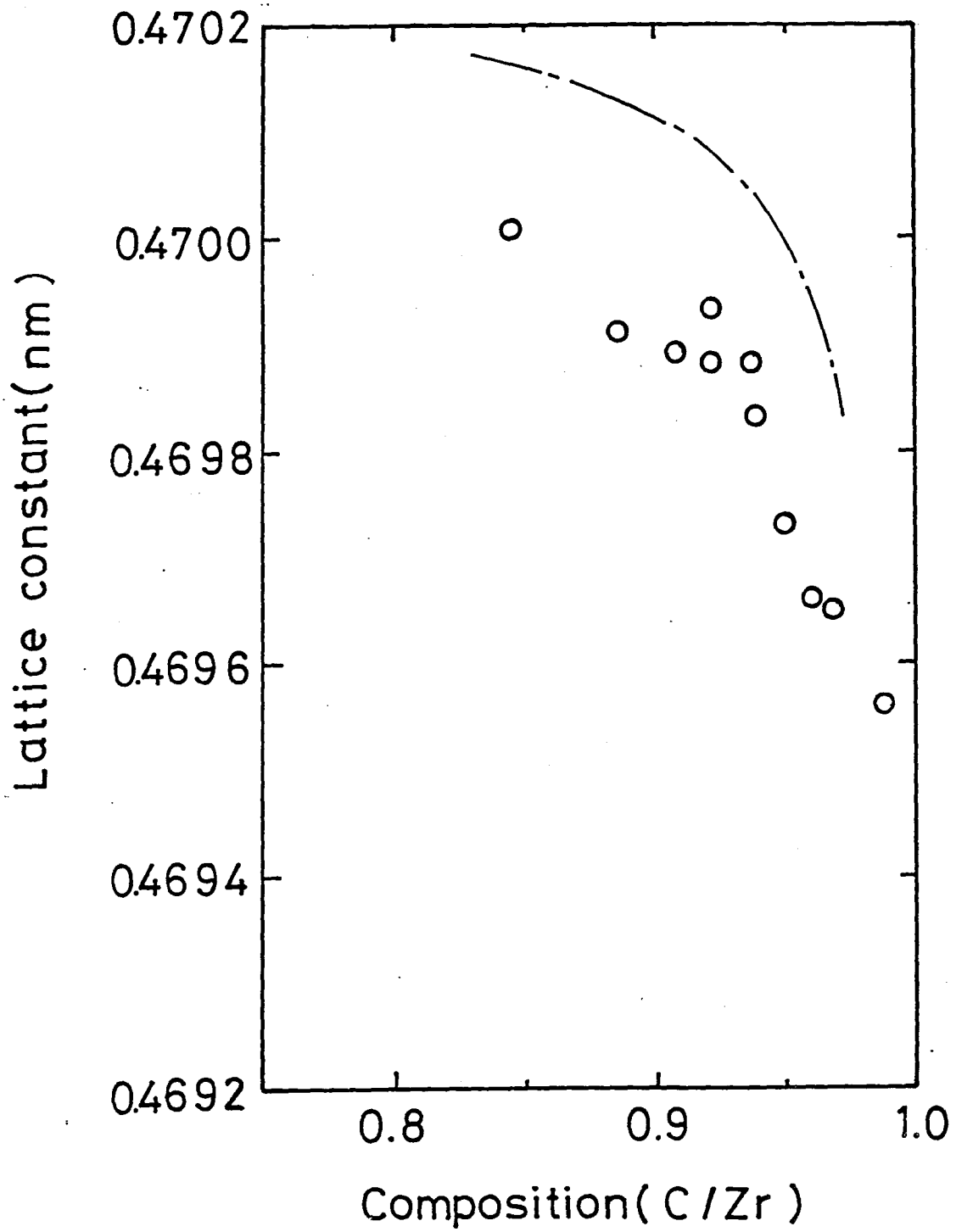

Fig.17 Relationship between the chemical composition and the lattice constant. A dash-dotted line is estimated by Toth[12].

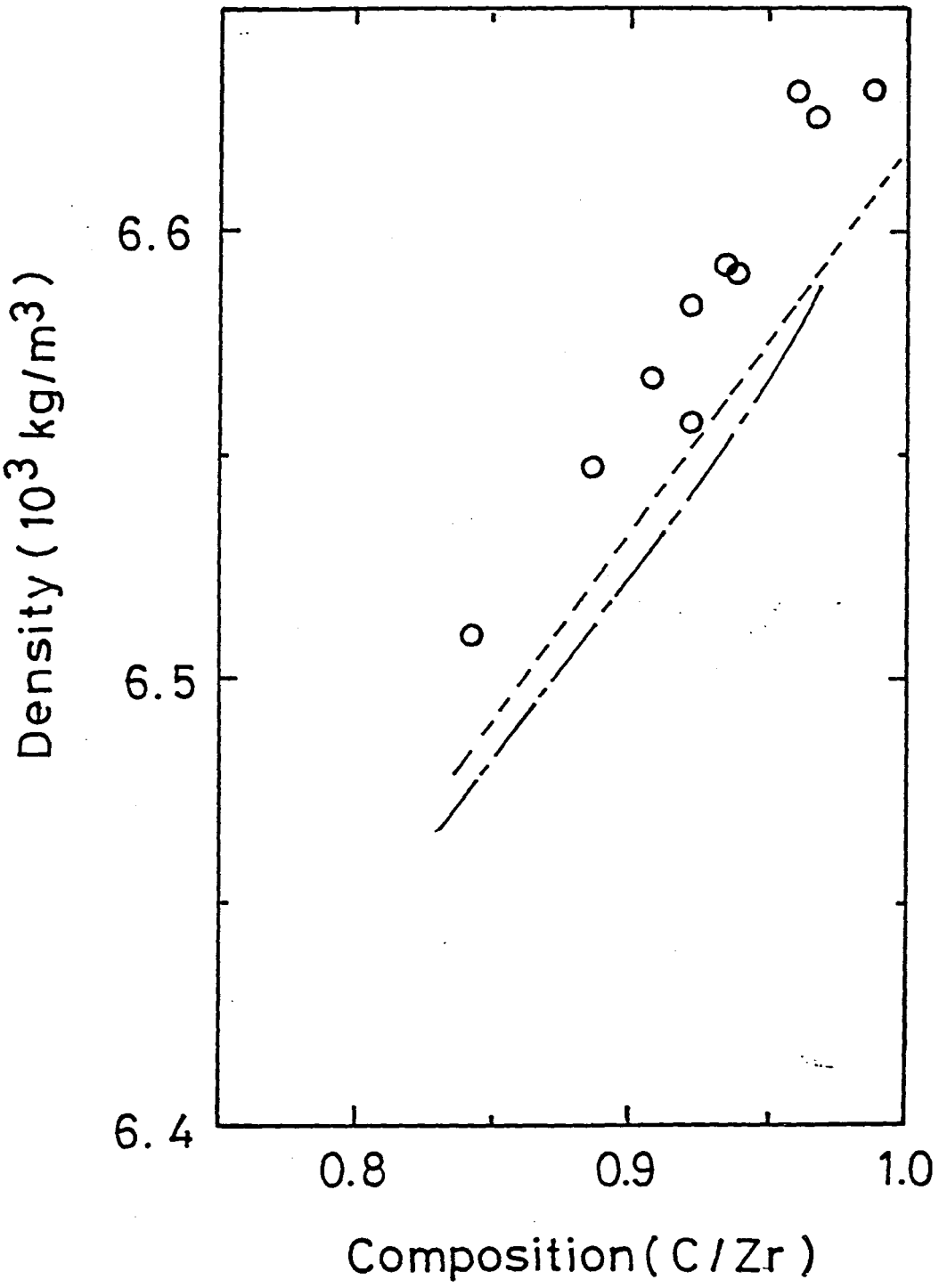

Fig. 18 Relationship between the chemical composition and the density. A dash line is obtained from the lattice constants in Fig. 17. A dash-dotted line is obtained from the estimated lattice constants in Fig. 17.

Table 14 Chemical compositions calculated from the atomic ratios, lattice constants and densities; c is atomic ratio, which is obtained from carbon analysis; a is lattice constant; d is density

c (C/Zr) ±0.005	a (nm) ±0.00004	d (kg/m^3) ±0.1	Crystal composition
0.987	0.46956	6631.4	$Zr_{1.003}C_{0.990}$
0.939	0.46983	6590.4	$Zr_{1.004}C_{0.942}$
0.922	0.46993	6556.9	$Zr_{1.002}C_{0.923}$
0.886	0.46991	6547.2	$Zr_{1.004}C_{0.890}$
0.842	0.46989	6509.7	$Zr_{1.003}C_{0.845}$
0.812	0.46975	6501.5	$Zr_{1.003}C_{0.816}$

4) Appearance, cross section and etch pit pattern

The size of $ZrC_{0.93}$ crystal rod is 6-7 cm long and about 9 mm in diameter, as shown in Fig. 19. The longitudinal section of the final part in the crystal rod is shown in Fig. 20(a). The crystal rod consists of a polycrystalline rim of approximately 1 mm thickness and a large single grain at the center of the rod. This thin rim can be made uniformly by only rotating the growing crystal and keeping the feed rod stationary, and under these growing conditions the central grain of the growing crystal became larger. The peripheral region of the central grain is composed of subgrains with orientations off a few degrees, judging from the results of splitting of the Laue spots. The central part of growing crystal rod is a good perfection crystal, as shown in Fig. 20(b).

The growth directions of $ZrC_{0.98}$ crystal rods were examined by a back-refection Laue method. Figure 21 shows the growth direction on a part of a Wulff-net. It is apparent that $ZrC_{0.98}$ crystals have no preferential growth direction.

The etch pits on the (100) cleavage planes of $ZrC_{0.98}$ are shown in Fig. 22. The shape in the pits were pyramidral. The etch pit densities were estimated to be $5 \times 10^6/cm^2$.

5) Conclusion

ZrC_x single crystals with constant chemical compositions have been prepared in the compositional region of higher than

Fig. 19 $ZrC_{0.93}$ single crystal rod prepared by the method shown in Fig. 15.

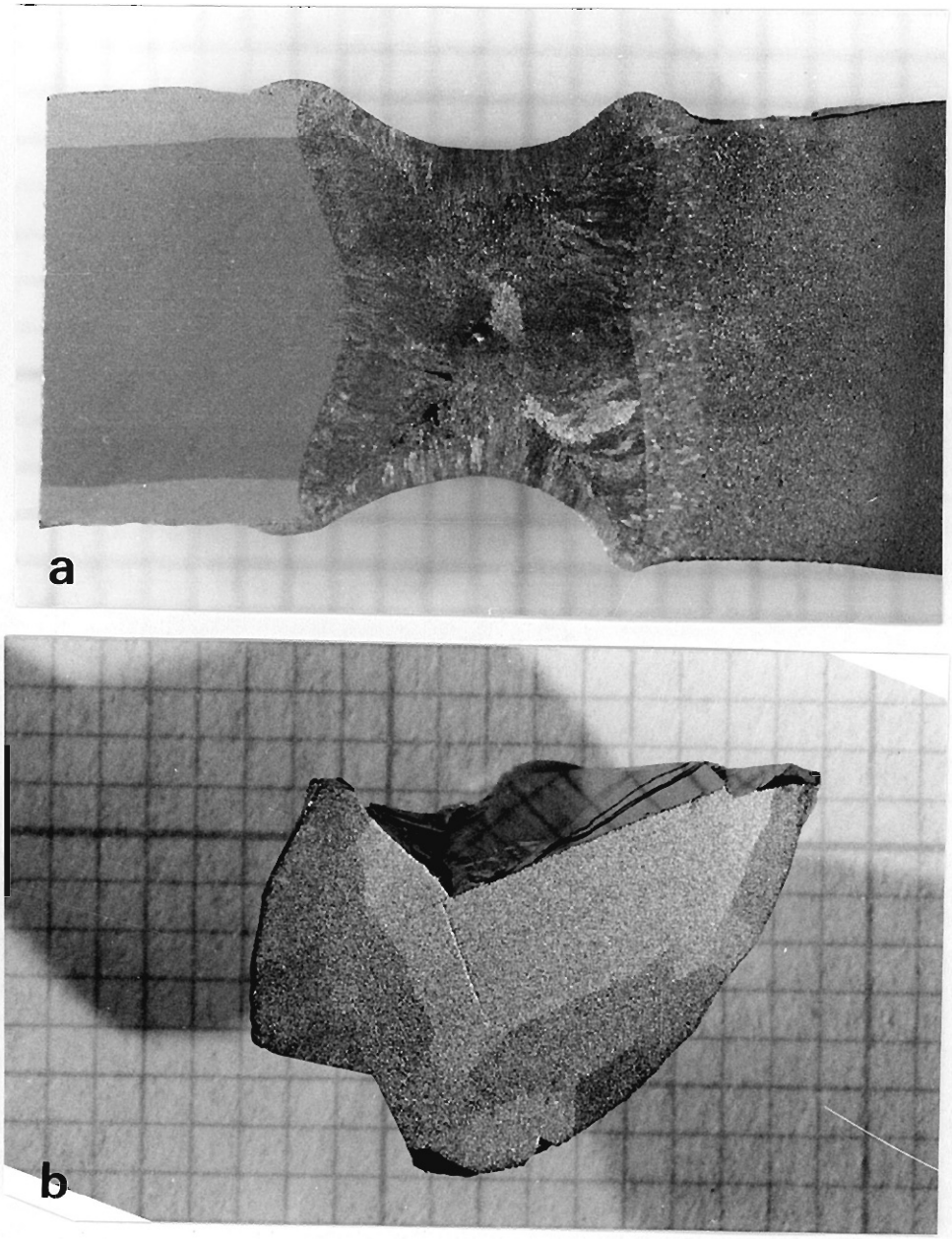

Fig. 20 (a)Longitudinal cross section of the final part of the $ZrC_{0.98}$ crystal rod. (b) The (100) section of the crystal rod and the (100) cleavage plane. A crystal rod consists of a polycrystalline rim and a central single crystal grain. The central grain is a good perfection crystal.

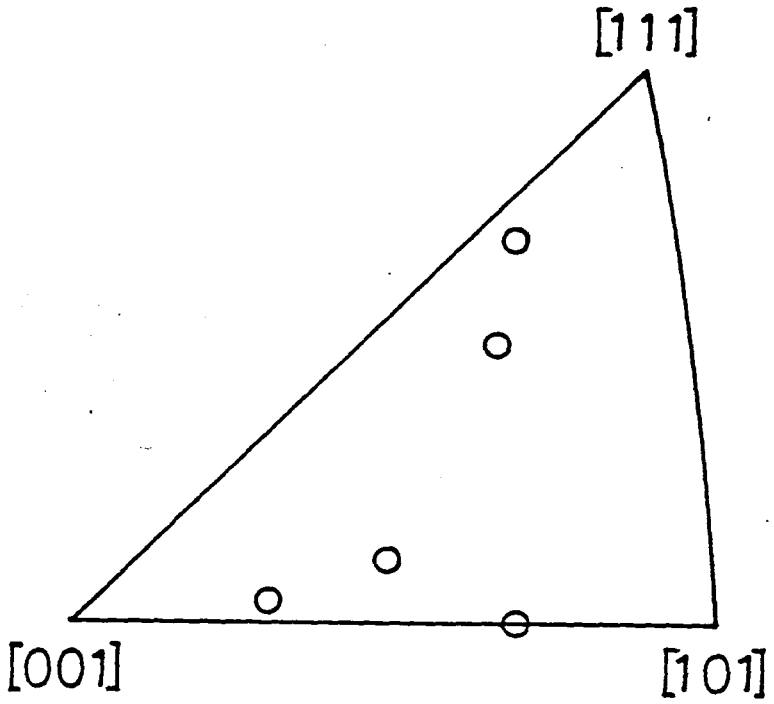

Fig. 21 Cyclographic projections onto a Wulff net of the growth directions of $ZrC_{0.98}$ single crystals.

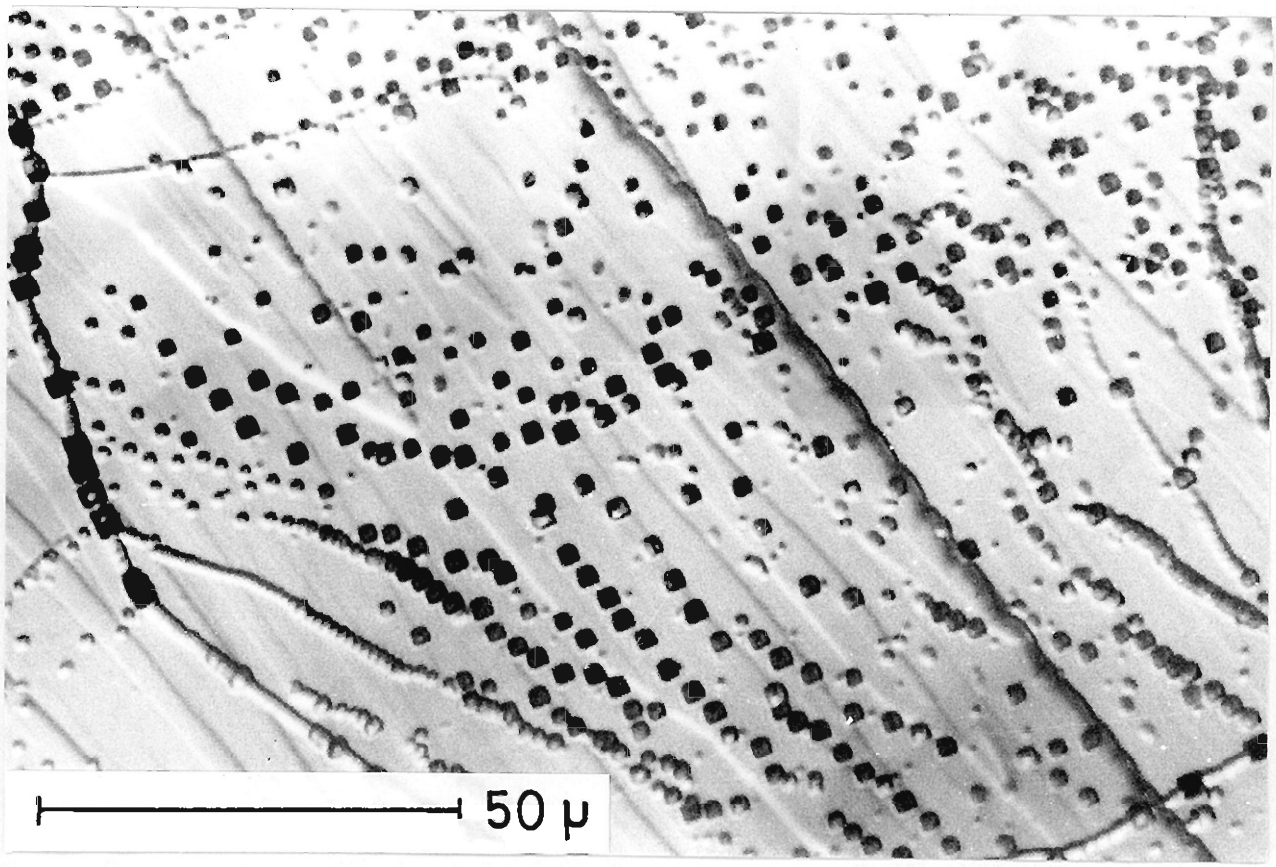

Fig. 22 An etch pit pattern in the (100) cleavage plane of $ZrC_{0.98}$ crystal. The etchant is a $HF:HNO_3:H_2O$=1:1:2 solution.

C/Zr=0.8 using a modified zone leveling method. High purity crystal with less than C/Zr=0.8 can not be prepared because of violent Zr evaporation. The relationship among the composition, lattice constant and density was obtained in the compositional region of C/Zr > 0.8.

2-4-3 HfC_x

HfC is one of the materials with the highest melting points. The maximum melting point is 3928°C, as shown in Fig. 23. Therefore, preparation of HfC crystal had been seldom tried. Only Haggerty et al. reported on the preparation of HfC crystals by a RF induction heating floating zone technique[7]. They carried out the zone pass at a very high growth rate(5 cm/h) for less than one hour. There were no detail describtions on the size and quality of the crystal in their report. The most difficulty comes from the high melting point because the temperature must be elevated up to 3900°C, as shown in Fig. 23, in order to melt a commercial powder(C/Hf=0.98). Therefore, we applied a modified zone leveling method to prepare the crystals at the temperature condition of a little above the HfC-C eutectic temperature(3180°C)[39].

1) Prepararion of HfC_x single crystals

In order to prepare the HfC crystal at a little above the HfC-C eutectic temperature, the molten zone composition must be kept near the eutectic composition(C/Hf=1.86), as deduced from Fig. 23.

As for the chemical composition of the initial molten zone, a nominal chemical composition of C/Hf=1.7 was selected. The eutectic composition was not used as the molten zone composition because the crystal often contained much free carbon. Further, in order to determine the chemical composition of the feed rod,

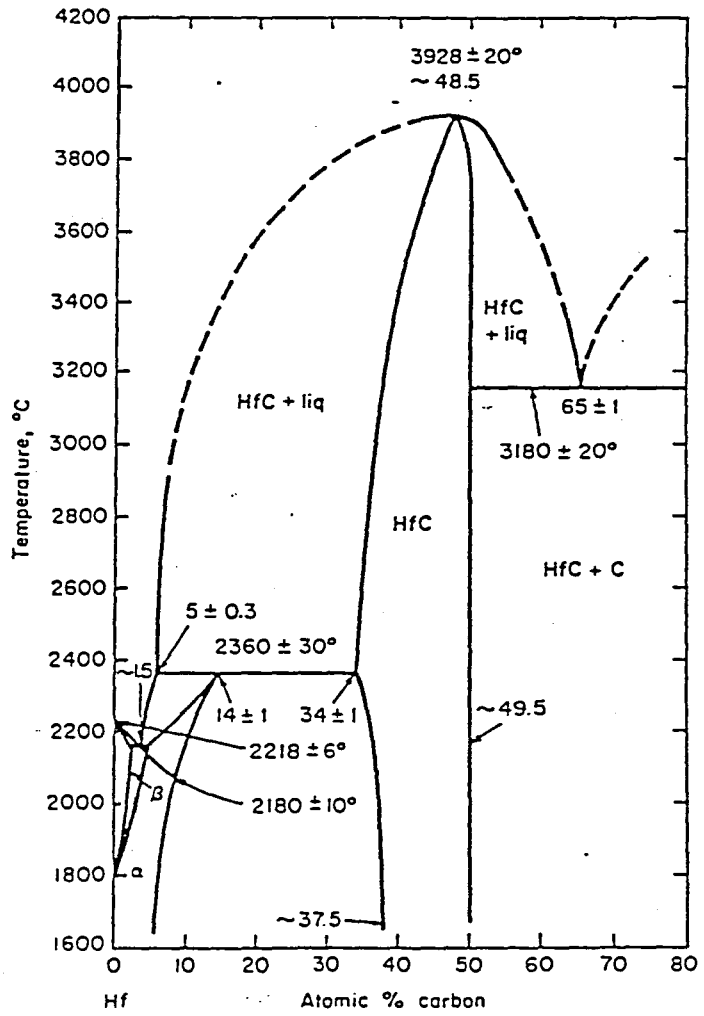

Fig. 23 Phase diagram of hafnium-carbon(after Rudy[20]).

the following experiment was carried out. Sintered feed rods with various chemical compositions(nominal ratios of C/Hf=1.09, 1.18, 1.32 and 1.51) were prepared. The molten zone was passed through each of the rod, using the initial molten zone having a nominal molar ratio of C/Hf=1.7. If the molten zone composition was kept constant, the heating power would be nearly constant. When the feed rod with C/Hf=1.32 was used, the heating power hardly changed during a zone pass.

The major problem in preparation of HfC_x single crystal was to evaporate violently from the molten zone. The evaporation products were HfC_x and graphite. Therefore, the molten zone was contact with the evaporation products deposited on the inside of the work coil, and then began to freeze from the part of the contact. This problem was solved by using a coil with large inside diameter(15 mm) and by counter-rotating the upper and lower shafts. The molten zone stirred by rotation had an effect on melting the evaporation products which touched the molten zone. The evaporation products on the inside of the work coil were removed by the rotating upper feed rod. Fortunately, since the molten HfC has a high viscosity, the zone pass itself could be easily carried out.

The content of carbon and Zr in the crystal rod were analyzed. The results are listed in Table 15. The crystal rod had no free carbon and almost constant chemical composition, but its composition(C/Hf(Zr)) slightly changed from 0.956 to 0.977. Much carbon might have been lost due to evaporation during a

Table 15 Carbon and Zr content in the crystal rod

	TC (wt%)	FC (wt%)	CC (wt%)	Zr (wt%)	Composition
Cry-I	6.13	0.00	6.13	1.61	$Hf_{0.967}Zr_{0.033}C_{0.956}$
Cry-M	6.18	0.00	6.18	1.75	$Hf_{0.964}Zr_{0.036}C_{0.962}$
Cry-F	6.28	0.00	6.28	1.93	$Hf_{0.961}Zr_{0.039}C_{0.977}$
M	10.55			5.36	$Hf_{0.889}Zr_{0.111}C_{1.66}$
S	8.05			2.30	$Hf_{0.952}Zr_{0.048}C_{1.27}$

period from the beginning of heating, especially from the beginning of the formation of the initial molten zone, to the start of zone pass, because carbon has a very high vapor pressure(0.2-0.3 atm)[36] at about 3300°C where the initial molten zone is formed. Therefore, when the molten zone began to be passed, the chemical composition of the molten zone changed to a carbon poorer composition than that of the desired composition(C/Hf=1.7). As the zone was passed, carbon was concentrated to C/Hf=1.66 in the molten zone. In order to prepare a crystal rod with a more constant composition, the nominal chemical composition of the initial molten zone must be richer in carbon to compensate for the violent carbon evaporation from the molten zone.

2) Impurities

The crystal contained 250 ppm oxygen and 340 ppm nitrogen, as listed in Table 16. This crystal of HfC contained more oxygen impurity than those of TiC and ZrC, which contained less than 10 ppm and 20 ppm, respectively. The nitrogen was the same level as that contained in TiC and ZrC crystals.

Metal impurities in the crystal(final part), starting material, feed rod and evaporation product were analyzed by X-ray fluorescence spectroscopy. All detectable impurities are tabulated in Table 17. Each peak height was normalized by the Hf peak heights. The main impurities in the starting material were Zr and W, whose contents were 2.3 wt% and 0.26 wt%, respectively.

Table 16 Oxygen and nitrogen impurity content in the sintered rod and crystal

	Oxygen (wt%)	Nitrogen (wt%)
S	0.14	0.21
Cry	0.025	0.034

Table 17 Impurities in the crystal, starting material, feed rod and evaporation product(peak heights)

	Crystal	Starting material	Feed rod	Evaporation product	Ratio (Evap./Feed)
Ti $K\beta$	-	-	-	112	>224
V $k\alpha$	-	-	-	63	>126
Cr $K\alpha$	-	1.5	0.5	185	370
Fe $K\alpha$	-	7	0.6	234	390
Co $K\alpha$	-	-	-	9	>18
Ni $K\alpha$	-	2.5	0.5	171	340
Zr $K\alpha$	56	63	64	230	3.6
W $L\alpha_1$	13	13	13	4.5	0.35
U $L\alpha_1$	-	1.5	1.5	72	48

The another impurities were less than a few hundred ppm. Cr, Fe and Ni were partially refined by sintering. Most of impurities are perfectly refined by evaporation during a zone pass. Zr and W, which have low vapor pressure, were not refined. Therefore, in order to prepare the high puritiy crystals, the starting material without Zr and W must be used.

3) Apperarance, cross section and etch pit pattern

The size of obtained crystal rod is about 6 cm long and 0.9 cm in diameter, as shown in Fig. 24. The outward appearance of the crystal rod was not smooth; although the zone was passed stably, the feed rod was not melted into the molten zone smoothly because the evaporation products adhered to the feed rod, and the evaporation products deposited on the work coil touched the crystal rod. The initial part of the crystal was polycrystalline, but a single crystal could be obtained from the last half of the crystal rod. The longitudinal section of the molten zone and the final part of the crystal rod are shown in Fig. 25. The cental single crystal grain is surrounded by a polycrystalline rim, like TiC_x and ZrC_x. The rim is thicker than those of TiC_x and ZrC_x. The grains in the rim are found to grow from the surface. A good-perfection crystal with 3-4 mm diameter could be obtained from the central part of the rod. The crack(cleavage) in the final part might have come from decreasing the heating power too rapidly at the end of the zone pass because the other parts did not have cracks.

Fig. 24 As grown $HfC_{0.96-0.98}$ crystal rod.

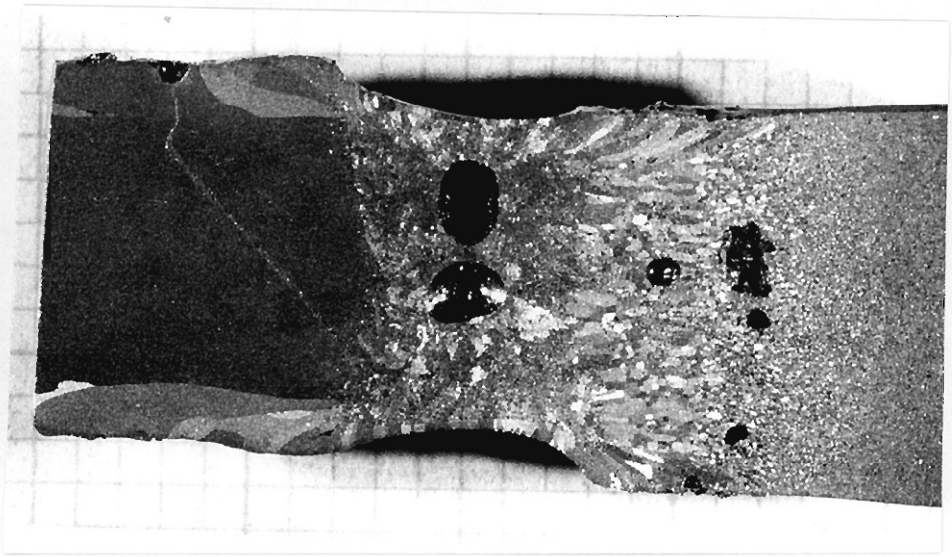

Fig. 25 Longitudinal section of the molten zone and final part of the HfC crystal rod.

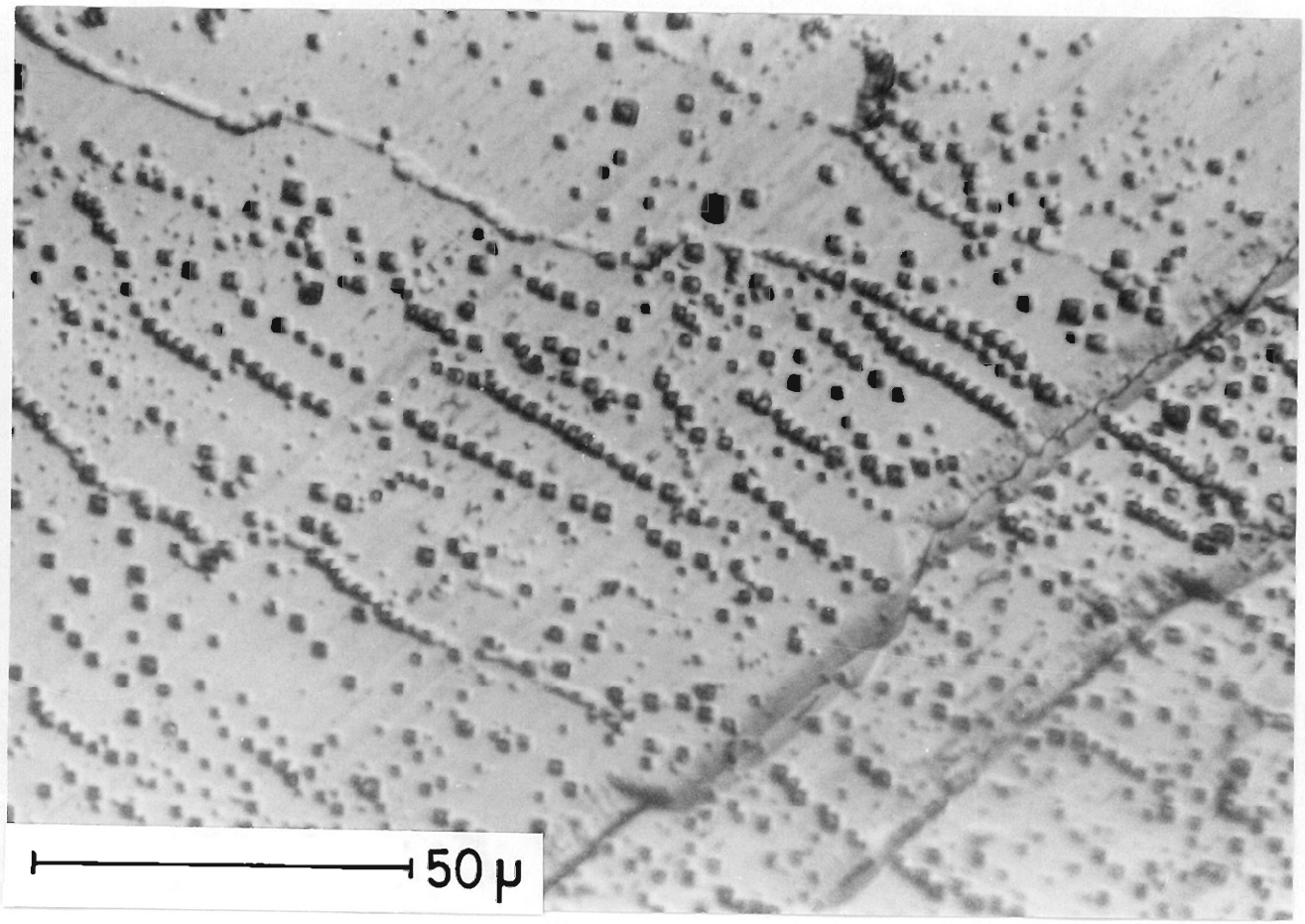

Fig. 26 An etch pit pattern in the (100) cleavage plane of HfC crystal.

Figure 26 shows the etch pit pattern on the (100) cleavage plane. The etch pit density is estimated to be 10^7 /cm^2.

3) Conclusion

HfC single crystal rods with 6 cm length and 0.9 cm diameter have been prepared by controlling the chemical compositions of the feed rod and the initial molten zone(a modified zone leveling method). The chemical composition(C/Hf(Zr)) of crystal was 0.956-0.977. The impurities were refined by evaporation, depending on their vapor pressures. The residual impurities were Zr and W. Therefore, the starting material without Zr and W must be used to prepare the high purity crystal.

2-4-4 VC_x

VC_x has two kinds of superstructures(V_8C_7 and V_6C_5) due to long range ordering of carbon defect. It is well-known that the defect ordering strongly influences the properties[12]. Therefore, the single phase VC_x crystals with homogeneous chemical compositions are indispensabale to understanding of the properties.

VC_x crystals were already prepared by a floating zone technique[6,33,40]. Precht et al.[6] indicated that the crystal rod prepared by a usual floating zone method has a composition gradient along the growth direction. Up to date, the crystal rods with uniform chemical compositions have not been prepared yet. In this section, the solidus-liquidus relation and the compositional change due to evaporation are examined under growth conditions, and further the compositional regions where V_8C_7, V_6C_5 and VC_x phases exist as single phases are examined by X-ray powder diffraction method. On the basis of the above three results, the single phase crystals with homogeneous chemical compositions are prepared by a modified zone leveling method[41].

1) Preparation of the single phase crystals

1-2) Determination of the composition diagram

In order to determine the solidus-liquidus relationship and the compositional change due to evaporation under the growth conditions, the following experiment was carried out. The

crystal rods were prepared using feed rods with various chemical compositions(C/V= 0.90, 0.86, 0.85, 0.77, 0.71) by a usual floating zone method. Several parts of the obtained crystal rods were analyzed. The results are listed in Table 18. The carbon content in the crystal rod increased as the zone passes in the carbon rich region(C/V >0.84) and decreased in the carbon poor region(C/V < 0.84). A rod of composition $VC_{0.85}$ exhibited little variation in chemical composition. This result indicates that the chemical composition with maximum melting point is about C/V=0.84. This value is consistent with that reported by Adelsberg et al.[42]. The last example listed in Table 18 was carried out in order to determine the VC-C eutectic composition. A rod with C/V=0.90 where VC and free carbon coexist in the phase diagram[42,43] was zone-passed. It is found that a steady state has been reached because the final part(Cry-F) has the same chemical composition as that of the feed rod(S). Therefore, the zone composition is equal to the VC-C eutectic composition, which is C/V=0.98. This value does not agree with that of Adelsberg et al.[42], but that of Rudy et al.[43].

A pair of the compositions of an initial part(cry-I) and a feed rod(S), and another pair of those of a final part(cry-F) and a zone(M) correspond to the solidus-liquidus relation, as shown in Fig. 3. Further, the compositional change due to evaporation can be obtained from the results of the chemical compositions in the final part(Cry-F) and the feed rod(S) because the zone pass distance(about 6 cm) is enough long to

Table 18 Carbon content and chemical compositions of VC_x crystals prepared by a usual floating zone method; TC is total carbon; Cry-I, -M and -F are the initial, middle and final parts of the crystal rod, respectively; S is the feed rod; M is the molten zone.

	TC (wt%)	Composition (C/V)
Cry-I	15.84	0.798
Cry-F	14.59	0.724
M	10.42	0.493
S	14.41	0.714
Cry-I	16.26	0.824
Cry-F	15.44	0.774
M	12.97	0.632
S	15.29	0.766
Cry-I	16.68	0.849
Cry-F	16.78	0.855
M	16.96	0.866
S	16.73	0.852
Cry-I	16.79	0.856
Cry-F	16.96	0.866
M	17.94	0.927
S	16.89	0.862
Cry-I	16.93	0.864
Cry-F	17.52	0.901
M	18.84	0.985
S	17.49	0.899

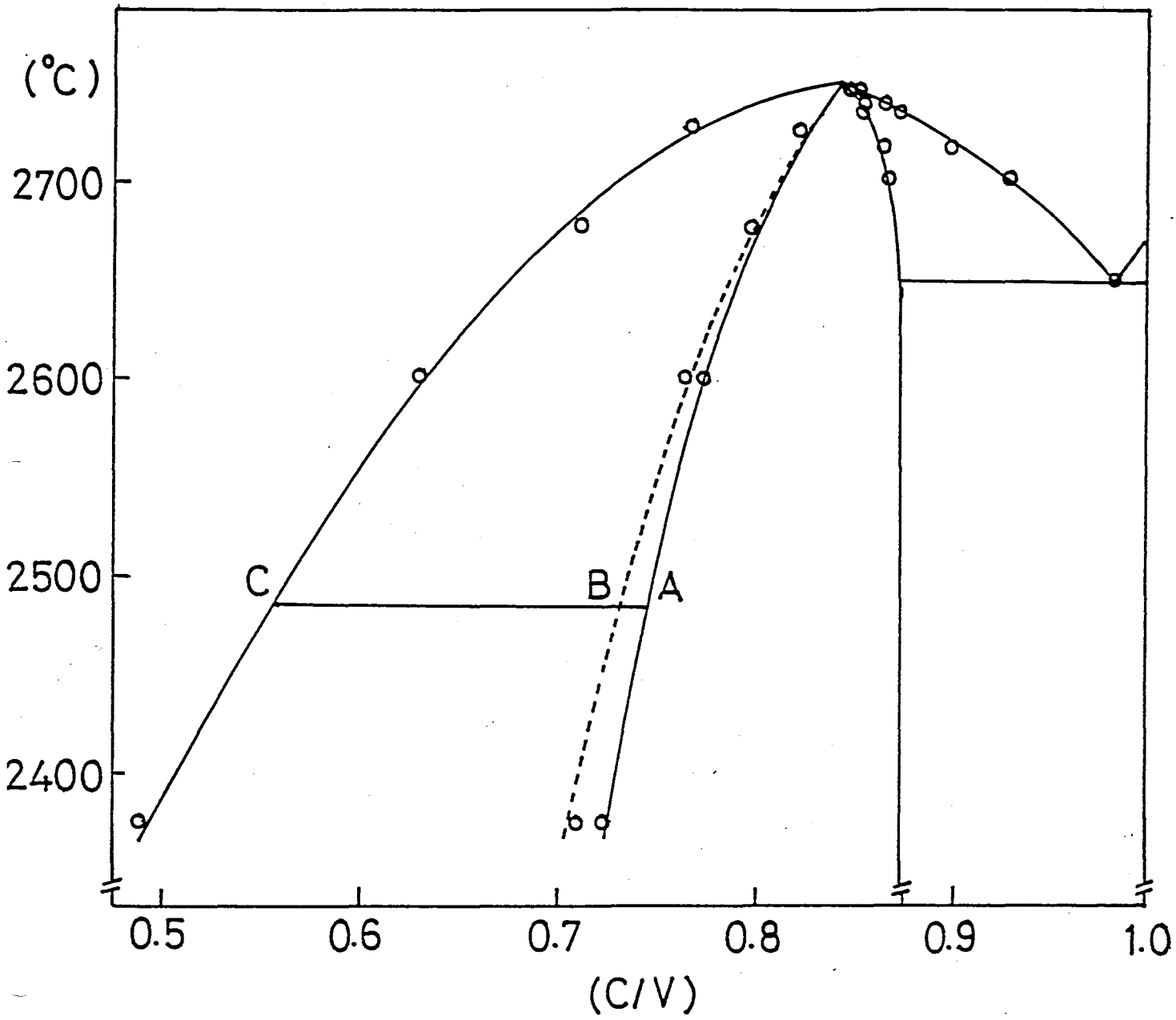

Fig. 27 A composition diagram of VC. The ordinate is referred by that of the phase diagram of Adelsberg et al.[42].

reach the stady state. If the chemical composition is not changed due to evaporation, the final part(Cry-F) ought to have the same chemical composition as that of the feed rod(S). In the carbon rich region, the chemical composition did not change due to evaporation, as described by Precht et al.[6]. However, in the carbon poor composition, the composition changes to be about 1 at% carbon richer due to evaporation. These results are summerized in Fig. 27. The ordinate is referred by that of the phase diagram of Adelsberg et al.[42]. The solid lines show the solidus and liquidus lines. The dashed line shows the feed rod composition. This diagram shows that the crystal rod with a composition A can be prepared by using a feed rod with B and an initial molten zone with C.

1-2) Determination of the compositional regions of single phases

The existence of two kinds of superstructures(V_8C_7 and V_6C_5) due to ordering of carbon defects are known in the vanadium carbide. The compositional regions where they exist as single phases were examined using the prepared crystals by X-ray powder diffraction method. The superstructures can be observed by the powder diffraction method because metal lattice is slightly disdorted by the carbon defect ordering. Two ordered phases, V_8C_7 and V_6C_5, and one disordered phase of VC_x were found to exist as single phases in the nonstoichiometric compositional range. The X-ray powder patterns of V_8C_7 and V_6C_5 are complex though they can be indexed as simple cubic[44] and pseudo-hexagonal

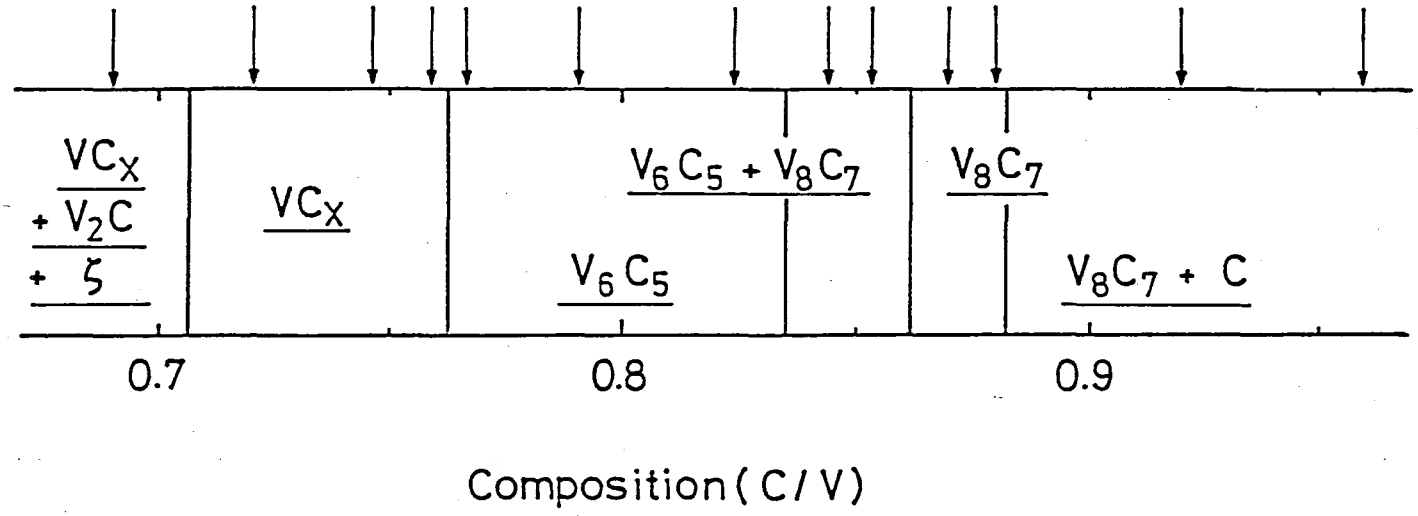

Fig. 28 Compositional regions of V_8C_7, V_6C_5 and VC_x phases. The arrows indicate the examined compositions.

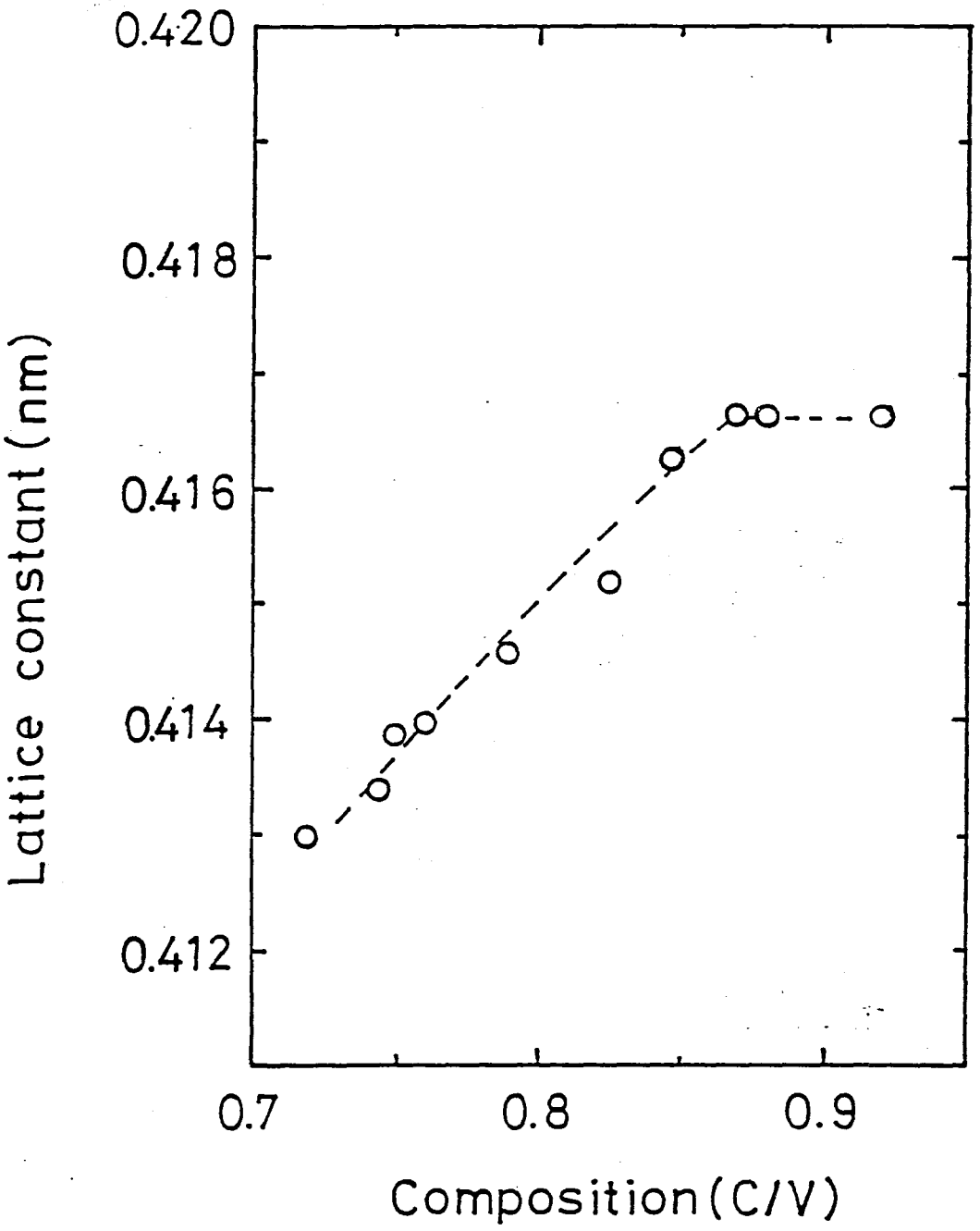

Fig. 29 Lattice constant of VC as a function of chemical composition. A dash line shows that estimated by Toth[12].

symmetry[45,46], respectively. The compositional regions for both phases were determined from the results of X-ray diffraction peaks diffracted in the low angle due to long range ordering. The composition boundary between the V_6C_5 and VC_x phases was determined from the results of X-ray diffraction patterns that the strong peaks of V_6C_5 are split, but not split and there are no peaks in the low angle due to defect ordering for VC_x phase. The results are shown in Fig. 28. The compositional regions of V_8C_7, V_6C_5 and VC_x were determined to be C/V=0.88-0.86, 0.84-0.76 and 0.76-0.71, respectively. These results are almost consistent with that of reported by Billingham et al.[47].

Figure 29 shows the lattice constant of VC as a function of composition. In this figure, the lattice constants of V_8C_7 phase are ploted as half of the values and those of the V_6C_5 phase are calculated as the lattice constants of the NaCl-type structure because the structure of V_6C_5 phase deviates only slightly from a NaCl structure. The composition-lattice constant relationship was already estimated by Toth[12]. The result reported by Toth is also shown as a dashed line in Fig. 29. The present result agreed well with the estimated one.

1-3) Preparation of the V_8C_7, V_6C_5 and VC_x crystals

Fig.28 suggests that V_8C_7, V_6C_5 and VC_x phases exist as single phases in the compositional regions of C/V=0.88-0.86, 0.84-0.76 and 0.76-0.71, respectively. Therefore, we prepared $VC_{0.87}$, $VC_{0.80}$ and $VC_{0.73}$ crystal rods.

In order to prepare the $VC_{0.87}$(V_8C_7 phase) crystal, a feed rod with C/V=0.87 and an initial molten zone with C/V=0.96 were used. An initial molten zone was formed by putting a certain amount of graphite disk between the upper and lower sintered rods and melting the part around the disk. The obtained crystal rod has a constant chemical composition along the growth direction, such as C/V=0.881, 0.872 and 0.873, as listed in Table 19. In addition, in order to examine the compositional change along the radial direction, a 5 x 5 x 15 mm^3 block was cut from the central part of the crystal. The block and the rest(peripheral part) were analyzed. The chemical compositions of the central and peripheral parts were C/V=0.875 and 0.876, respectively. Therefore, the obtained crystal rod is found to have the homogeneous chemical composition within 1 at%.

The $VC_{0.80}$ crystal(V_6C_5 phase) was prepared using a feed rod with C/V=0.79 and an initial molten zone with C/V=0.75. The initial molten zone was formed by melting the sintered rod with C/V=0.75. The analytical results are listed in Table 20. The crystal rod has a homogeneous chemical composition along the growth direction, such as C/V=0.803, 0.804 and 0.801.

The VC_x phase crystal with C/V=0.73 was prepared using a feed rod with C/V=0.68 and an initial molten zone with C/V=0.54. The molten zone was formed by putting a small amount of V metal disk between the upper and lower sintered rods. Table 20 also shows the analytical results. The difference in chemical composition between the feed rod(C/V=0.68) and the crystal(

Table 19 Results of carbon analysis of the V_8C_7 crystal rod; FC and CC are free and combined carbon, respectively; Cry-M, -C and -P are the middle, central and peripheral parts of the crystal rod, respectively.

$VC_{0.87}$ (V_8C_7 phase)

	TC (wt%)	FC (wt%)	CC (wt%)	Composition (C/V)
Cry-I	17.20	0.00	17.20	0.881
Cry-M	17.06	0.00	17.06	0.872
Cry-F	17.07	0.00	17.07	0.873
M	18.52			0.964
S	17.16			0.879
Cry-C	17.10			0.875
Cry-P	17.12			0.876

Table 20 Results of carbon analysis of the V_6C_5 and $VC_{0.73}$ crystal rods.

	$VC_{0.80}$ (V_6C_5 phase)		$VC_{0.73}$ (VC_x phase)	
	TC (wt%)	Composition C/V	TC (wt%)	Composition (C/V)
Cry-I	15.91	0.803	14.76	0.734
Cry-M	15.94	0.804	14.64	0.727
Cry-F	15.89	0.801	14.47	0.718
M	15.03	0.750	11.21	0.535
S	15.76	0.794	13.84	0.681

C/V=0.72-0.73) arose from evaporation. The evaporation product consisted of V_2C and unknown phase. Vanadium metal does not evaporate from a molten zone. This is a charactristic of the 5a carbides. The $VC_{0.73}$ crystal has the homogeneous chemical composition within about 1 at%.

2) Impurity refining

Oxygen and nitrogen impurity content in the V_8C_7, V_6C_5 and VC_x crystals and their feed rods are listed in Table 21. The crystals contained less than 200 ppm oxygen, which does not depend on a chemical composition of crystal. On the other hand, the nitrogen content in the V_8C_7 and V_6C_5 crystals were less than 50 ppm and 340 ppm, respectively. VC_x crystal had much nitrogen impuritiy(0.6 wt%).

Metal impurities, which are heavier than Ti, in the crystal($VC_{0.87}$), starting material, feed rod and evaporation product were analyzed by X-ray fluorescence spectroscopy. All detectable impurities are listed in Table 22. The main impurities in the starting material are W and Mo metals whose content are 400 ppm. Each peak height was nomarized by the V K peak. Comparing the metal impurities of the starting material with those of the feed sintered rod, Zn was perfectly refined. Fe, Co, Cr and Ni were found to be refined partially during sintering. The other impurities are not refined at all.

Each impurity peak height in the feed rod(Feed) was compared with that in the evaporation product(Evap). The ratio

Table 21 Oxygen and nitrogen impurities in crystals and sintered rods.

		$VC_{0.87}(V_8C_7)$	$VC_{0.76}(V_6C_5)$	$VC_{0.73}(VC_x)$
Oxygen	S	0.048	0.097	0.21
	Cry	0.018	0.016	0.015
Nitrogen	S	< 0.005	0.011	0.18
	Cry	< 0.005	0.034	0.60

Table 22 Impurities in the crystal($VC_{0.87}$), starting material, feed rod and evaporation product analyzed by X-ray fluorescence spectroscopy(peak heights normalized by V K_{α} peak height).

	Crystal	Starting material	Feed rod (Feed)	Evaporation product(Evap.)	Ratio (Evap./Feed)
Ti(K_{α})	0.5	0.5	0.5	-	<1
Cr(K_{β})	-	-	-	5	>10
Fe(K_{α})	-	2	1	64	64
Co(K_{α})	-	0.5	-	15.5	>31
Ni(K_{α})	-	0.5	-	16	>32
Zn(K_{α})	-	5	-	0.5	>1
Mo(K_{α})	33	34	33	0.5	0.03
W (L_{α_1})	1.5	2	2	-	<0.25

(Evap/Feed) of each impurity peak is tabulated in Table 22. The ratio means the evaporation rate ratio of impurity to VC. When an impurity is entirely refined by evaporation, the ratio becomes maximum. In the case of the present preparation condition, about 1.6 wt% of VC is lost due to evaporation. The maximum value of the ratio is about 63(=1/0.016). Cr, Fe, Co and Ni were found to be entirely refined by evaporation during a zone pass. The values of ratio in Ti, Mo and W metals show that their evaporation rates are lower than that of VC. Therefore, these impurities can not be refined by evaporation at all. In addition, it is not expected that these impurities are refined by zone refining because they form the solid solution with VC and their distribution coefficents are not far less than unity. Therefore, these impurity content in the crystal depend on the impurity content in the starting material. In order to prepare the high purity VC crystal, the starting material should contain no impurities which have low vapor pressures.

3) Appearence, cross section and etch pit pattern

An as-grown crystal rod of $VC_{0.87}$(V_8C_7 phase) is shown in Fig. 30. The size of crystal rod is 9 mm in diameter and about 6 cm long. Fig. 31(a) and (b) show the longitudinal cross sections of the initial and final parts of a $VC_{0.87}$ crystal rod, respectively. The initial part consists of several grains. However, as the molten zone passed, the central grain grew larger, and then the central part became a single crystal after a

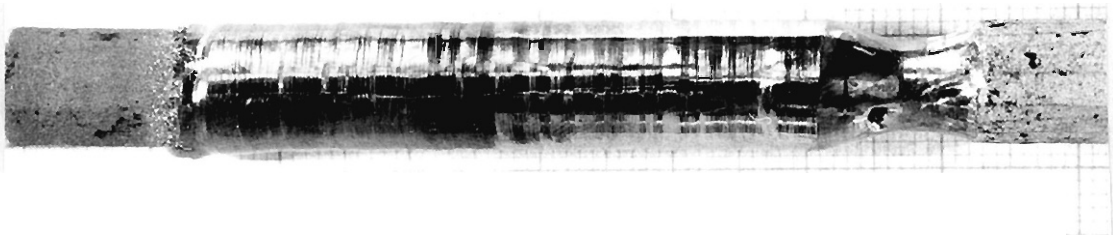

Fig. 30 $VC_{0.87}$(V_8C_7 phase) as-grown crystal rod.

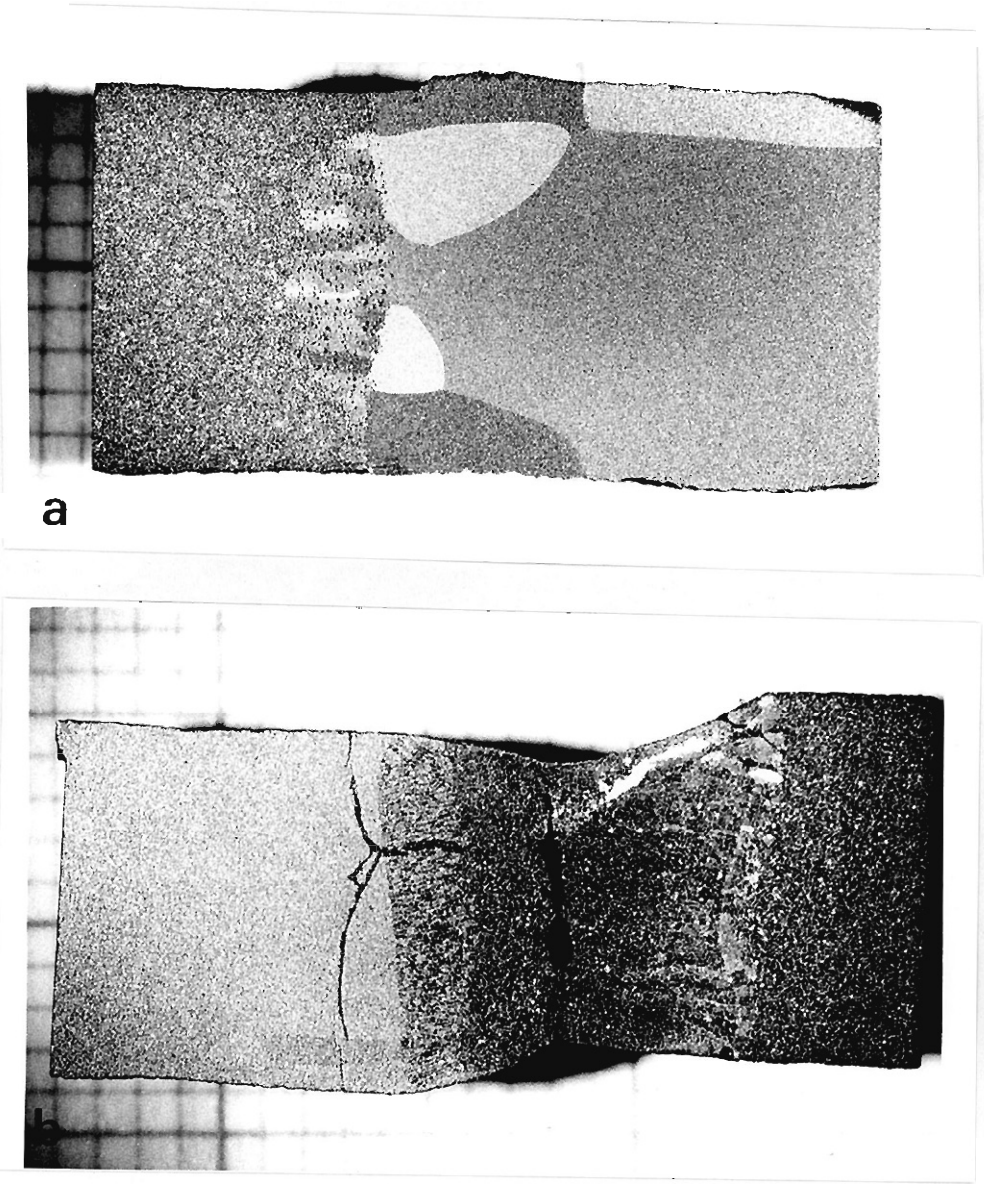

Fig. 31 Longitudinal cross sections of V_8C_7 crystal rod: (a)initial part and (b)final part.

1 cm zone pass. Fig. 31(b) shows the final part of the crystal rod. The cracks might be formed by decreasing the heating power too rapidly at the end of the zone pass. The crystal rods often had cracks, especially, when the crystal has a carbon rich composition, at the beginning of the growth. However, the crystals were almost prevented from cracking by a stable zone pass and a low growth rate(5 mm/hr).

The growth directions of the eleven $VC_{0.87}$ crystal rods were examined by a back-reflection Laue method. Fig. 32 shows the growth directions on a part of a Wulff net. It is apparent that $VC_{0.87}$ crystal has no preferred growth direction.

The etch pits on the (100) clevage plane of V_8C_7 crystal are shown in Fig. 33(a) and (b). Two kinds of etch pits were found: the large, flat bottomed pits and the small pits. The large pits appear at the first stage of etching, and the small pits appear at the next stage. The large ones, which were also observed in the TiC crystal, are formed by the existence of carbon inclusions[36]. The etch pit density depends on the place of the crystal rod. The densities were 10^3 and 10^4 /cm^2 at the central and peripheral parts, respectively, as shown in Fig. 33. In addition, the large etch pits decrease with decreasing the carbon content in the crystal. The etch pit density in the V_6C_5 crystal was less than 10^2 /cm^2. The small pits correspond to the dislocations and its density was 10^6 /cm^2, which does not depend on the place or chemical composition of crystal.

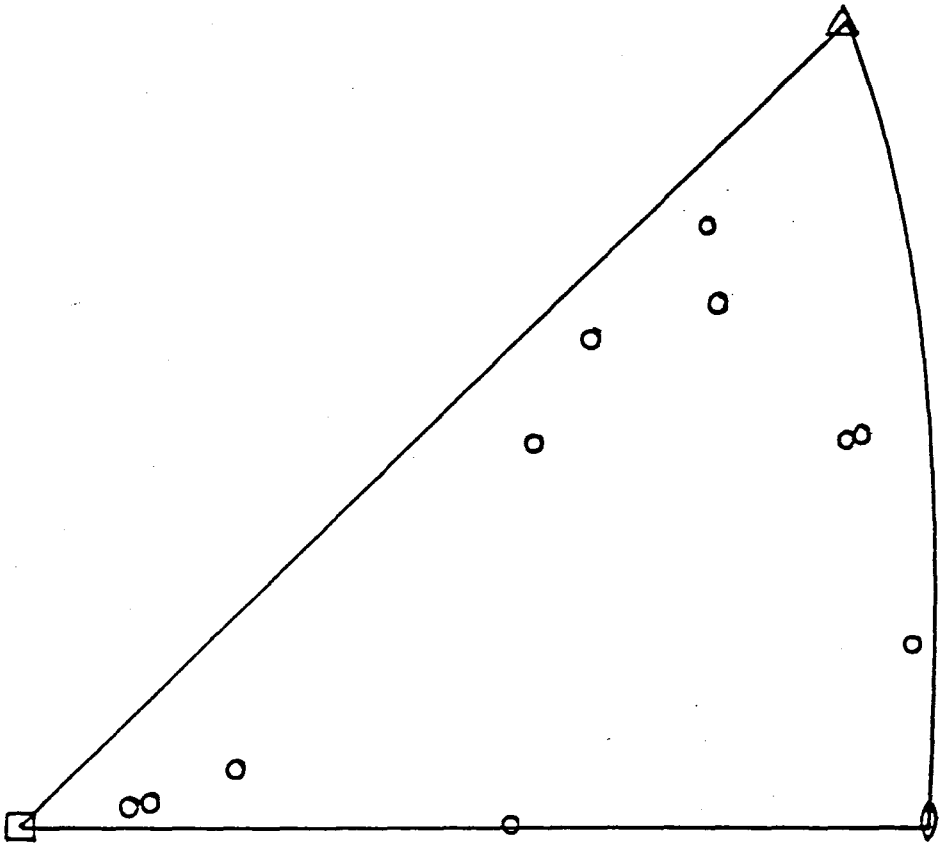

Fig. 32 Cyclographic projections onto a Wulff net of the growth directions of V_8C_7 crystal rods.

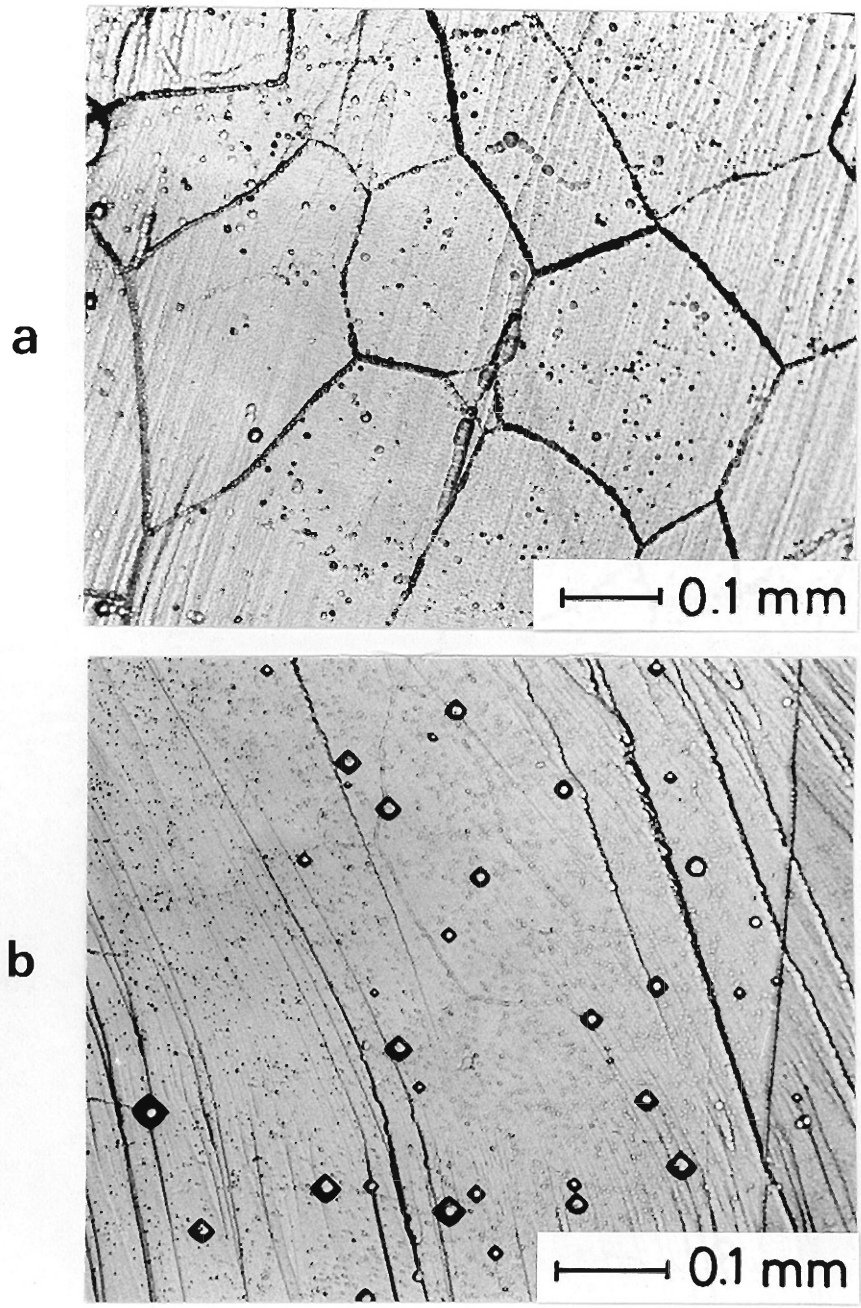

Fig. 33 Etching pattern of the (100) cleavage plane of V_8C_7 crystal. (a)central part and (b)periphral part.

4) Conclution

From the results of the solidus-liquidus relation, the compositional change due to evaporation and determination of the chemical compositioal ranges where V_8C_7, V_6C_5 and VC_x phases exist as single phases, the single phase crystals of V_8C_7, V_6C_5 and VC_x were prepared. The size of crystal rods were 6 cm long and 0.9-1.0 cm in diameter. Cracks were hardly formed in the crystal. The homogeneity of the chemical composition in crystal was within about 1 at%. It was found that impurities are refined by evaporation, depending on the vapor pressures of impurities. Therefore, selecting a commercial carbide powder with low content of Mo and W impurities(400 ppm), the high purity crystals were prepared.

2-4-5 NbC_x

NbC crystals were prepared by a floating zone technique by several workers[33,48]. The large single crystals were not prepared yet. The main problem is that a stable zone pass could not be carried out because of its high melting point, as shown in Fig. 34. Consequently, a large single crystal without cracks have not been grown yet. In addition, no attention was paid to the preparation of the crystals with controlled chemical compositions. In this chapter, the large single crystals with the desired chemical compositions and crack free are prepared over the entire composition range[49].

1) Preparation of crystals with desired chemical compositions

When the growth temperature is high, like in the case of NbC_x, many preliminary experiments must be carried out in order to find out the best growth conditions(the helium pressure, the growth rate, the coil configuration(especially the inside diameter) and so on). It was found from the present experimental results that 10^6 Pa of helium gas pressure and 1.25 cm/h of growth rate are the best conditions. The inside diameter of the work coil must be determined in mm unit when the evaporation is violent. The work coil with too small diameter causes the touch between the molten zone and the evaporation product deposited on the coil. The work coil with too large diameter makes the heating power higher. In the present case, when the carbon rich crystal is prepared, the inside diameter of the work coil became

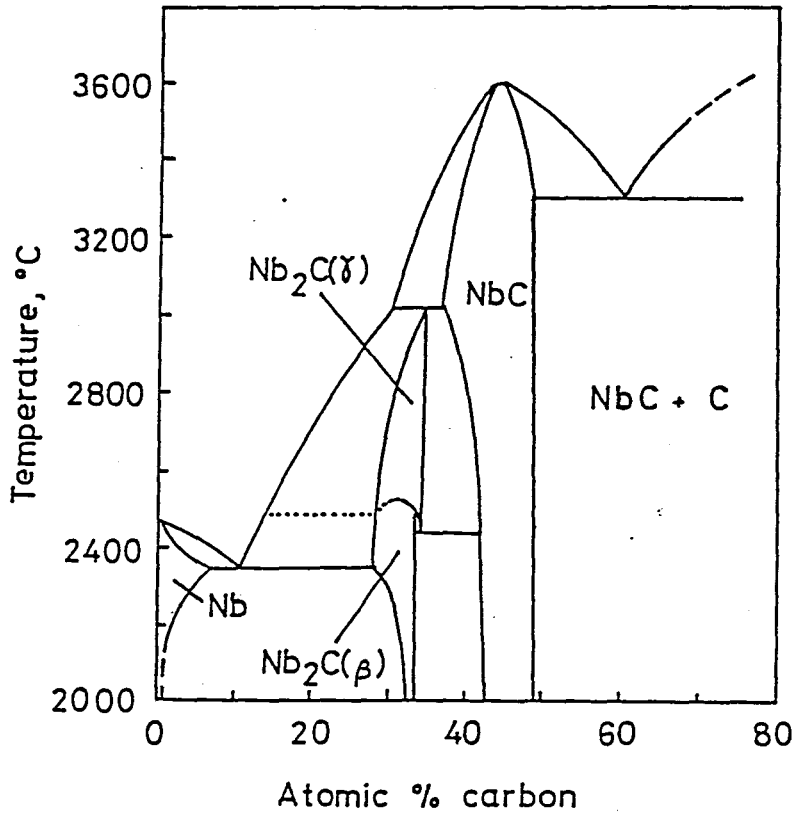

Fig. 34 Phase diagram of Nb-NbC system[12]

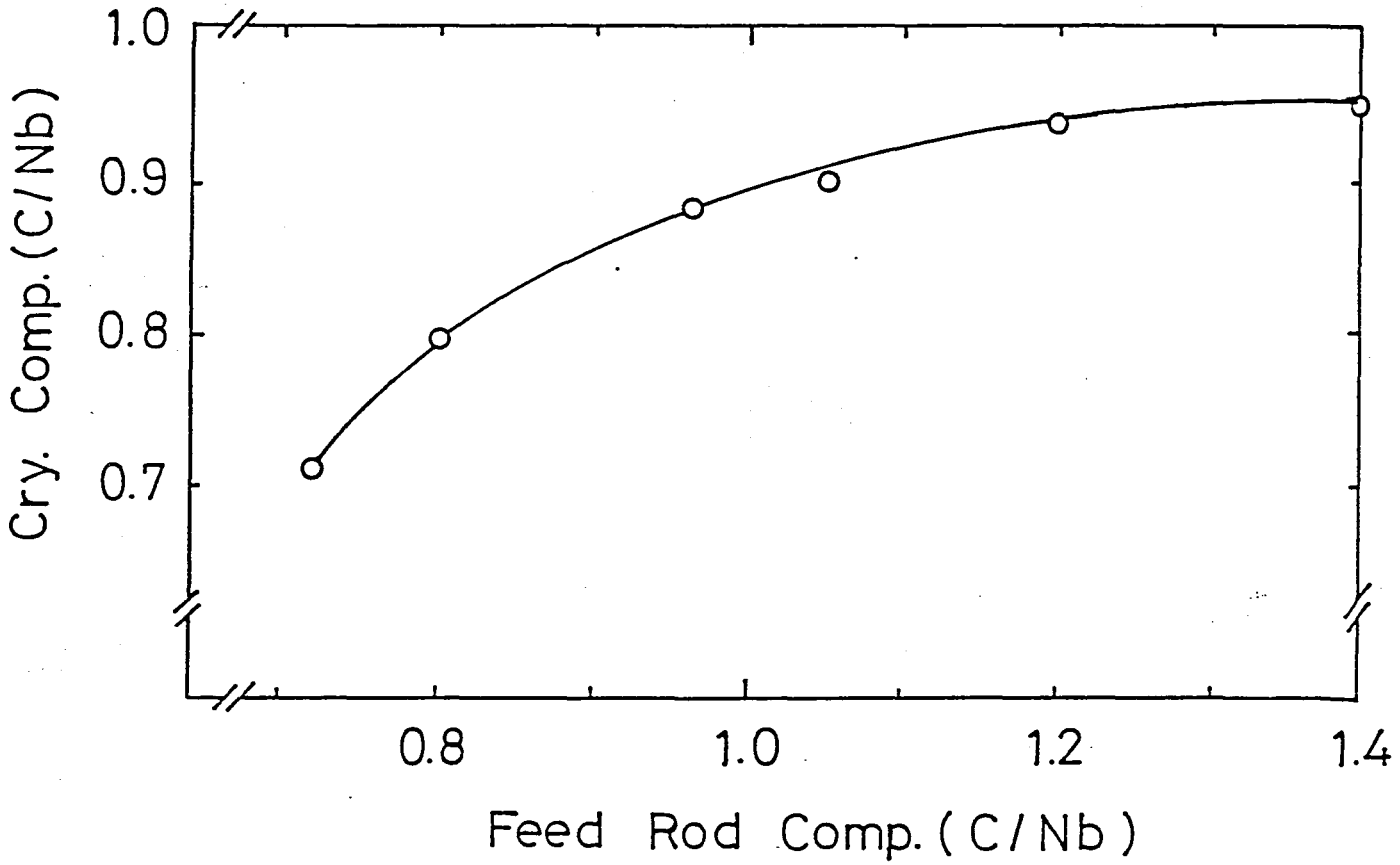

Fig. 35 Relationship in chemical composition between the feed rod and the crystal.

an important factor. It was found that the crystals were easily prepared using a work coil with 16 mm in inside diameter.

In order to prepare a crystal with the desired chemical composition, the solidus-liquidus relation and the compositional change due to evaporation must be determined. The former was obtained from the phase diagram(Fig. 34). The initial molten zone composition was controlled by putting a carbon or Nb metal disk between the upper and lower sintered rods, as shown in Fig. 4. The latter was examined by the following experiment. The crystal rods 4-5 cm in length were prepared using feed rods with various chemical compositions. In this case, the zone leveling condition has already reached after a 4-5 cm zone pass. The feed rod and the final part of the crystal rod were analyzed. The results are shown in Fig. 35. The differences in chemical composition between the crystal and the feed rod are caused by evaporation. The feed rod composition was then determined from the experimental results mentioned above.

In order to prepare $NbC_{0.95}$ crystal, a feed rod with C/Nb=1.20 was used on the basis of the results shown in Fig. 35. A carbon disk with 0.12 g weight was used to form a molten zone with chemical compostion C/Nb=1.24. The obtained crystal rod had no free carbon and a nearly constant chemical composition along the growth direction, such as C/Nb=0.929, 0.950 and 0.950, as listed in Table 23. The initial part of the crystal rod had a lower carbon content than the middle and final parts. This result is due to the chemical composition of the initial molten

Table 23 Carbon and chemical compositions in the $NbC_{0.95}$ crystal rod; S' is the feed rod just above the zone.

	TC (wt%)	FC (wt%)	CC (wt%)	Ta/Nb(Ta)	Composition C/Nb(Ta)
Cry-I	10.57	0.00	10.57	0.017	0.929
Cry-M	10.79	0.00	10.79	0.016	0.950
Cry-F	10.79	0.00	10.79	0.016	0.950
M	13.70			0.010	1.24
S'	11.90			0.016	1.06
S	13.30			0.016	1.20

zone was C/Nb=1.15, which was different from the ideal chemical composition of C/Nb=1.24. It is difficult to form the initial molten zone with the desired chemical composition because the chemical composition of the initial molten zone depends on the time required for the zone pass to start due to violent evaporation. However, in the present method, even though the initial zone composition changed from the liquidus composition, the zone leveling condition was soon reached because the initial molten zone had a near-liquidus composition. Therefore, the middle and final parts of the crystal rod had the desired chemical composition. The feed rod(S') just above the molten zone has less carbon(C/Nb=1.06) than the feed rod(S)(C/Nb=1.20). It was found that the three quaters of the carbon added to the feed rod had already sublimed before the feed rod melted into the molten zone. Most of the evaporation product was carbon. The weight of NbC was about 20 % in the evaporation product.

In addition, the compositional change along the radial direction of the crystal rod was examined. The sample was the final part of the crystal rod which was prepared by the same way as mentioned above. A 5 x 5 x 15 mm^3 piece was cut from the central part of the crystal rod(9 mm diameter) by a spark corrosion cutter. The chemical compositions of the central part and the remainder(peipheral part) were analyzed. The chemical compositions of central part and peripheral parts were C/Nb(Ta)=0.955 and 0.956, respectively. The cetral and

peripheral parts have the same chemical composition within the limits of errors. As seen in the experimental results listed in Table 23, it is found that a crystal with the desired chemical compostion can be prepared within an error of 1 at%.

A $NbC_{0.89}$ crystal was prepared by using the initial molten zone with C/Nb=1.0 and feed rod with C/Nb=0.98. The analytical results are listed in Table 24(a). The crystal rod had a constant chemical composition along the growth direction, such as C/Nb=0.881, 0.888 and 0.893. The difference in chemical composition between the feed rod and crystal was 9 at%(= 0.98 - 0.89), which is explained by carbon evaporation.

Table 24(b) shows the analytical result of the $NbC_{0.79}$ crystal rod. The niobium metal pellet(0.15 g) was put between the upper and lower sintered rods, and then an initial molten zone was formed. The chemical compositions(C/Nb) of cry-I, -M and -F were 0.798, 0.794 and 0.789, respectively. A composition change did not occure due to evaporation because the crystal and feed rod had the same chemical composition. This result is well explained by a decrease of the carbon content in the molten zone because carbon has the highest vapor pressure among NbC, Nb and C. The amount of the evaporation product was small, compared with those of $NbC_{0.95}$ and $NbC_{0.89}$.

The lattice constants of the $NbC_{0.95}$, $NbC_{0.89}$ and $NbC_{0.79}$ crystals were determined to be 0.4468, 0.44628 and 0.44488 nm, respectively. These results were compared with the reported expression[50]:

Table 24 Carbon and chemical compositions in the $NbC_{0.89}$ and $NbC_{0.79}$ crystal rods

	TC (wt%)	FC (wt%)	CC (wt%)	Ta/Nb(Ta)	Composition C/Nb(Ta)
(a) $NbC_{0.89}$					
Cry-I	10.09	0.01	10.08	0.017	0.881
Cry-M	10.16	0.00	10.16	0.016	0.888
Cry-F	10.21	0.00	10.21	0.016	0.893
M	11.40			0.012	1.01
S'	10.70			0.016	0.94
S	11.10			0.016	0.98
(b) $NbC_{0.79}$					
Cry-I	9.23	0.00	9.23	0.015	0.798
Cry-M	9.21	0.00	9.21	0.013	0.794
Cry-F	9.15	0.00	9.15	0.013	0.789
M	7.30			0.012	0.62
S'	8.97			0.013	0.77
S	9.19			0.013	0.79

$a = 0.409847 + 0.071820(C/Nb) - 0.034570(C/Nb)^2$.

The prepared crystals have little smaller lattice constants than the calulated ones, namely by about 0.0001 nm. Oxygen and nitrogen impurities play a role to increase the lattice constants in NbC_x. Therefore, the present results suggested that the purity of the prepared crystals is higher than that of already reported.

2) Impurities

Oxygen and nitrogen imputrity content in the crystals and feed rods are listed in Table 25. The crystals contained less than 500 ppm oxygen and less than 100-200 ppm nitrogen over the entire compositional range. These impurity levels were almost the same as those in the other 5a group carbide(TaC)[51]. The impurity content in the crystals depended on those in the feed rod. Therefore, it is necessary to use a feed rod having a low oxygen and nitrogen contents in order to prepare a pure crystal.

Metal impurities in the crystal, starting material, feed rod and evaporation product were examined by X-ray fluorescence analysis. All detectable impurities are listed in Table 26. Only Ta is detected in the crystal. The other impurities is less than 100 ppm. The Ta impurity, which is not refined by evaporation at all, has a distribution coefficient(k) higher than unity, as seen in Table 23 and 24. Therefore, Ta impurity is not refined by zone refining, either, as shown in Fig. 51. In order to prepare the high purity crystal, the starting material

Table 25 Oxygen and nitrogen impurities in $NbC_{0.95}$, $NbC_{0.89}$ and $NbC_{0.79}$ crystals and their feed rods(wt%).

		$NbC_{0.95}$	$NbC_{0.89}$	$NbC_{0.79}$
Oxygen	S	0.140	0.110	0.099
	Cry	0.046	0.048	0.028
Nitrogen	S	0.007	0.006	0.074
	Cry	0.009	0.005	0.002

Table 26 Impurities in the crystal($NbC_{0.95}$), starting material, feed rod and evaporation product analyzed by X-ray fluorescence spectroscopy(peak heights normalized by Nb $K\beta_{1,3}$ peak height).

	Crystal	Starting material	Feed rod (Feed)	Evaporation product(Evap.)	Ratio (Evap./Feed)
Ti Kα	-	-	-	26	> 52
V Kα	-	-	-	1	> 2
Cr Kα	-	1	0.5	188	376
Mn Kα	-	-	-	4	> 8
Fe Kα	-	1.5	-	204	408
Co Kα	-	-	-	3	> 6
Ni Kα	-	1	-	8	16
Zr Kα	-	-	-	15	> 30
Ta $L\alpha_1$	120	120	120	7	0.1

A dash means less than 0.5.

without Ta must be chosen.

3)Appearance, cross section and etch pit pattern

An as-grown crystal rod of $NbC_{0.95}$ is shown in Fig. 36. The size of crystal rod is 9 mm in diameter and 6 cm long. The sintered rod(S') just above the molten zone is found to lose carbon, and to shrink because of the low density of the sintered rod. The crystal rod surface was not smooth, although the crystal rod was prepared under a constant heating power. This result is thought to be due to a consequence of the contact between the molten zone and the evaporation product deposied n the work coil.

The growth directions of the seven $NbC_{0.95}$ crystal rods were examined by a back-reflection Laue method. Figure 37 shows the results of growth directions on a part of a Wulff net. It is apparent that $NbC_{0.95}$ has no prefered growth direction.

The longitudinal cross sections of the initial and final parts of the crystal rod is shown in Fig. 38. The initial part (Fig. 38(a)) consists of several grains. However, as the zone was passed, the central grain grows larger and the central part becomes single crystal after a 2 cm zone pass. Figure 38(b) shows the final part of the crystal rod, the molten zone and the feed rod. The crystal-zone interface is convex toward the zone at the central part, and nearly flat at both ends. The interface shape sometimes becomes concave at the end of the interface, as shown in Fig. 38(b). In this situation, a new grain starts to

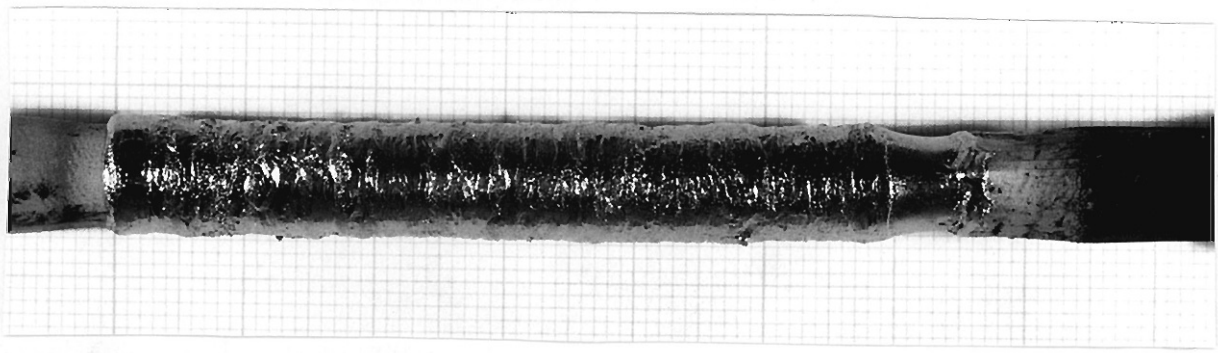

Fig. 36 As-grown $NbC_{0.95}$ crystal rod with 6 cm length and 9 mm diameter.

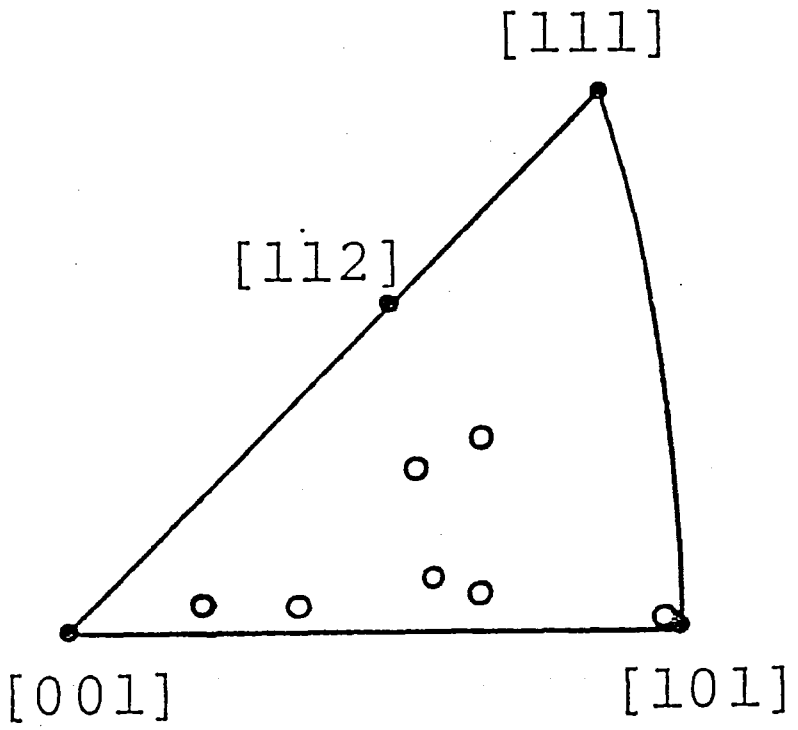

Fig. 37 Cyclographic projections onto a Wulff net of growth directions of $NbC_{0.95}$ single crystals.

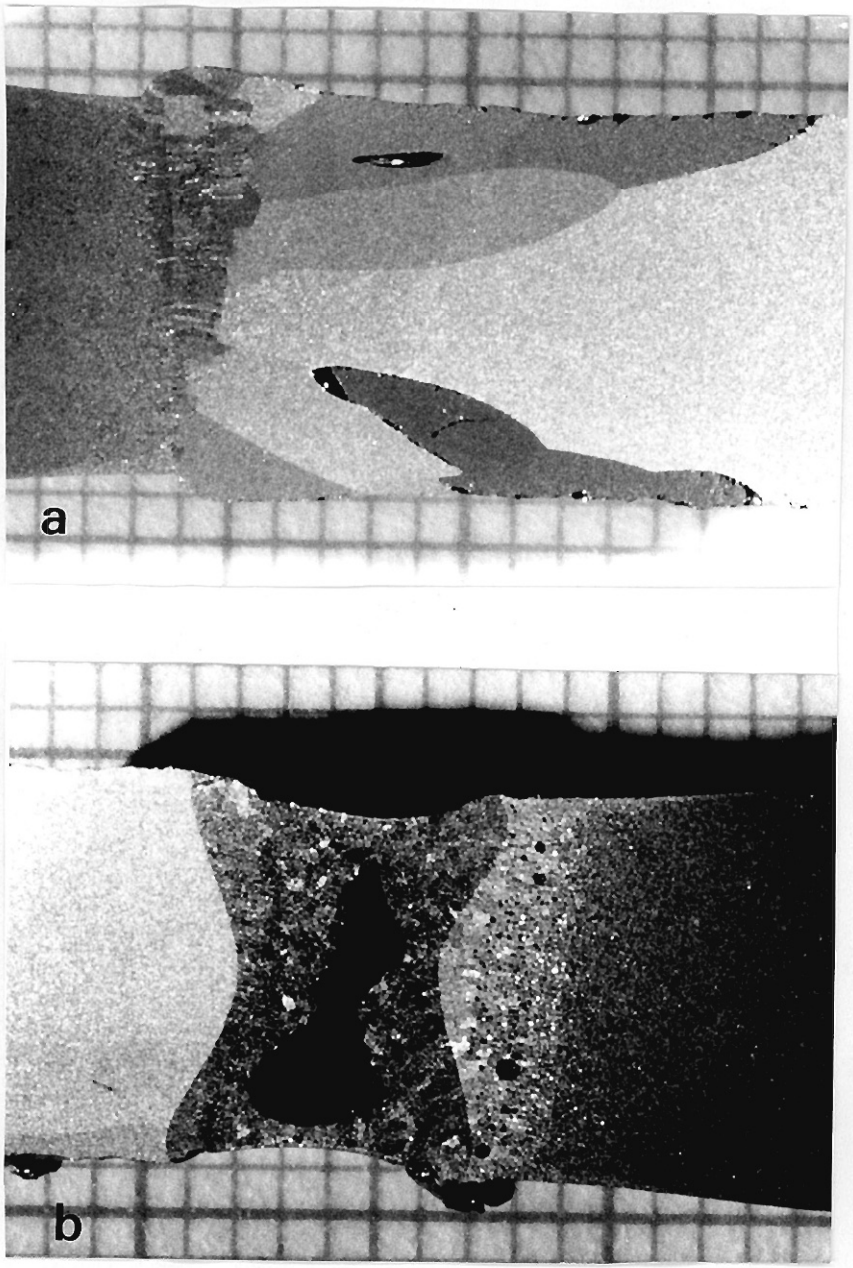

Fig. 38 Longitudinal cross sections of (a) the initial part, (b) the final part and the zone and of the $NbC_{0.95}$ crystal rod.

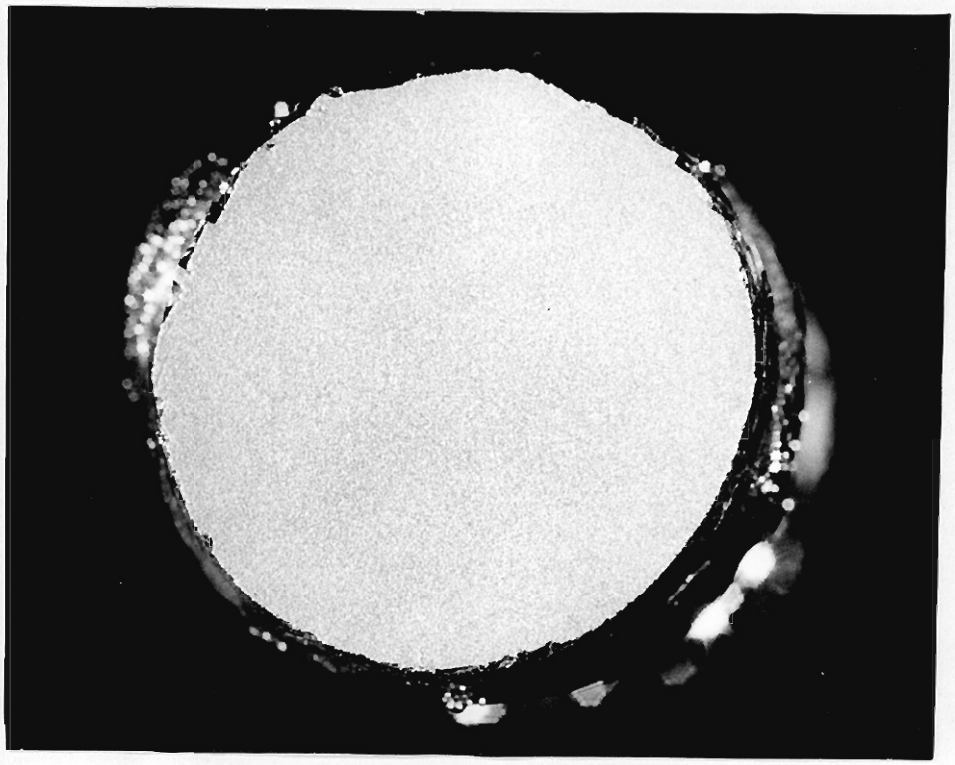

Fig. 39 Cross section of $NbC_{0.95}$ crystal rod.

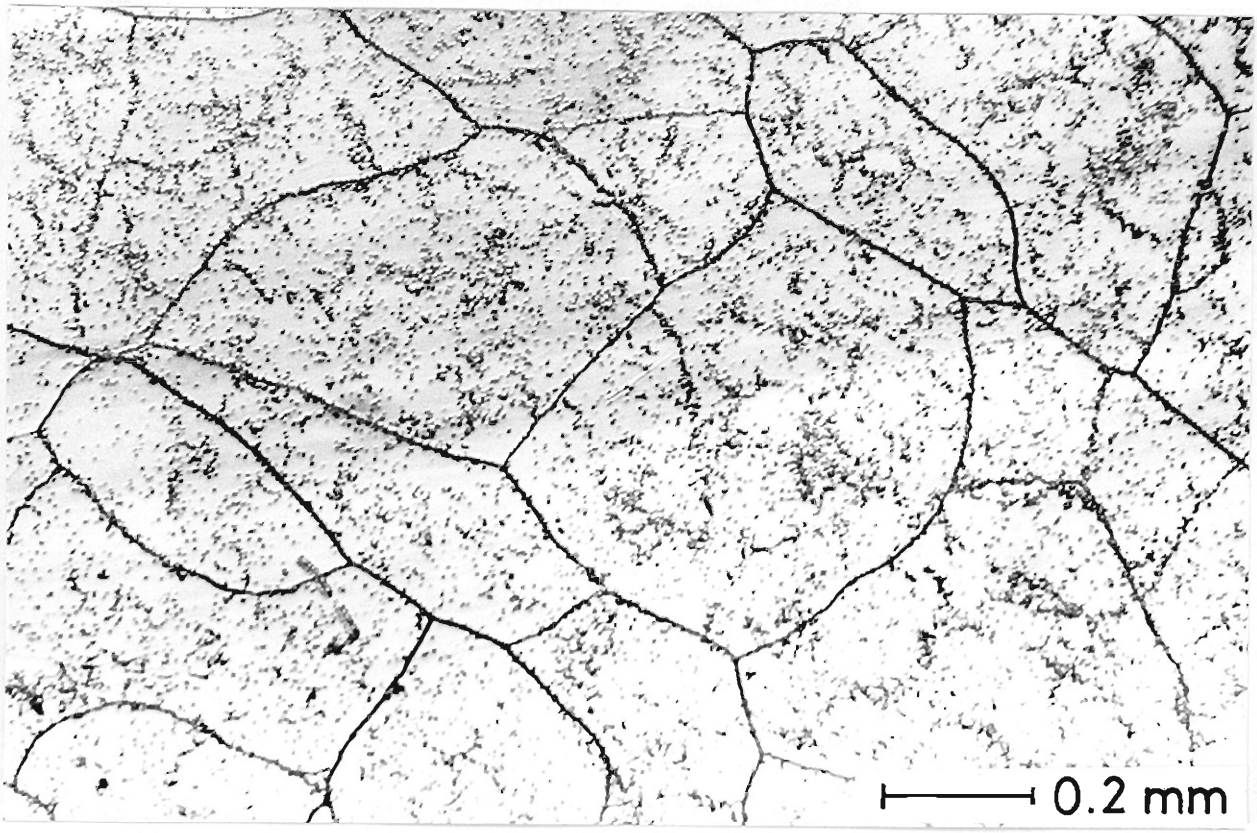

Fig. 40 Etch pit pattern of the (100) cleavage plane of $NbC_{0.95}$ crystal.

grow from the outside of the crystal rod. However, the new grain does not grow into the central part. The thickness of the outside grain is about 1 mm. The new outside grain grows out, as the zone is passed. This is explained by the fact that the crystal grows normal to the interface[51,52] because NbC has no preferential growth directions, as shown in Fig. 37. The cross section of the final part of the crystal rod is shown in Fig. 38. The quality of the crystal was examined by a back-reflection Laue method. The crystal was found to be of good crystalline perfection except for the peripheral part where the Laue spot separation was often observed.

Figure 40 shows the etch pit pattern on the (100) cleavage plane. The etch pit density is estimated to be 10^7 /cm^2.

4) Conclusion

NbC_x single crystals with desired chemical compositions were prepared by a modified zone leveling method. The size of crystal rods were 6 cm long and 8-9 mm in diameter. The grown crystals had highly homogeneous chemical compositions within 1 at% and were confirmed to have a good crystalline perfection as determined by the back-reflection Laue method. It was found that all impurities, except Ta, were entirely refined by evaporation. In order to prepare the high purity crystals, starting material which does not contain impurities of low vapor pressures should be used and a feed rod with low oxygen and nitrogen impurity contents must be prepared.

2-4-6 TaC_x

TaC has the highest melting point among the inorganic materials. A few trials of preparation of TaC crystals by a floating zone technique were reported[7,33,53]. However, the trials did not succeed yet. In the present experiments, the preparation of TaC single crystals was carried out by applying a modified zone leveling method[51]. In this method, TaC crystal can be prepared at a little higher temperature condition of TaC-C eutectic temperature(3400 °C), as shown in Fig. 41.

1) Preparation of TaC crystals with constant chemical compositions

1-1) Estimation of compositional change due to evaporation

In order to prepare the TaC crystal with a nearly stoichiometric composition at a little above the TaC-C eutectic temperature, the molten zone composition must be kept near the eutectic composition during a zone pass. From the present author's experience in preparation of HfC crystals[39], TaC crystal with a nearly stoichiometric composition was tried to be prepared using a feed rod with C/Ta=1.3 and an initial molten zone with nearly eutectic composition. An initial molten zone with such a composition could be obtained. However, as soon as the zone started to pass, the heating power had to be increased. The obtained crystal rod had a compositional gradient along the growth direction. The chemical composition of the crystal rod obtained after 0.5 cm zone pass was near the highest melting

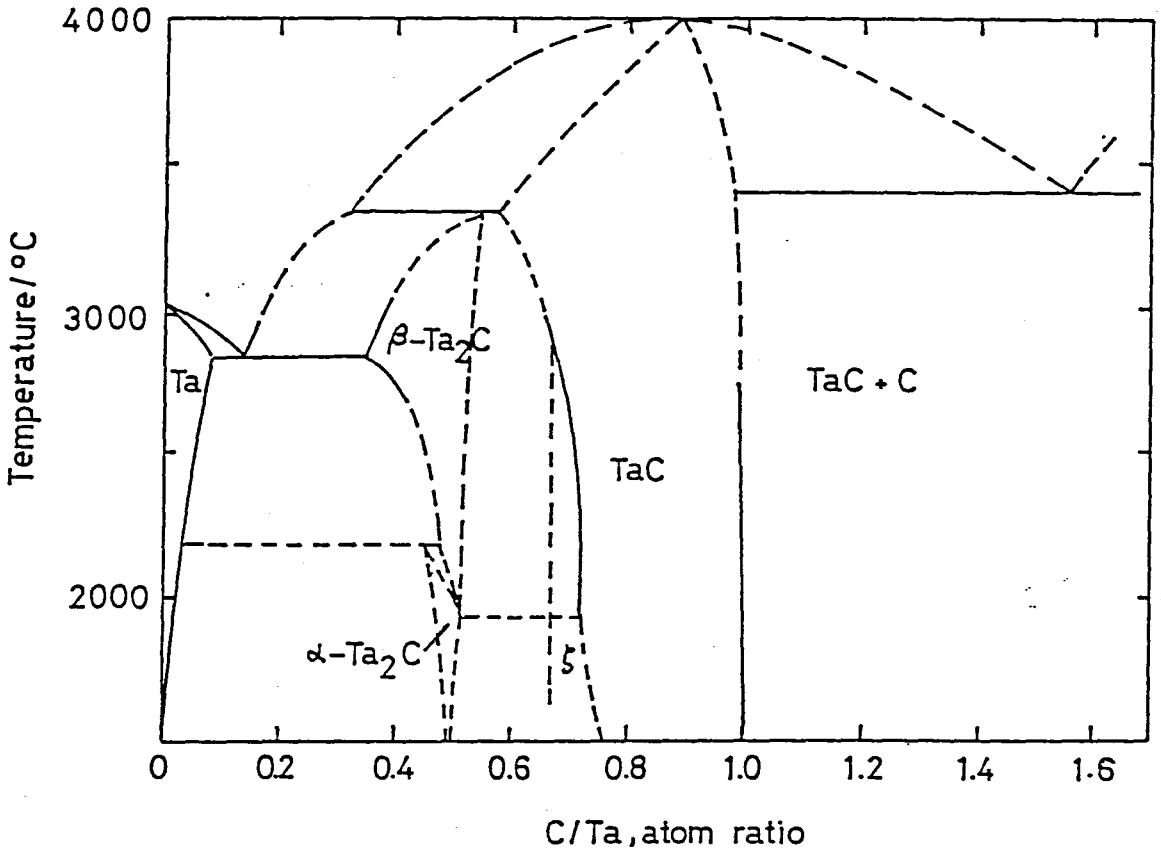

Fig. 41 Phase diagram of Ta-TaC system[12]

point composition(C/Ta=0.89). The vapor pressure of carbon(graphite) was about 10^5 Pa at this temperature range(3400-4000 ℃). Therefore, when the initial zone started to pass, the feed rod with low carbon content was melted into the molten zone, and the initial zone composition could not be kept constant.

In order to estimate the effective sublimation loss of carbon from the feed rod, TaC crystal rods with about 3 cm length were prepared under the same growth conditions, using the feed rods with various chemical compositions(C/Ta=1.3, 1.35, 1.45, 1.5, 1.7, 1.9 and 2.2). The chemical compositions of the initial(at 0.5 cm zone pass) and the final(at 3 cm zone pass) parts of the obtained crystal rods were determined from the results of lattice constant measurements on the basis of the expression[54]:

$C/Ta(\pm 0.01) = -25.641 + 59.757a.$

The results are shown in Fig. 42. The obtained crystal rods had compositional gradients along the growth direction. Fig. 42 shows that free carbon was deposited already from the initial part using the feed rod with more than C/Ta=2.2. Further, using a feed rod with more than C/Ta=1.5, a single phase could not be obtained under the steady state, at least, after 3 cm zone pass. Therefore, in order to obtain a crystal rod with C/Ta=0.96-97, one has to use a feed rod having a ratio of C/Ta=1.4, whose initial part(about 2 cm length) has a composition of C/Ta=2.2.

1-2) Preparation of TaC single crystal with constant chemical

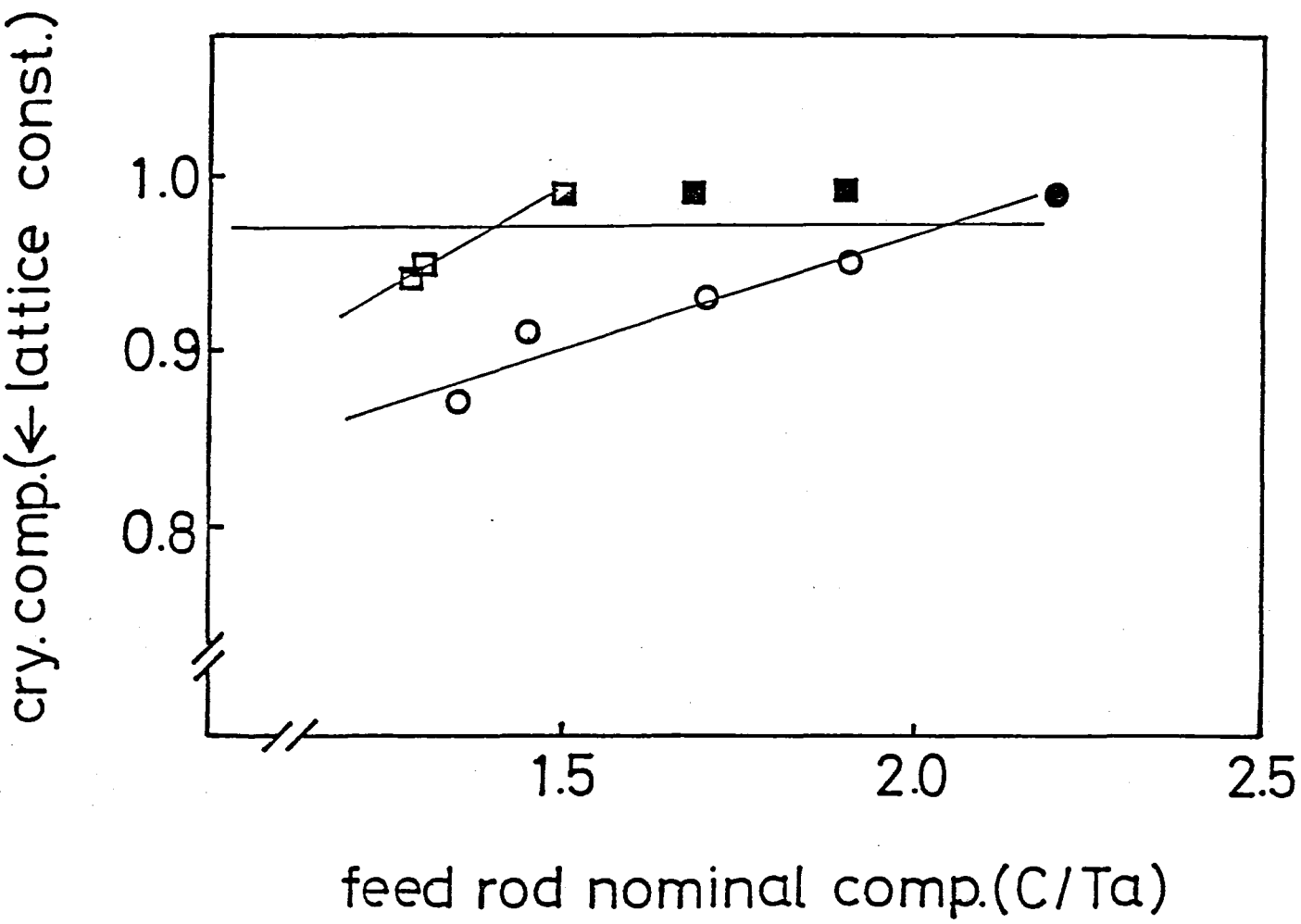

Fig. 42 The relationship in chemical composition between the feed rod and the initial(at 0.5 cm zone pass)(○) and final (at 3 cm zone pass)(□) parts of the crystal rods. (●) and (■) show free carbon deposition.

1-2) Preparation of TaC single crystal with constant chemical composition

The initial part of the feed rod must have an excess of carbon, i.e., C/Ta=2.2(not 2.1), because the carbon content in the initial part becomes deficient when the zone is not formed smoothly. This serious problem often occured. Even though the zone is formed smoothly and the zone has excess carbon, the steady state is easily reached soon due to violent evaporation.

The arrangement and procedures to prepare the single crystal are shown in Fig. 43(a), and the several analyzed parts of the obtained crystal rod are shown in Fig. 43(b). Carbon and niobium(which is a main impurity) were analyzed. The results are listed in Table 27. The crystal contained no free carbon and was constant chemical composition, such as C/Ta=0.946, 0.951 and 0.955. The feed rod(S') just above the zone has less carbon content(C/Ta=1.25) than the feed rod(S)(C/Ta=1.40). It was found that a part of added carbon had already sublimed before the feed rod was melted into the zone. The value of C/Ta=1.25 is an average value obtained from the result of analysis for the feed rod with about 5 mm length just above the zone. Therefore, when the feed rod was melted into the zone, still more added carbon would be lost. On the other hand, carbon hardly sublimes from the growing crystal because this is the carbon sublimation from TaC, while the carbon sublimation from the feed rod is the sublimation of graphite.

In order to examine the chemical compositions of the central

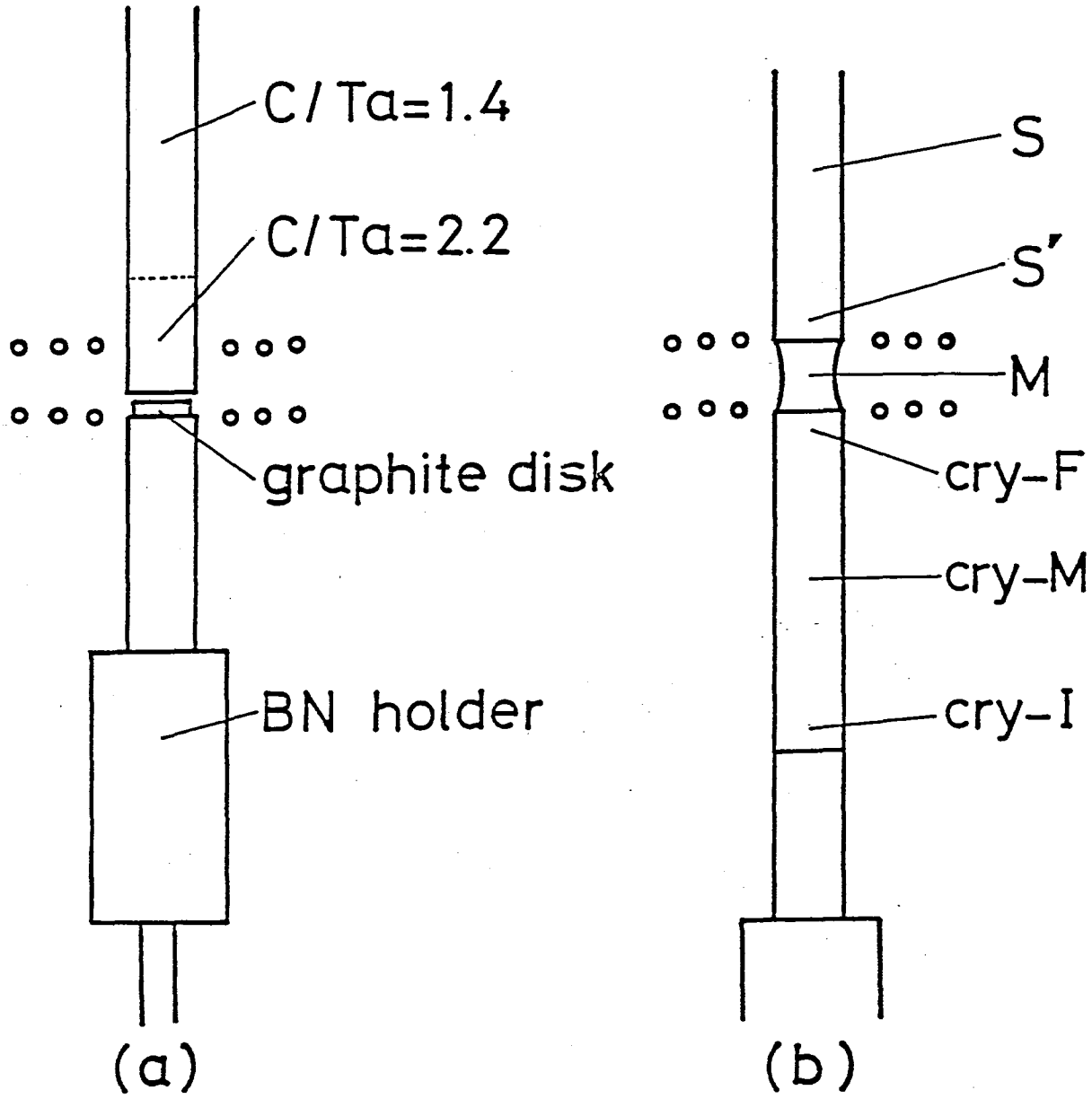

Fig. 43 (a)Arrangement of preparation of TaC single crystals The length of feed rod with C/Ta=2.2 is about 2 cm. After the initial zone is formed, the feed rod is passed downwards. (b) The parts to be analyzed are shown.

Table 27 Carbon content and chemical compositions in the TaC crystal rod.

>

	TC wt%	FC wt%	CC wt%	Nb/Ta	Composition C/Ta(Nb)
Cry-I	5.94	0.00	5.94	0.012	0.946
Cry-M	5.97	0.00	5.97	0.013	0.951
Cry-F	6.00	0.00	6.00	0.014	0.955
M	8.38			0.017	1.37
S'	7.70			0.014	1.25
S	8.53			0.014	1.40

Table 28 Carbon content and chemical compositions of the central and peripheral parts in the crystal rods

	TC wt%	FC wt%	CC wt%	Nb/Ta	Composition C/Nb(Ta)
Center	5.98	0.00	5.98	0.003	0.957
Periphery	5.95	0.00	5.95	0.003	0.952
Center	5.92	0.00	5.92	0.013	0.942
Periphery	5.85	0.00	5.85	0.013	0.930

and peripheral parts of the crystal rods, a 5 x 5 x 15 mm^3 block was cut from the central part of the crystal rod by a spark corrosion cutter. The chemical compositions of the central part and the rest(peripheral part) were analyzed, as listed in Table 28. The central part has a tendensy to contain a little more carbon than the peripheral part by about 1 at%. Furthermore, the difference in chemical composition along the growth direction is less than 1 at%, as seen in table 27. Therefore, the obtained crystal rod was found to have homogeneous chemical composition within 1 at%.

2) Impurities

The crystal, which was prepared in the same method as shown in Fig. 43, contained 160 ppm oxygen and 260 ppm nitrogen impurities, as shown in table 29. These impurity levels were almost the same as those in the IVa group carbide crystals. These impurities in the crystal did not change by a zone pass.

Metal impurities in the crystal($TaC_{0.95}$), starting material, feed rod and evaporation product were examined. The results are listed in Table 30. The evaporation rate was 0.45 g/h, when $TaC_{0.95}$ crystal was prepared. Ta content in the evaporation product is only 8 wt% and the rest was carbon. It is found that 0.3 % of TaC evaporated because about 14 g of TaC crystal was prepared per hour(= 0.45 x 0.08 / 14). Therefore, when impurity is perfectly refined, the value ratio(Evap./Feed) is about 350(= 1/0.003). All impurities except Nb were refined

Table 29 Oxygen and nitrogen impurity content in the feed rod and crystal($TaC_{0.95}$)

	Oxygen (wt%)	Nitrogen (wt%)
S	0.023	0.022
Cry	0.016	0.026

Table 30 Impurities in the crystal($TaC_{0.95}$), starting material, feed rod and evaporation product analyzed by X-ray fluorescence spectroscopy(peak heights normalized by Ta peak heights).

	Crystal	Starting material	Feed rod (Feed)	Evaporation product(Evap.)	Ratio (Evap./Feed)
Ti Kα	-	-	-	48	> 96
Cr Kβ	-	-	-	120	>240
Mn Kα	-	-	-	124	>248
Fe Kβ	-	2.5	-	250	>500
Co Kβ	-	1	-	58	>116
Ni Kα	-	1	-	36	> 72
Nb Kα	27	27	27	108	4

A dash means less than 0.5.

Table 31 Chemical compositions calculated from the densities and the lattice constants; d is density; a is lattice constant.

Analytical composition	Composition from d and a	d (kg/m^3)	a (nm)	Composition from a
Cry-I 0.946	0.937	14421	0.44485	0.940
Cry-M 0.951	0.939	14414	0.4449	0.945
Cry-f 0.955	0.951	14408	0.4450	0.950
Cry 0.867	0.879	14529	0.4437	0.870

due to evaporation. In order to prepare the high purity crystals, the starting material without Nb must be used.

3) Relationship among chemical composition, lattice constant and density

The lattice constants, densities and Nb contents of the crystal were measured, and the chemical compositions were derived by assuming that vacancies exist only on the carbon sites. The results are shown in Table 31. These results agreed well with those of chemical analysis within the limits of errors. Furthermore, the chemical compositions were calculated from the lattice constants, on the basis of the the expression described in ref.[54]. In addition, Table 31 also shows the results of the lattice constant, density, Nb content and chemical composition on the crystal with a ratio of C/Ta=0.867, which has almost a maximum melting point(3983 ℃)[12]. From these results, the nonstoichiometry is found to come from only the carbon defects.

4) Appearance, cross section and etch pit pattern

The size of crystal rod obtained by the method shown in Fig. 43 was about 6 cm long and 0.9-1.0 cm in diameter, as shown in Fig. 44. The color of the crystal rod was golden. Its color depends on the chemical composition. The crystal with C/Ta=0.867 was almost silvery.

It is noted that the outward appearance of the crystal rod is not smooth. This is due to both violent evaporation from the

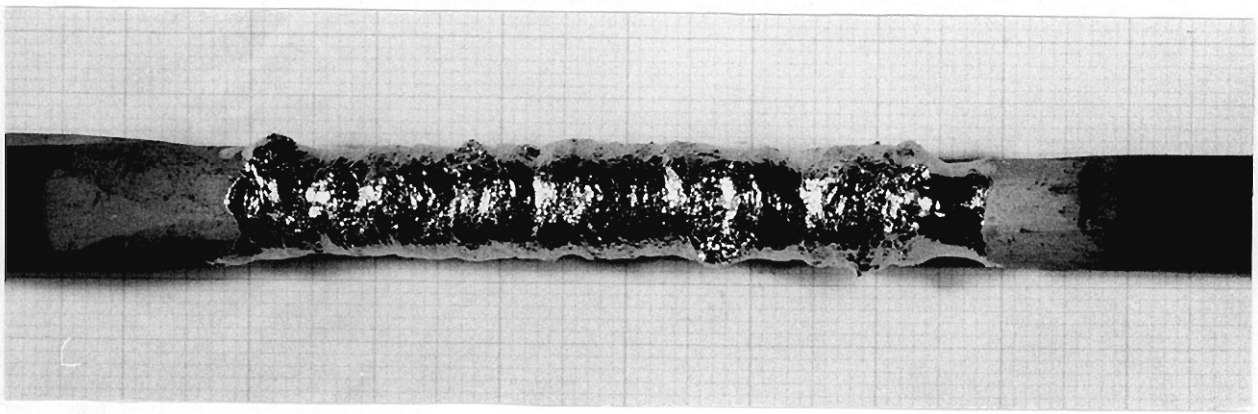

Fig. 44 As-grown $TaC_{0.95}$ crystal rod

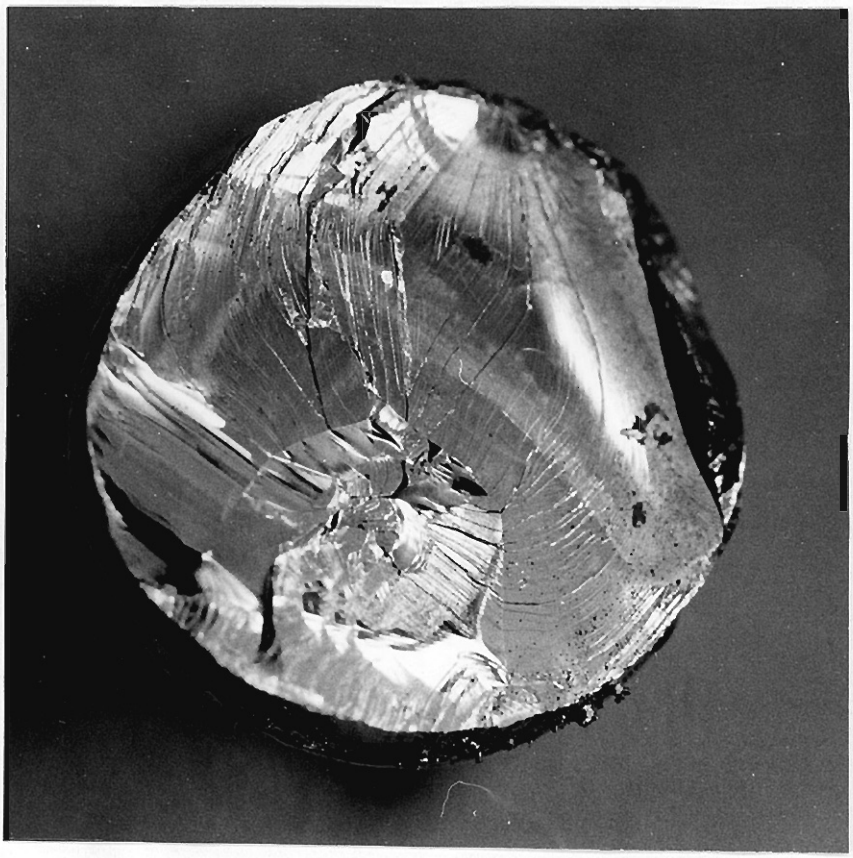

Fig. 45 The (100) cleavage plane of TaC single crystal at about 1 cm zone pass.

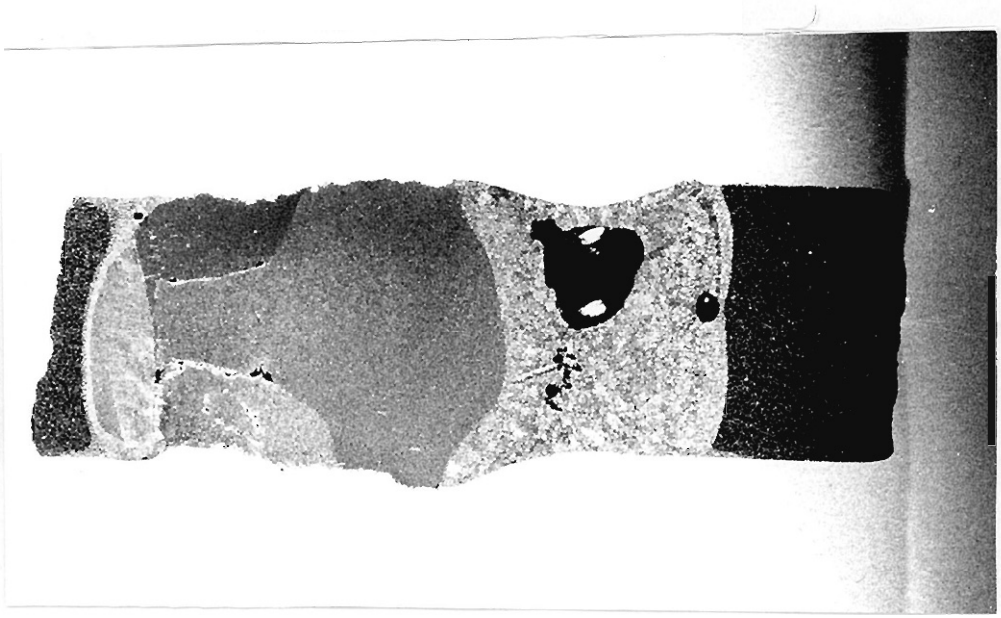

Fig. 46 Longitudinal cross section of $TaC_{0.95}$

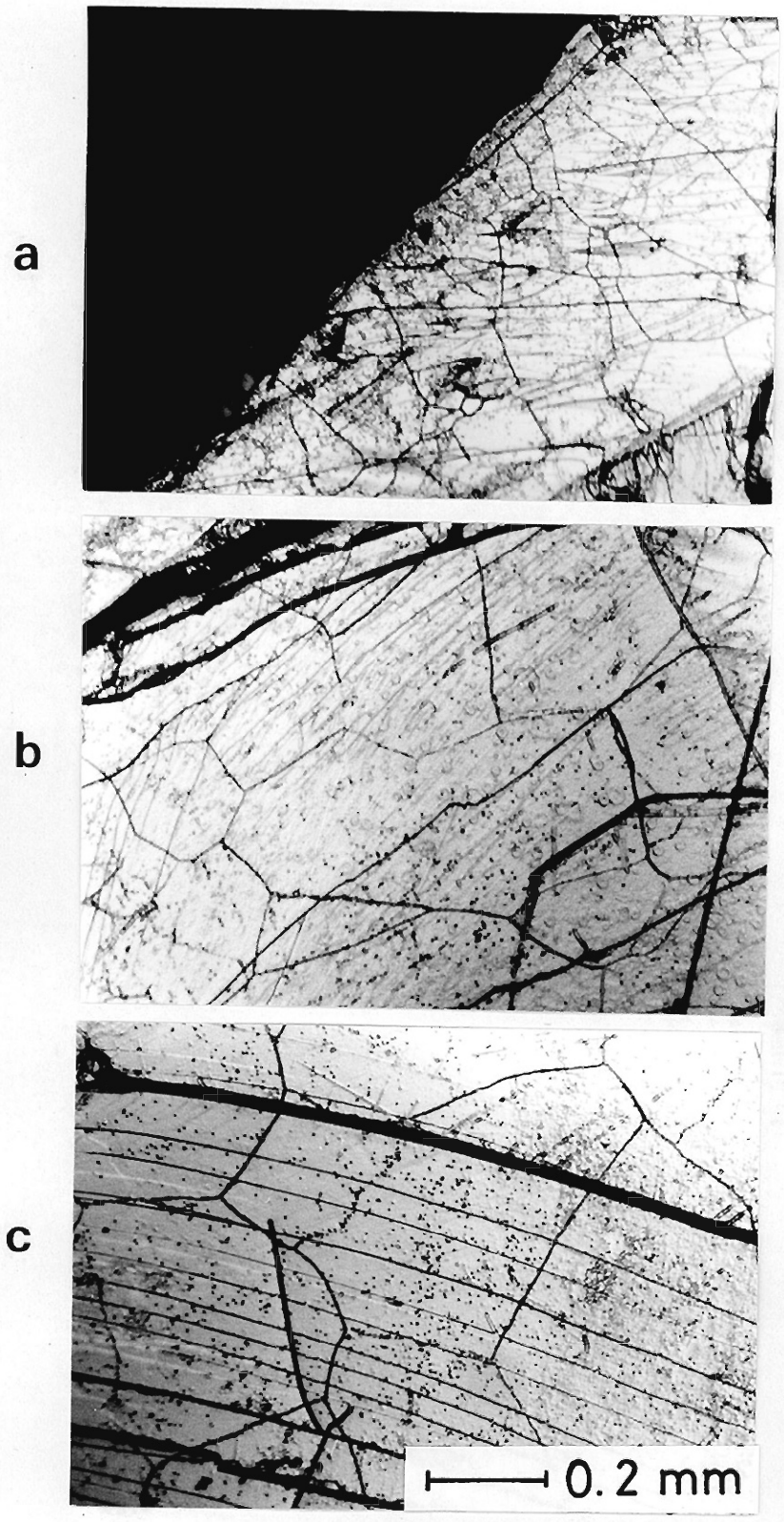

Fig. 47 Etch pit pattern of the (100) cleavage plane of $TaC_{0.95}$ crystal: (a) surface part, (b) part between the surface and the central parts and (c) central part of the crystal rod.

molten zone and carbon sublimation from the feed rod surface just above the molten zone. The former problem caused the contact of the molten zone with the evaporation products on the work coil. The latter problem was occured that the feed rod was not melted into the molten zone smoothly. The surface of the feed rod just above the molten zone with about 0.5 mm thickness changed to yellow in color due to carbon evaporation. Therefore, the feed rod surface was not melted into the molten zone smoothly because the surface part has a higher melting point.

Although the outward appearance of the crystal rod was not smooth, a good quality crystal could be obtained. The (100) cleavage plane at 1 cm zone pass is shown in Fig. 45. It was found that the crystal rod became almost a single crystal even after 1 cm zone pass. A longitudinal cross section is shown in Fig. 46. TaC has a small number of nucleation sites. A single crystal can be obtained from the part after a 1 cm zone pass and the crystal rod has no polycrystalline outward rim.

Figure 47 shows the etch pit patterns on the (100) cleavage plane of $TaC_{0.95}$ crystal. The network is small at the peripheral part. The etch pit density is estimated to be 10^7 /cm^2.

5) Conclusion

TaC single crystals with about 6 cm length and 0.9-1.0 cm diameter could be prepared by a modified zone leveling method. The crystal rod have homogeneous chemical compositions(C/Ta(Nb)= 0.95-0.96), and do not contain any free carbon. The analytical

compositions agrees well with those calculated from the lattice constants and densities. All impurities, except for Nb, were refined only by evaporation.

2-5 Discussion of crystal growth of the carbides

2-5-1 Influence of ah ambient helium gas

The crystals must be prepared under the ambient helium gas condition. Therefore, the influences of helium gas pressure on heating power, the evaporattion rate and the crystal quality were examined in the case of TiC. Figure 48 shows the relationship between the magnitude of gas pressure and the heating power. The temperatures in this figure indicate those at the middle part of the crystal rod with 8 cm in length during heating. The differece in heating power between the gas pressures of 3×10^5 Pa and 3×10^6 Pa was about 12 %. Acually, the crystals were prepared at the helium gas pressure lower than 10^6 Pa. Therefore, the influence of gas pressure on the heating power was found to be small. This result indicates that most of the supplied power is lost due to radiation.

Figure 49 shows the influence of gas pressure on the evaporation rate. The measurements were carried out by preparing $TiC_{0.96}$ crystals at various gas pressures using a modified zone leveling method. The evaporation rate was obtained from the weight loss, the growth time and the surface area of the molten zone. It was found that the evaporation rate was proportional to $p^{-0.75}$. Haggerty et al.[7] pointed out that the rate is proportional to $p^{-0.5}$ using the mathematical model. From the results of the present experiments, the effect of helium gas pressure on evaporation rate was found to be a slightly larger than that obtained from the theory. Figure 49 also shows the

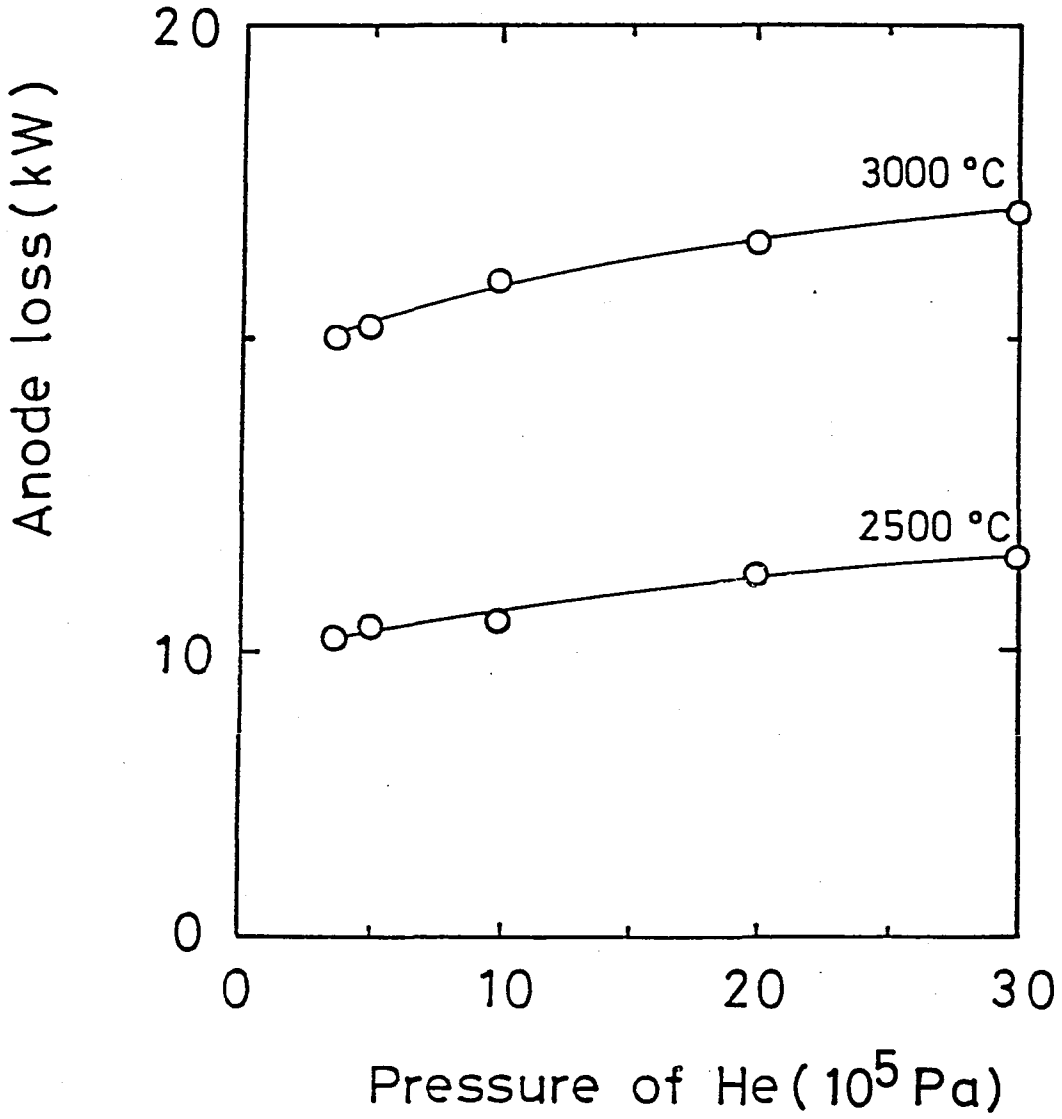

Fig. 48 Relationship between the helium pressure and the heating power(Anode loss).

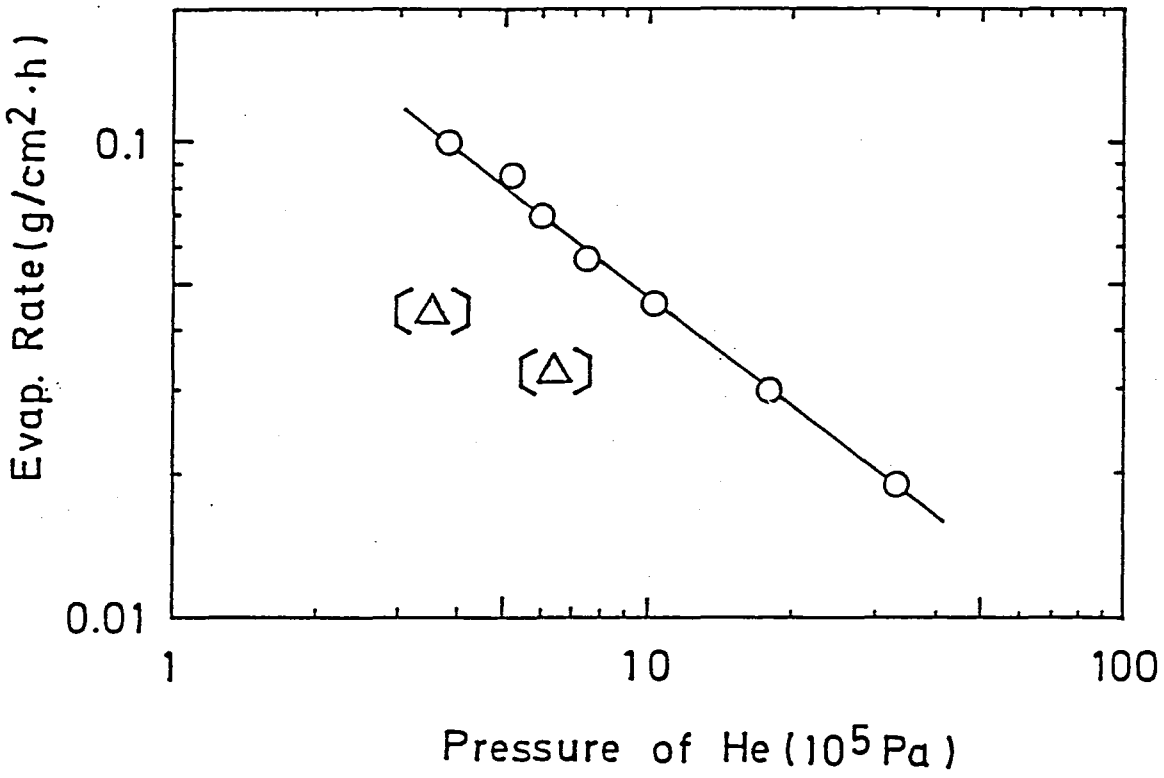

Fig. 49 Relationship between the helium gas pressure and the evaporation rate of a molten TiC(C/Ti=1.35). The triangle shows the measured point under argon gas.

results obtained in the case of Ar ambient gas. These values could not be measured accurately because the small arc discharge often occured during a zone pass. The evaporation rate becomes half, compared with the result in the case of helium gas.

Crystal rods of $TiC_{0.96}$, 4 cm long, were prepared at 5 x 10^5 Pa and 3 x 10^6 Pa of helium gas. Figure 50 shows the longitudinal cross section of the molten zone, the cross section of the crystal rod and the cleavage plane. The crystal prepared at 3 x 10^6 Pa has a polycrystalline rim, and does not have a plain cleavage plane because the central part consists of several grains. On the other hand, the crystal prepared at 5 x 10^5 Pa has a single grain at the central part and has a clear cut cleavage plane, as seen in Fig. 50(a). When the gas pressure is even lower than 4-5 x 10^5 Pa, evaporation becomes more violent. Many evaporation products adhere to the work coil and touch the molten zone and the crystal. Many dendrites grow on the crystal rod surface. The crystal part which contains dendrites becomes a heat sink. New grains start to grow from the dendrites and a single crystal rod can be obtained no longer. The best ambient gas pressure to obtain TiC crystals with the best quality is 4-5 x 10^5 Pa.

From these results, it was found that an ambient helium gas does not influence to the heating power so much, but does to the evaporation rate and the crystal quality.

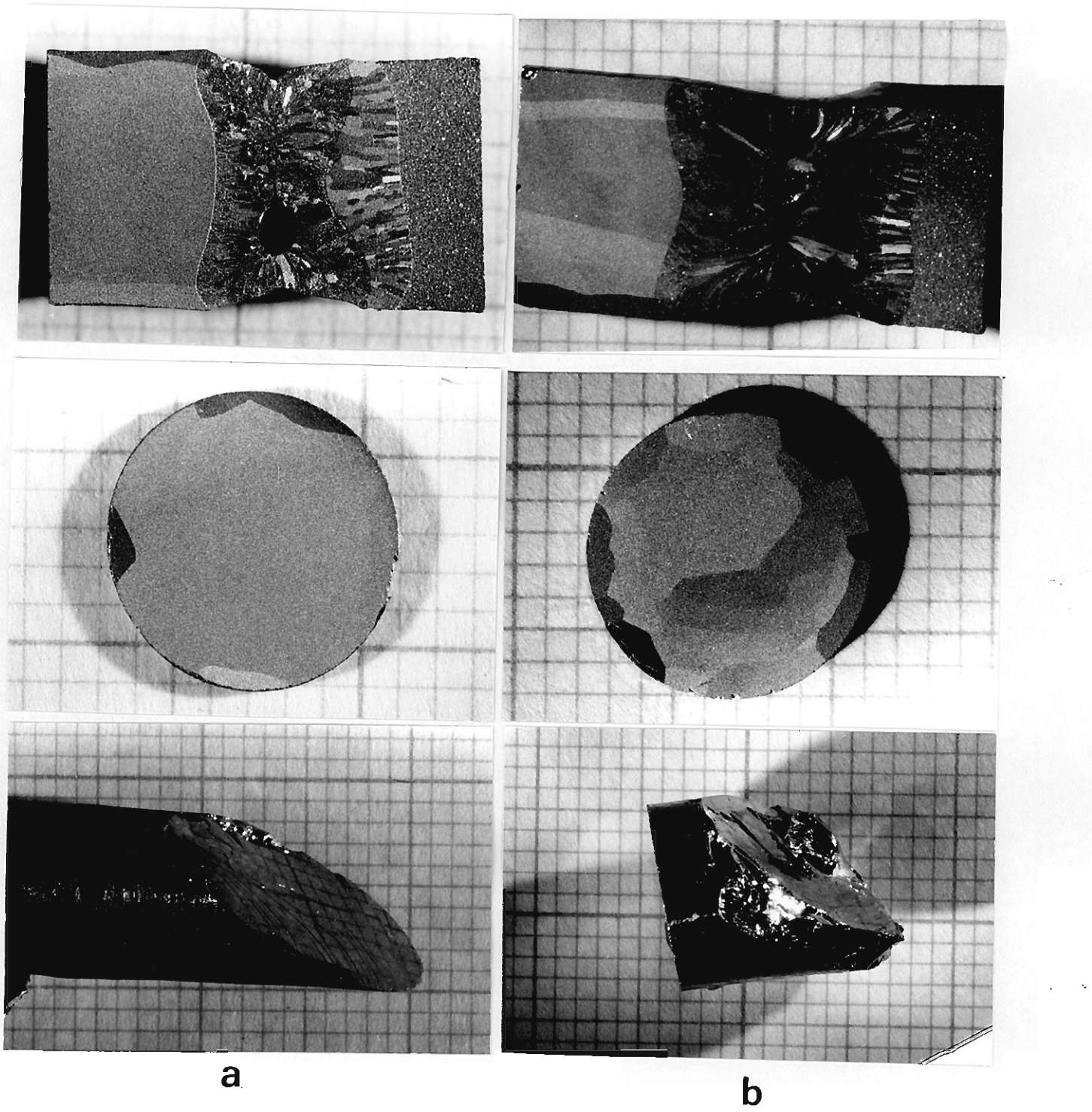

Fig. 50 Longitudinal cross sections of the zones, cross sections and cleavage planes of the crystal rods prepared at (a) 5×10^5 Pa and (b) 3 MPa of helium.

2-5-2 Crystal growth

Every single crystals of the IVa and Va group carbides were prepared by a modified zone leveling method. The size was 5-6 cm long and 0.8-1.0 cm in diameter. The homogeneity of chemical composition is within 1 at%. The single crystals of TiC_x and ZrC_x, which belong to the IVa group carbides, were prepared in the compositional region with C/M higher than 0.85. The Va group carbides of VC_x and NbC_x were prepared over the entire compositional range. HfC_x and TaC_x crystals, which have the highest melting points among materials, were prepared in the carbon rich compositional region.

In order to prepare the carbide crystals by a modified zone leveling method, the relationship between the solidus and liquidus compositions and the compositional change due to evaporation must be determined under the growth conditions. The former agrees well with some of the phase diagrams which had already been reported. This result suggests that these crystals were prepared nearly under the equilibrium state. Besides, it is expected that the phase diagram of the high melting materials can be determined by a floating zone method. Actually, when an initial molten zone is formed on the basis of the solidus-liquidus relation, a little experience is needed. For oxample, as shown in Fig. 4, the carbon or metal disk is put between the upper and lower sintered rod, and the part around the disk is melted to form the initial molten zone with the liquidus composition which coexists with the desired chemical composition

of crystal. Therefore, the zone composiiton depends on the weight of the disk, the setting position and the density of the sintered rod which is set below the initial molten zone. In the case of the high growth temperature, the initial molten zone composition also depends on the time required to form the molten zone because of violent evaporation. In addition, the form of the disk is an important factor to form the initial molten zone with the same form as that during a zone pass because the zone volume must be kept constant.

On the other hand, the latter(compositional change due to evaporation) was found to depend on the zone composition and growth temperature. In the carbon-rich compositional region, the evaporation products are generally the carbide(MC) and carbon. The carbon evaporation mainly caused the compositional change. In the carbon poor compositional region, the evaporation products are the carbide(MC) and metal in the case of the IVa carbides, but the carbides(MC and M_2C) in the case of the Va carbides. Therefore, the IVa carbide crystals with C/M less than 0.80 could not be prepared because the zone composition quickly changed to the carbon rich composition due to violent metal evaporation. This phenomena was occured when the parent metals have very high vapor pressures, compared with the carbides. On the other hand, the Va carbide crystals could be prepared over the entire compositional range because of the following two reasons. The amount of the evaporation product is small during a zone pass because the M_2C carbide has lower vapor pressure than the metal.

In addition, the compositional change due to evaporation is small because only the metal component is not lost.

The preparations of single crystals of the IVa and Va carbides are compared with each other. In the preparation of the crystal with carbon rich composition, the growth can be divided into two groups depending on the growth temperature; the preparation of the carbides at a high growth temperature of 3300-3500 ℃ and the other at the temperature lower than 3000 ℃. The crystals prepared at the high temperature are of TaC, HfC and NbC. These crystals are prepared under about 10^5 Pa of the carbon vapor pressure. Therefore, there are two major problems: the high temperature and violent evaporation. The former was solved by the technique described in section 2-1. The latter introduced the contact between the molten zone and the evaporation product on the work coil because the evaporation product adheres to the work coil. Therefore, the crystals are prepared using a work coil with a relatively large inside diameter(16 mm), although the molten zone is effectively heated using a work coil with a small inside diameter. A higher pressure of helium gas(10^6 Pa) was used to lower the evaporation rate and to carry away the evaporation product from the molten zone surface by convection. In addition, the growth rate was higher (1.25-1.5 cm/h) than that in the case of $TiC_{0.96}$ crystal preparation(0.5 cm/h). As an additional problem, a part of the molten zone surface was often solidified during a zone pass because carbon evaporates non-uniformly due to an asymmetric

temperature distribution around the molten zone. This problem was solved by rotating the upper and lower shafts. Rotation also play an important role to melt the feed rod into the molten zone smoothly. In order to prepare the crystal more smoothly, the feed rod density must be increased. The feed rod, to which much carbon is added, has the density less than 50 % of the theoretical density. The low density of the feed rod introduces the unsmooth zone pass because the bouble in the molten zone becomes large and the cracks are formed in the feed rod just above the molten zone.

The single crystals of $TiC_{0.96}$, $ZrC_{0.98}$ and $VC_{0.87}$ can be prepared at a relatively low growth temperature(less than 3000 ℃) without problems described above. However, there are other problems which are caused by the properties of each carbide. In the case of TiC, the crystal rods which consist of several subgrains are often prepared[33]. The cross section is like that of salami. This may come from the fact that a molten TiC has relatively high viscousity. Therefore, this problem was solved by decreasing the growth rate(5 mm/h) and secelting a commercial carbide powder with low W content(500 ppm). In the case of ZrC, since the molten ZrC has a low viscosity, it is easy to drop out the molten zone during a zone pass. This problem was solved by using a thin work coil[38]. In the case of VC, cracks are easily formed in the crystal rod. This problem is not perfectly solved yet, but became small by a stable zone pass and the low growth rate.

In the case of the preparation of the single crystal with carbon poor compositional region, the crystals of TiC_x and ZrC_x belonging to the IVa group carbides could not be prepared because of violent metal evaporation, as already described. On the other hand, the Va group carbide crystals of VC and NbC can be prepared in the same method as the carbon-rich crystal. The problem of the compositional change due to evaporation is not perfectly solved yet. This is a weak point of a floation zone technique because of a small volume of the molten zone.

2-5-3 Impurities

1) Oxygen and nitrogen impurities

The oxygen and nitrogen impurities occupy the carbon defect sites. These impurities, especially oxygen, influence the properties of carbides, as described in Chapter 1. Therefore, the high purity crystals must be prepared and the content of these impurities in the sample should be checked. Generally, it is said that the carbide with impurities less than a few hundred ppm shows intrinsic properties[25].

The distributions of these impurities in the crystal rod are determined by the equiliblium among the crystal, zone and pertial pressure in the ambient gas. The content of impurity in the crystal is mainly determined by the partial pressure in the ambient gas because these impurities are lost as gas phases during a heating[12]

Oxygen impurity content in the IVa carbide crystals

decreases by less than one tenth due to a zone pass, but in the case of the Va carbides it decreases, at most, by 50 %. This difference comes from the fact that the ambient gas may be refined during a zone pass by the evaporated IVa carbides, which have a getter effect[12]. Therefore, although the feed rods of the IVa carbides contained more than 1000 ppm oxygen, its content in the crystals are low. In the TiC and ZrC crystals, oxygen can not be detected. HfC contains 250 ppm oxygen. On the other hand, as for the nitrogen impurity, the content hardly changed due to a zone pass. The Va carbide crystal has nitrogen(about 100 ppm) in an amount less than the IVa carbide crystals(300 ppm).

The crystals with low oxygen and nitrogen impurity content are prepared from the feed rod with low oxygen and nitrogen impurity content.

2) Metal impurities

From the evaporation data of metal impurities, it was found that metal impurities can be divided into three groups; the first group impurities, such as Mn, Fe Co and so on, are perfectly refined by evaporation; the second ones have a evaporation rate lower than that of the host carbide; the third impurities do not evaporate during a zone pass. The order of the evaporation rate of metal impurities are as follows;

Zn > [Mn > Cr,Fe,Co,Ni] >> Ti > Zr > Hf > W

Ti >> Hf

Nb > Ta

Ti > V >> Mo > W

This tendency can be understood from the vapor pressure (or evaporation rate) of the impurity carbides[35].

The distribution of impurity along the growth direction was calculated under the same assumptions used in the construction of the theory for the zone refining; the constant zone length(L), the constant distribution coefficient(k), the uniform solute concentration(C_0) through the feed rod, the uniform solute concentration(C_L) in the molten zone, and so on. Additional assumptions were made: impurity concentration in the evaporation product is proportional to that in the zone; the evaporation rate is constant during a zone pass; b% of the host carbide is lost during a zone pass due to evaporation. The effective solute concentration(C_0') through the feed rod is introduced:

$$C_0' = 100/(100-b)\ C_0. \qquad (1)$$

When the zone with unity cross section advances by dx, the amounts of impurity entering the zone is $C_0' dx$, and that leaving it is $kC_L dx$ due to zone refining, and $k_{evap}C_L dx$ due to evaporation from the zone. The net change(ds) in the impurity amount in the zone is:

$$ds = C_0'dx - kC_Ldx - k_{evap}C_Ldx, \qquad (2)$$
$$= C_0'dx - k'C_Ldx,$$

where $k' = k + k_{evap}$. (3)

Formula(2) has the same form as that in the theoretical consideration of zone refining[35]. The solute concentration in the zone can be easily obtained as follows:

$$C_L/C_0' = (1/k')(1-(1-k')\exp(-k'x/L)). \qquad (4)$$

Therefore, the solute concentration(C_0') in the crystal rod at any x is given by

$$(C_S/C_0') = k(C_L/C_0')$$
$$= (k/k')(1-(1-k')\exp(-k'x/L)). \qquad (5)$$

Substituting (1) into (5),

$$(C_S/C_0) = 100/(100-b)(k/k')(1-(1-k')\exp(-k'x/L). \qquad (6)$$

In the case of preparation of the carbide crystals, their evaporation loss was, at most, 10 wt% in the present growth conditions. Therefore, b is assumed to be 10. The first class impurities hardly solid-solute into the carbides and these impurities have melting points lower than the carbides.

Therefore, k is assumed to be 0.01. The k_{evap} is 10 because these impurities have vapor pressure two order higher than the carbides whose k_{evap} is 0.1(= 10 % of evaporation loss). The second group impurities are the IVa, Va and VIa metals, which form solid-solution with the carbides and have a magnidude of vapor pressure approximate to those of the carbides. Therefore, it is assumed that k is between 0.4(Zr in HfC) and 1.4(Ta in NbC) and k_{evap} is 0.1. In the case of the third impurity group, k_{evap} is zero and k is 0.8 for W in TiC and 1.2 for Mo in VC. The concentration of impurity along the growth directions was calculated,as shown in Fig. 51. The impurity content at the initial part of the crystal rod is determined by the distribution coefficient(k). After being kept at the steady state, the impurity content is determined by the product(100/(100-b)(k/k')) of the condensation due to the host carbide evaporation and the refining due to the impurity evaporation. In the case of k_{evap}=0, the impurity content increases by the loss of host carbide at the steady state. In the case of k_{evap}=0.1, the impurity content in crystal hardly deviated from that in the feed rod. In the case of k_{evap}=10, that is, in the case of Cr, Mn, Fe, Co and Ni impurities, k' becomes large and the steady state is reached soon. These impurities are perfectly refined by evaporation. The dashed line in Fig. 51 shows the distribution in the case when these impurities do not evaporate at all.

The impurities left in the crystals are the IVa-VIa metals except Cr. These impurities are not refined due to evaporation

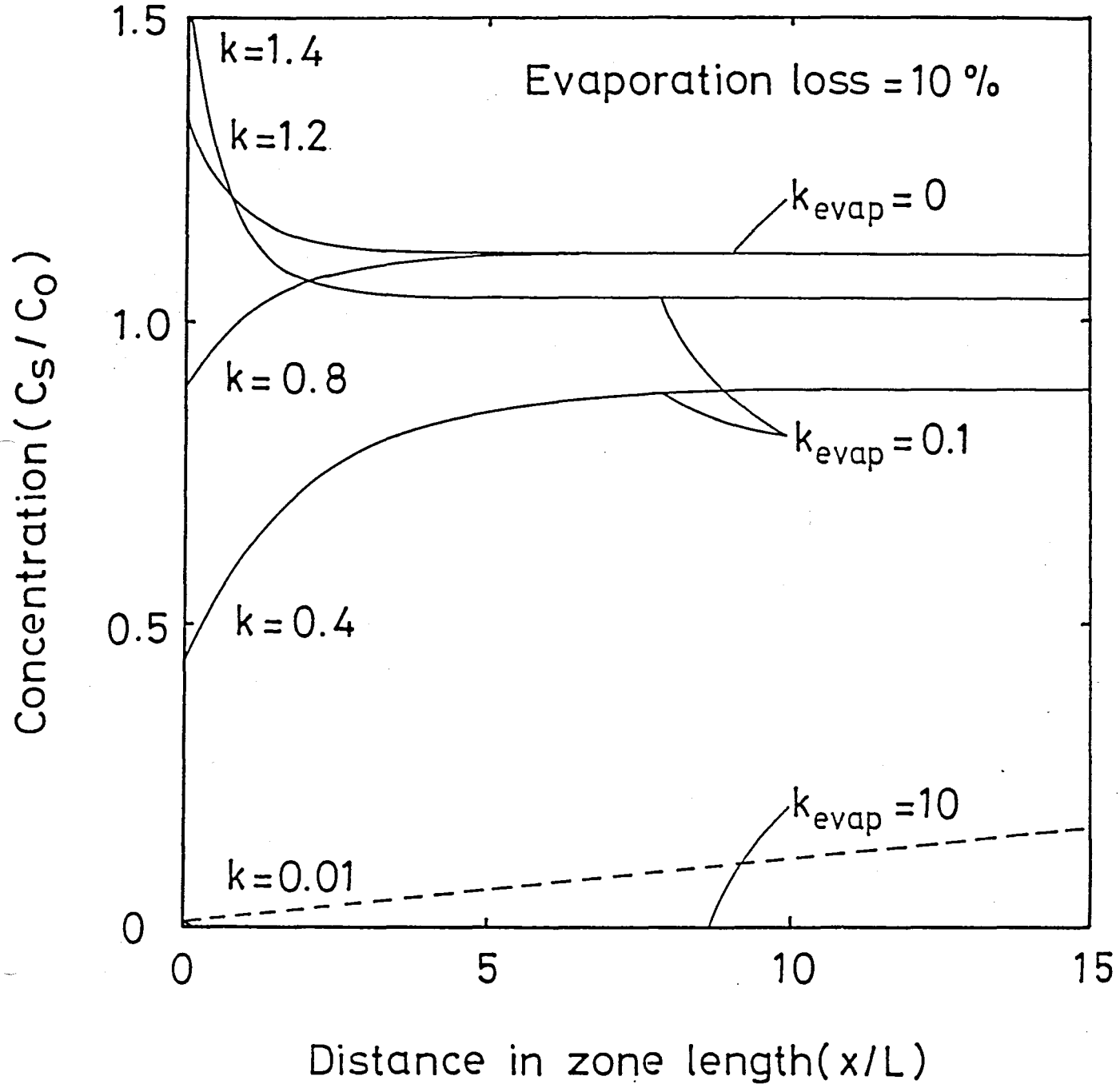

Fig. 51 Impurity distribution along the growth direction.

and zone refining, because all the carbides of these impurity metal have low vapor pressure and form the solid solutions. Therefore, in order to prepare the highly pure crystal, the IVa-VIa metal impurities except Cr should be eliminated from the starting materials.

2-5-4 Chemical composition, lattice contant and density of the IVa and Va transition metal carbides

On the basis of the above results, the high purity crystals were prepared. The carbon content, lattice constants and densities of these crystals were measured.

The lattice constants are influenced by the content of oxygen and nitrogen impurities. The existence of oxygen and nitrogen impurities contract lattice constants of the IVa carbides, and expand those of the Va carbides. Therefore, Toth[12] estimated the relationship between the chemical composition and the lattice constants from the highest and lowest values among the reported scattered values in each case of the IVa and Va carbides, respectively. It was confirmed that his estimation is almost valid. The IVa carbides have the largest lattice constants at the chemical composition of C/M= 0.83-0.89. The lattice constants become small with decreasing and increasing the carbon content. On the other hand, the lattice constants of the Va carbides decrease with decreasing the C/M atomic ratio. Further, it is confirmed that no defects exist at the metal sites and that the nonstoichiometry are derived from only the carbon

defect.

2-5-5 Appearance and cross section

The size of crystal rods prepared by a modified zone leveling method is about 6 cm long and 0.8-1.0 cm in diameter. The crystal rods with relatively low melting points, such as TiC, VC and ZrC, have a smooth surface. These crystals are found to be prepared smoothly. On the other hand, the crystal with high melting point has a rough surface. This is due to the violent evaporation, because the evaporation product adheres to the work coil, and touches the zone and the just grown crystal.

Figure 52(a) and (b) show the longitudinal cross sections of the IVa($ZrC_{0.98}$) and Va($TaC_{0.95}$) carbide crystals, respectively. The cross sections were grouned using the under 400 mesh powders of B_4C. The difference in reflection arises from the difference in the orientation of each grain. The appearant difference indicates that the orientations between the grains are quite different. A little difference in reflection corresponds to a few degrees. Therefore, the misorientation higher than one or two degrees in the crystal can be found from the observation of the cross section. In Fig. 52, the initial part of crystal consists of several grains. As the zone advances, one of the central grains becomes large, and then becomes a single crystal. The differences between the IVa and Va group carbides are that the number of grain at the initial part of the IVa crystal is more than that of the Va crystal, and that

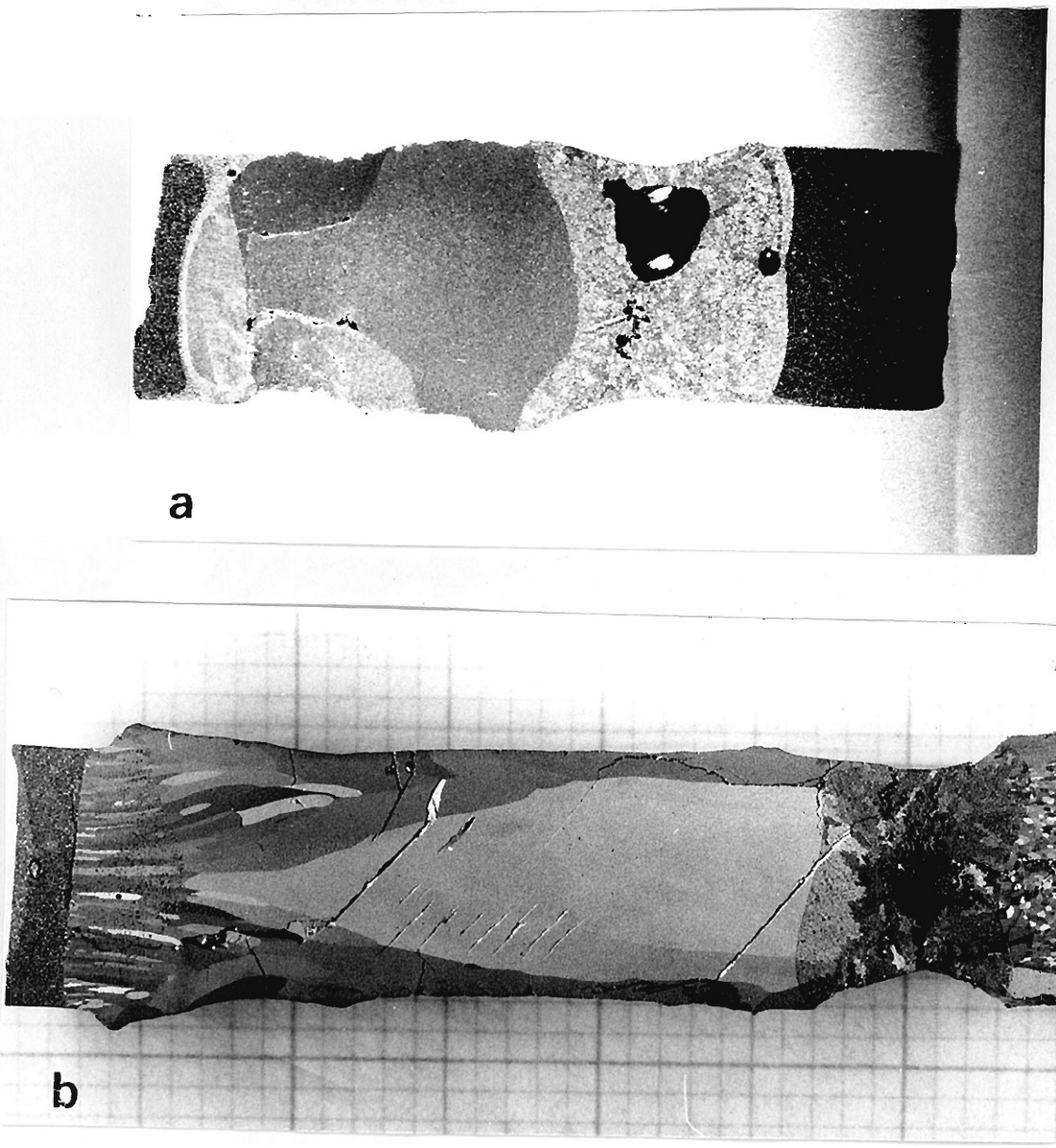

Fig. 52 Longitudinal cross sections of (a) $TaC_{0.95}$ and (b) $ZrC_{0.98}$.

all the IVa crystals are surrounded by a polycrystalline rim, but the Va crystal is not.

2-5-6 Crystal growth mechanism

The difference between the IVa and Va transition metal carbide crystals is that the IVa crystals are surrounded by a ploycrystalline rim, but the Va crystal is not. The reason is as follows.

Figure 53 shows the longitudinal cross section of the $TiC_{0.96}$ crystal with 1 cm length. As seen in this picture, the grains at the central part did not grow to a single grain yet. The boundaries between the grains were normal to the zone-crystal interface. This result indicates that each grain grows normal to the interface, which is considered to be reasonable from the fact that TiC does not have a prefered growth direction[52]. The shape of the interface is convex toward the molten zone at the central part and concave at the peripheral part. Therefore, the large grain growth takes place at the central part. At the surface, the grains grow from the rod surface to the concave point and form a polycrystalline rim with about 1 mm thickness. It can be explained from the interface shape that all IVa carbide crystals have a polycrystalline rim. On the other hand, the cross section of $TaC_{0.95}$ crystal is shown in Fig. 52. The interface shape is convex to the zone. A polycrystalline rim is not formed because the central grain grows to the surface. In the case of VC, the rim is not formed although the interface

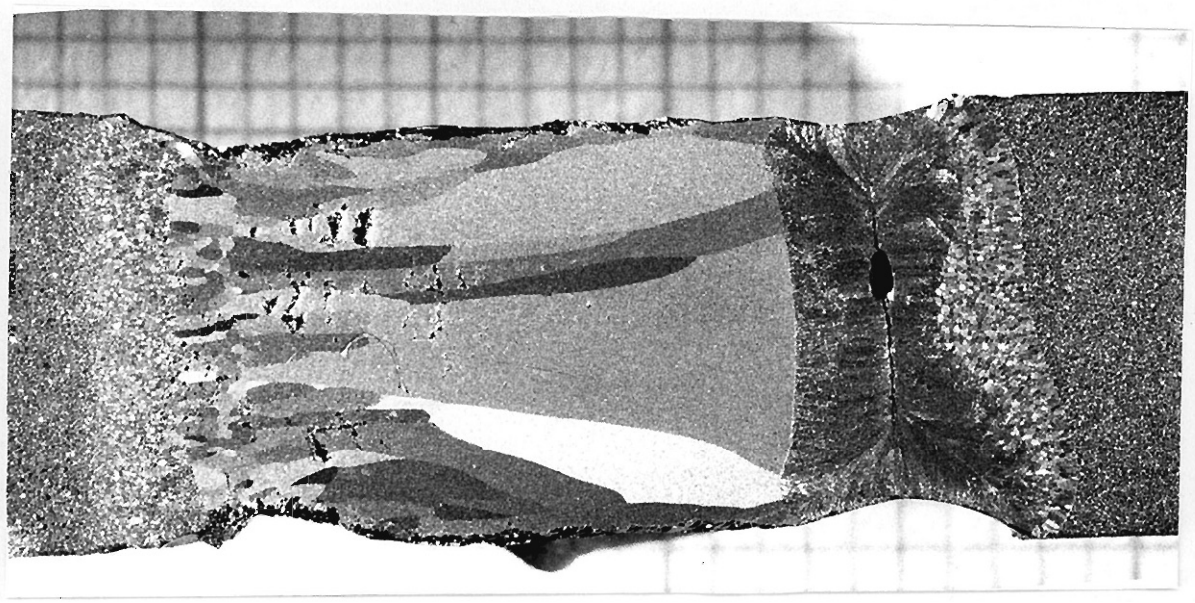

Fig. 53 Longitudinal cross section of $TiC_{0.96}$ crystal rod.

shape is similar to that of the IVa carbides. As shown in Fig. 31, the grains at the initial part of VC crystal rod are large though those grains grow on the sintered rod. Diameters of grains are larger than the thickness of the rim. It is difficult to form the rim because the small grain is not stable.

The interface shape is determined by both the radial temperature and chemical composition distributions near the interface because the carbides are compounds consisting of metal and carbon. In the case of the IVa carbide(TiC), the interface shape indicates that the temperature in both ends of the interface are lower than that in the central part and/or their carbon contents are also lower(equivalent to high melting point). According to the experimental results on carbon content listed in Table 2, the interface is found to be determined by the temperature distribution. On the othe hand, in the case of TaC, the interface is convex to the zone, as shown in Fig. 52. From the analytical results(Table 28), the central part contained more carbon content than that of the peripheral part. Therefore, it is found that the interface shape of TaC is mainly determined by the temperature distribution. Further discussion will be made in Chapter 3.

2-5-7 Etch pit pattern

In all the carbide crystals, the etch pit patterns are very similar in each other. The etch pits form the low grain boundaries. The boundaries form the mesh-like structure. The

mesh at the central part is larger than that at the peripheral part. The size of mesh depend on the growth temperature. The carbides with low melting points, such as TiC and VC, have the large mesh, compared with the high melting carbides, such as TaC, NbC and HfC. Therefore, the etch pit densities increase with increasing growth temperature as listed below:

TiC, VC	10^6	$/cm^2$
ZrC	5×10^6	$/cm^2$
TaC, HfC, NbC	10^7	$/cm^2$

The carbide crystals have the etch pit density of 10^{6-7} $/cm^2$.

Figure 54(a) and (b) show the X-ray topograph of (100) planes which are normal and parallel to the <100> growth direction, respectively. It is found from the lack in Fig. 54(a) that the periphearal part consists of several grains. However, the crystal, as a whole, has almost a uniform orientation. In the materials with high melting temperatures, the crystal of this kind is found to have a high quality. The crystal consists of the perfect crystals with the dimension less than 100 microns. Several or dozens of the perfect crystals gather with several seconds misorientation each other and form a crystal grain. The boundary between the crystal grains is observed in the etching patterns. The orientation difference between the crystal grains are about several minutes. Several crystal grains gather to form a large grain. The difference in their orientation are less than

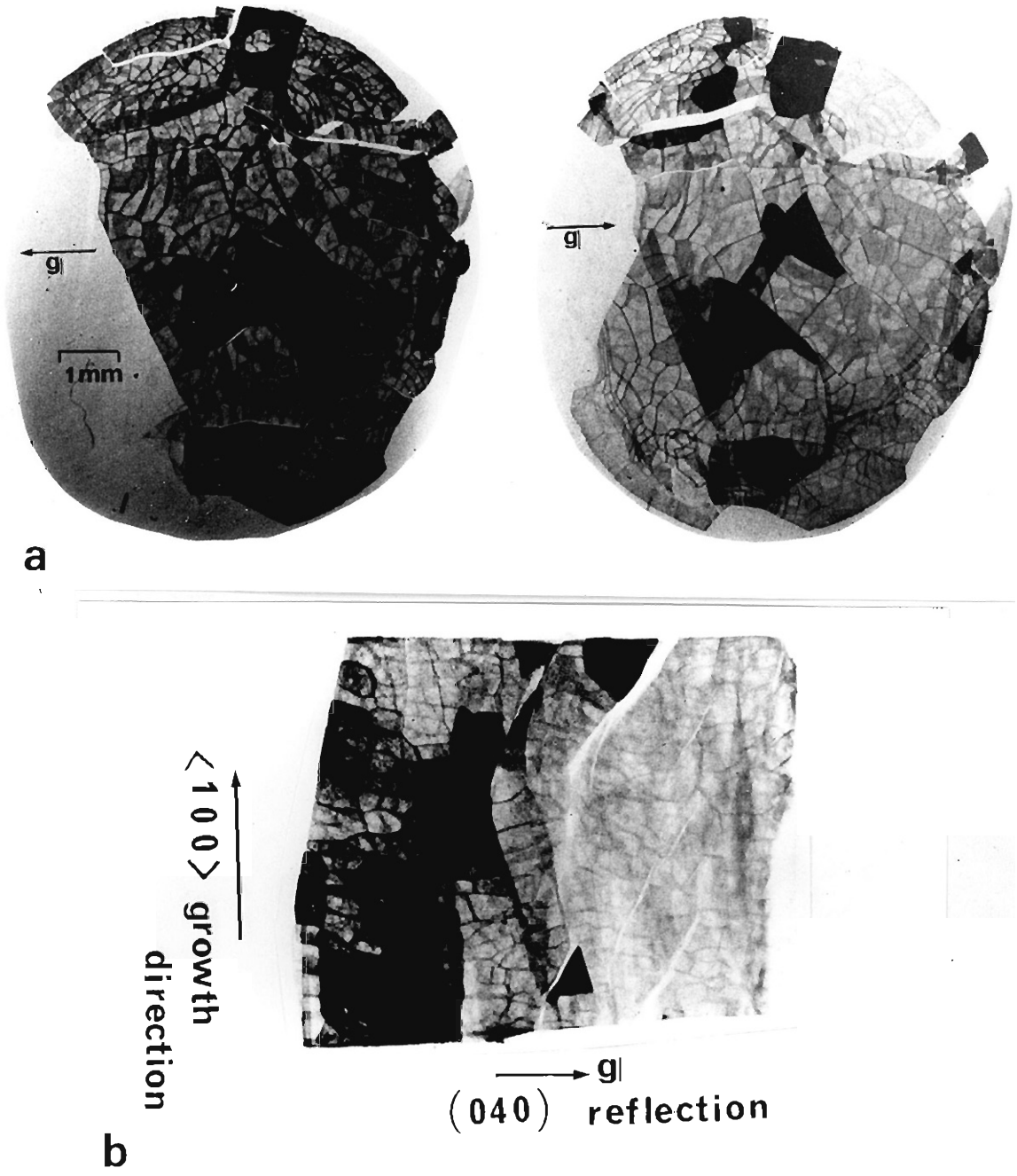

Fig. 54 X-ray transmission topographs of (a) normal plane (100) and (b) parallel plane (100) to the growth direction (100) of $TiC_{0.96}$ crystal rod. g denotes diffraction vector.

a few degrees. Several large grains constitute a crystal rod.

Figure 54(b) shows the topograph of (100) plane parallel to the growth direction. The parallel pattern along the growth direction was observed, but the crystallinity was essentially same as that shown in Fig. 54(a). The three dimensional network of the boundary is formed in the whole crystal. It is difficult to explain the existence of the three dimentional network formed during the growth because the defect structure do not prolong to the growth direction. Therefore, the three dimensional network is thought to be formed after growth. This defect structure was observed when the KCl crystal, which has low thermal conductivity and high thermal expansion, was prepared under the steep temperature gradient along the growth direction[55]. The carbide are not a material with so low thermal conductivity, but the crystal is prepared under the very steep temperature gradient(about 200 C/mm^2) because of their high melting point. Therefore, the microscopic defect is caused by a very steep temperature gradient along the growth direction.

2-6 Electrical resistivities of carbides

Transition-metal carbides have typically metallic properties. Their resistivities at room temperature are in the range of 20-250 x $10^{-8}\Omega$m[12]. However, these values are imperfectly known and varies widely from sample to sample. For example, the values for TiC range from 35 to 250 x $10^{-8}\Omega$m. The difference in resistivity values can usually be attributed to the sample(carbon-to-metal ratio, impurities, especialy oxygen, and porosity), as described in Chapter 1. Therefore, samples which were well characterized were prepared in the previous chapter and used in this measurement.

2-6-1 Sample preparation and measurement

Samples for measurements were cut from single crystal rods using a spark corrosion cutter. The rectangular samples which consisted of the (100) planes were etched briefly in a mixture of hydrofluoric and nitric acids at room temperature, and then washed in a supersonic bath to remove the surface residue. The size of samples was about 1 x 1 x 8 mm^3.

All resistivity measurements were performed at 4.2(or 77)K and 298K using a four-probe dc technique. Electrical currents were flown along the [100] axis. The uncertainty of measured resistivity is estimated to be $\pm$3 %, which is caused mainly by the uncertainty of distance between the potential probes. The uncertainty of composition analysis is estimated to be $\pm$0.3 %.

2-6-2 Results and discussion

The residual resistivity of TiC_x single-crystal is shown as a function of composition in Fig. 55. The residual resistivity arises mainly only from the carbon vacancies because the vacancies are main imperfections and not ordered. The resistivity increases with increasing the vacancy content. In order to explain the dependence of the resistivity on the composition, the following formula, which is used in the case of disordered alloy, was applied to this system:

$$\rho \propto \frac{x \cdot 1-x}{n} \qquad (1)$$

where ρ is a resistivity, x is a molar fraction of carbon vacancies and n is a carrier density.

In this case, the carrier density(n) can be thought to be 0.1 + x, because the stoichiometric TiC has about 0.1 conduction electron per mole[12], and also because the number of conduction electron per unit formula increases by the vacancy content in the nonstoichiometric carbides, according to the recent calculation of band structure[56]. The curve obtained from the formula(1) is also shown as a dashed line in Fig. 55. The measured values and the calculated curve agree well each other. Therefore, the residual resistivity of TiC could be explained from both the scattering of electron and the change in carrier density due to introduction of carbon vacancies.

Fig. 56 shows the residual resistivity of single-crystal NbC_x as a function of composition. Open circles show the values

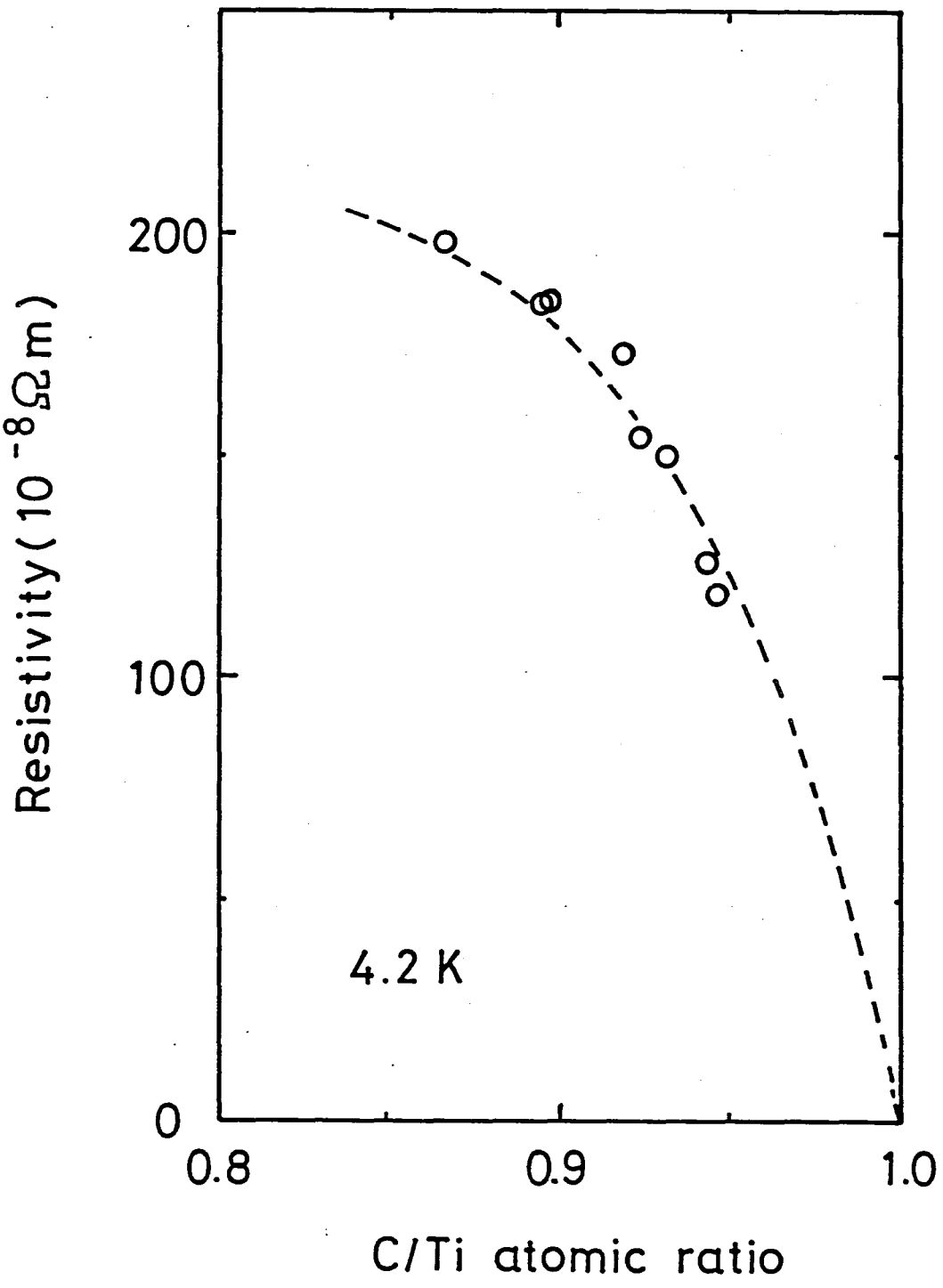

Fig. 55 Residual resistivity of single-crystal TiC_x as a function of composition. Open circles(O) show the measured values. The dashed line is derived from the formula($\rho \propto \frac{x \cdot 1-x}{0.1+x}$).

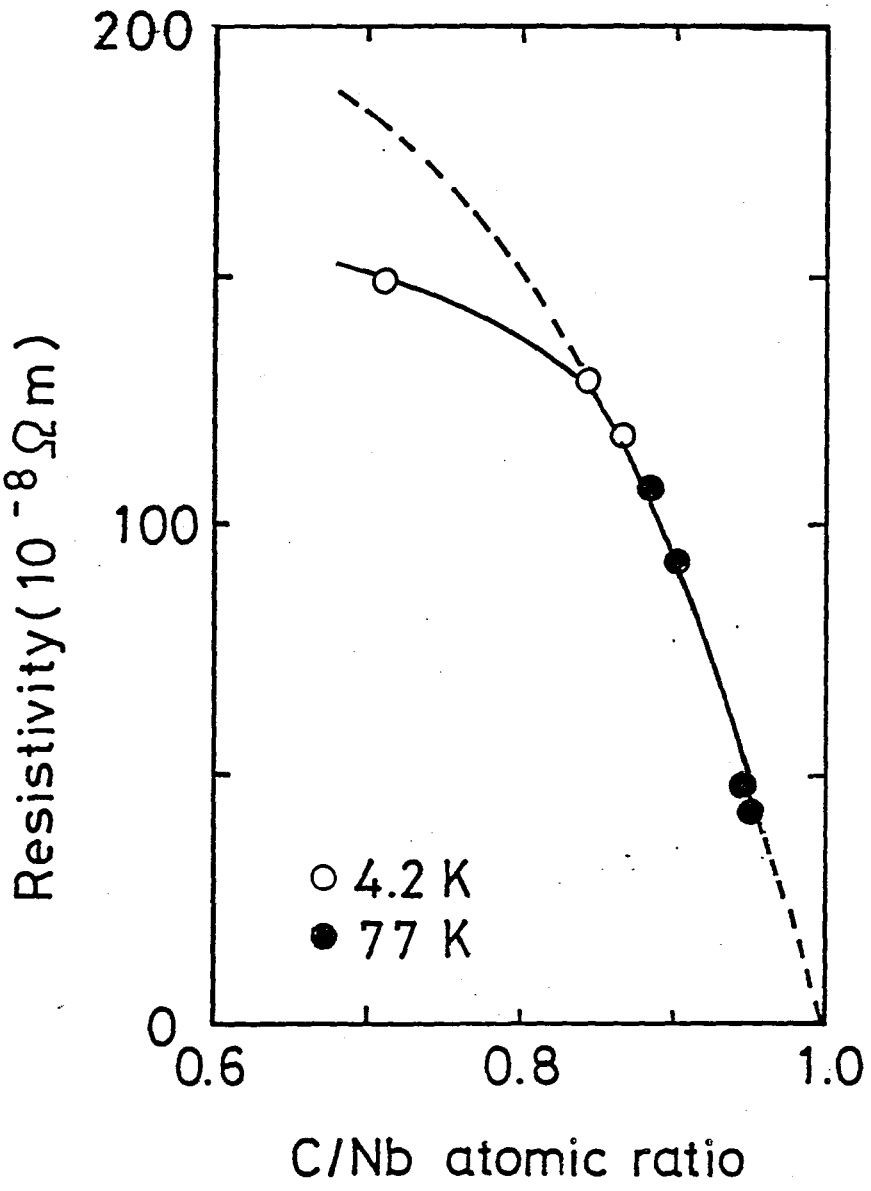

Fig. 56 Residual resistivity of single-crystal NbC_x as a function of composition. Open and close circles show the values measured at 4.2K and 77K, respectively. The dashed line is derived from the formula($\rho \propto \frac{x \cdot 1-x}{1+x}$).

measured at 4.2K. Close circles show the values at 77K. NbC became a superconductor at 4.2K in the composition region higher than 0.87-0.88 in C/Nb ratio. This result agrees well with the values already reported[12]. In the composition region higher than C/Nb=0.88, the residual resistivity was measured at 77K. The resistivity at 77K can be regarded as the residual resistivity because the resistivity of the carbides hardly change in the low temperature[12]. The dashed line in Fig. 56 shows the results calculated using the formula(1). Then, the depencence of carrier density (n) on the composition (1-x) was regarded as 1+x because a stoichiometric NbC has one conduction electron per mole[12] and the number of conduction electron increases by the content of introduced carbon vacancies, like the case of TiC[56]. The dashed line agrees well with the measured values in the composition region higher than C/Nb=0.85. However, when the carbon vacancy higher than 15 at% is introduced in the sample, the measured resistivity is lower than the calculated values. The reason is because the interaction between the vacancies lowers the increase of resistivity due to the reduction of effective vacancy concentration.

Figure 57 shows the resistivities of TiC_x and NbC_x as a function of composition at 298K. Their resistivities at 298K are almost the same as their residual resistivity. Therefore, their resistivities at room temperature are determined mainly by the introduction of vacancy. The difference between the resistivity at 298K and that at 4.2K is a few of $10^{-8}\Omega m$ in the defect-rich

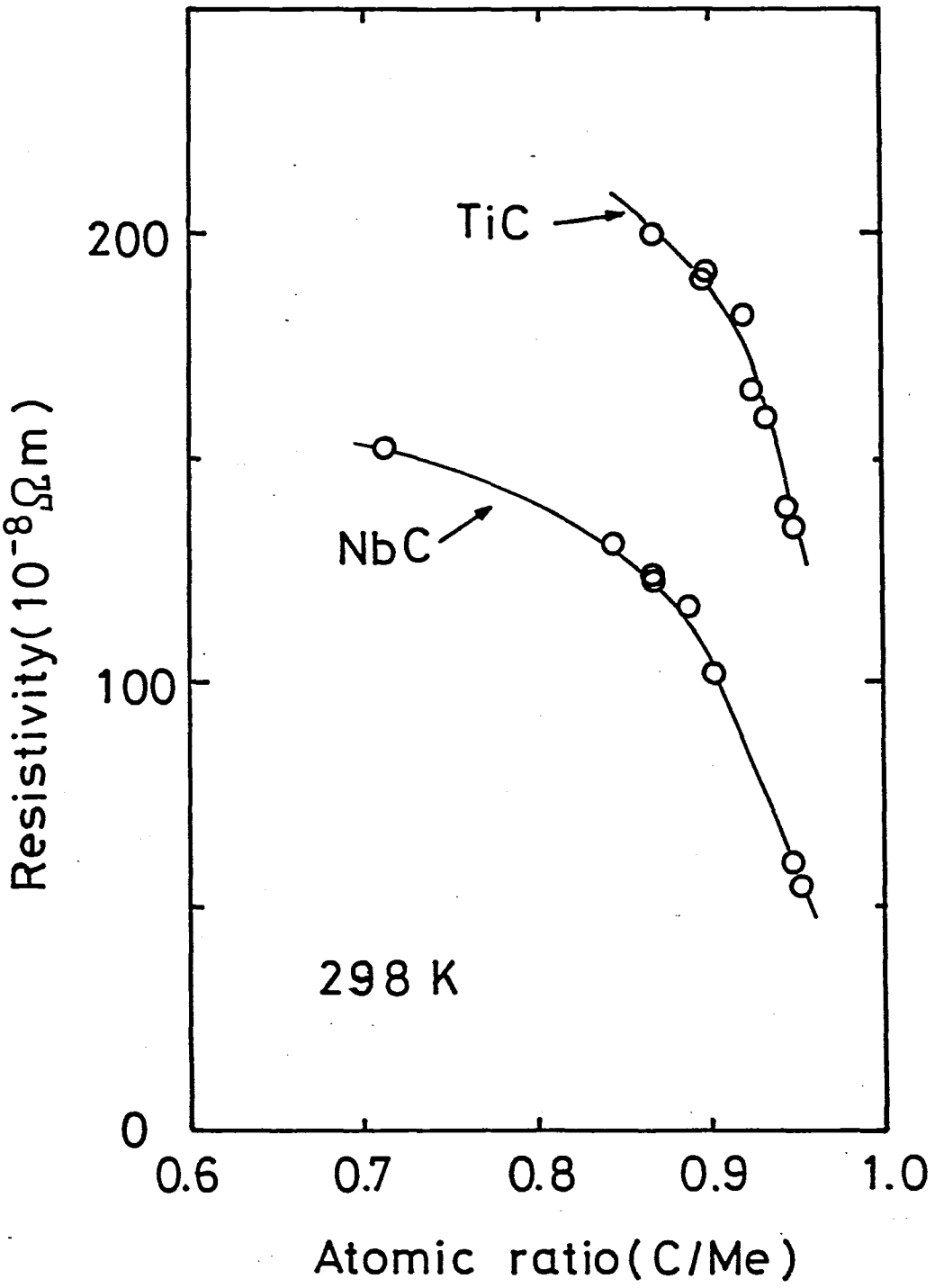

Fig. 57 Electrical resistivities of TiC_x and NbC_x as a function of composition at 298K.

region. The difference becomes larger as the composition approaches the stoichiometry. The cause is due to the fact that the carbide with near-stoichiometric composition have lower carrier density[57].

Figure 58 shows the resistivity of VC_x at 4.2K and 298K as a function of composition. VC_x has two ordered phases, that is, V_6C_5 and V_8C_7 phases. Their composition regions which were determined by X-ray powder diffraction are also shown in Fig.4. A disordered $VC_{0.749}$ has the highest resistivity and its resistivity at 4.2K and 298K is almost the same, like the case of TiC_x and NbC_x. However, in the composition region higher than C/V=0.76, the resistivity curves at 4.2K and 298K rapidly decrease with decreasing vacancy content although the resistivity of NbC_x did not decrease so much in the region of C/Nb=0.7 to 0.9, as shown in Figs. 56 and 57. This is due to the ordering of carbon vacancies. The resistivities at the ideal compositions of the V_6C_5 and V_8C_7 phases, that is, $VC_{0.833}$ and $VC_{0.875}$, show the minimum resistivity. In the V_6C_5 phase, the sample of $VC_{0.835}$ had the lowest residual resistivity of $27 \times 10^{-8} \Omega$ m. If the sample with the ideal composition($VC_{0.833}$) is prepared, the residual resistivity will decrease more. The lowest residual resistivity of V_8C_7 phase was 1.7×10^{-8} Ω m and its residual resistance ratio(RRR) was 17. This value is the best among the reported values($\rho = 3.2 \times 10^{-8} \Omega$ m, RRR= 10)[58]. In the V_6C_5 and V_8C_7 composition regions, the change in resistivity per one at% vacancy is small in the lower composition than the ideal

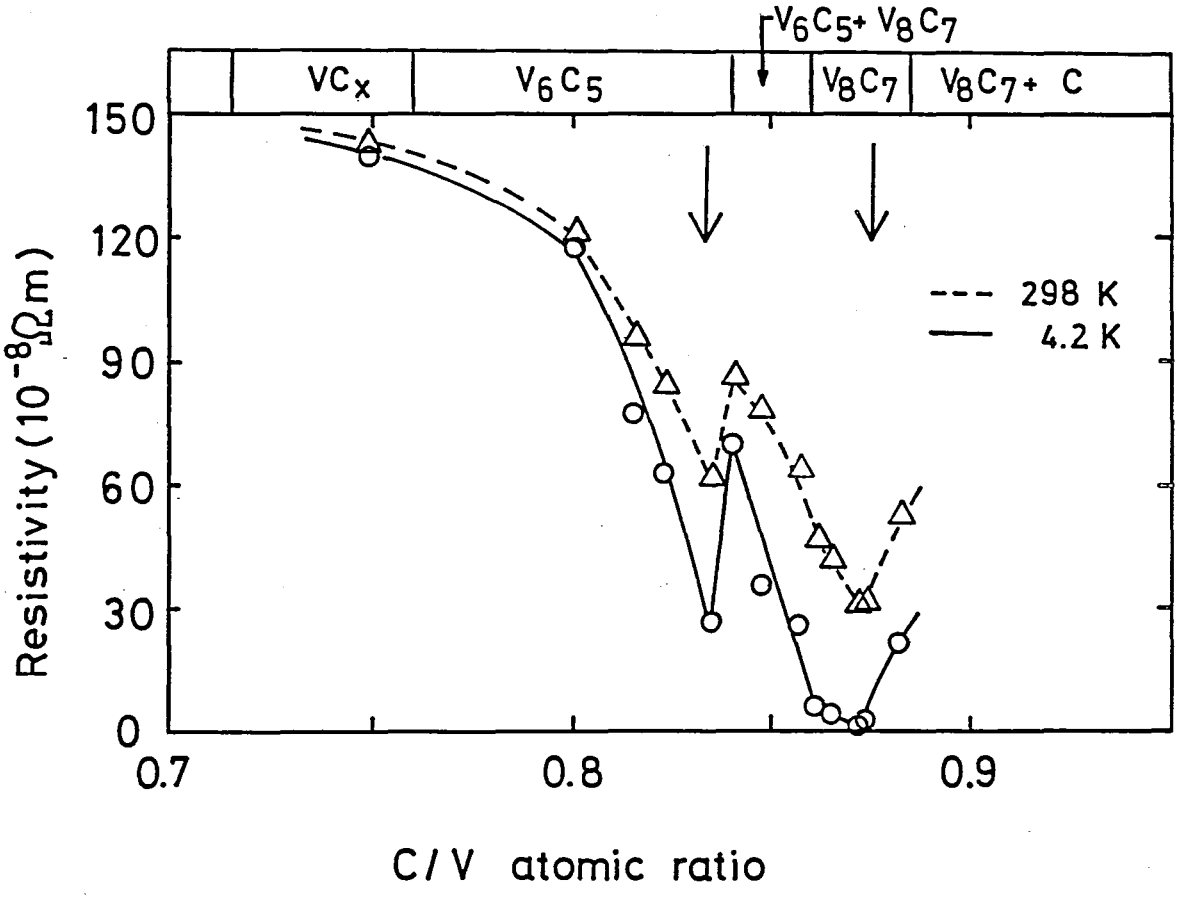

Fig. 58 Electrical resistivity of single-crystal VC_x as a function of composition at 4.2K and 298K.

composition, compared with that in the higher region. In both of phases, the vanadium sublattice is distorted a little by introduction of carbon into the octahedral sites because VC has the smallest octahedral sites among the carbides. Therefore, it can be easily understood that taking off carbon from the ideal V_6C_5 and V_8C_7 does not increase the resistivity so much as putting carbon into them.

2-6-3 Conclusion

In this section, the electrical resistivities of TiC_x, NbC_x and VC_x were measured at 4.2K(or 77K) and 298K. The measured results did not vary widely from sample to sample, compared with the already reported ones[12,58,59]. This is due to the fact that the high quality single crystal with defined compositions and low oxygen impurity content were prepared.

In TiC_x and NbC_x, the dependence of their residual resistivity on the composition were explained by the scattering of electron and the change in carrier density due to the introduction of carbon vacancies. However, in the composition region of higher than 15 at% of carbon vacancies of NbC_x, it was found that the interaction between the vacancies must be considered to understand the dependence of resistivity on the composition.

In VC, which has V_6C_5 and V_8C_7 ordered phases, the dependence of the resistivity on the composition corresponded to the composition regions where the ordered phases exist. The

lowest residual resistivity in V_8C_7 phase was $1.7 \times 10^{-8} \Omega m$, which was the lowest value among the reported ones. The residual resistivity will be become still lower by controlling the composition more strictly and removing the Mo and W impurities. If so, the Fermi-surface measurement will be made possible and the electronic structure and bonding characters of carbides will be understood more clearly.

3. TEMPERATURE DISTRIBUTION IN CRYSTAL RODS WITH HIGH MELTING POINTS PREPARED BY A RF FLOATING ZONE TECHNIQUE

The major problem of a floating zone technique is that the crystals are prepared under a steep temperature gradient because of the high melting points(> 2500 K). Hence, the temperature distribution within the growing crystal rod is an important factor to grow the good quality crystal. The temperature distribution can not be measured directly because of the high melting points. Therefore, the temperature distribution can be estimated only by calculation.

The temperature distribution along the thin rod and the power required to maintain the molten zone were calculated analytically using a one-dimensional model[60]. In this model, it is assumed that the zone temperature is maintained at the melting point, and the heat is conducted away through the crystal-zone interface into the crystal rod, and then the heat dissipated from the rod surface only by radiation.

The temperature distribution in a growing crystal rod and the power were already calculated numerically using a three-dimensional model in which the power is supplied to the rod surface[61]. However, unfortunately, this model can not be applied to the case of preparation of crystals by a RF floating zone technique, because the heat energy is supplied not only to the surface but also to the inner part of the molten zone and crystal. In the present study, using a simplified three-

dimensional model in which the power is supplied by RF heating, the temperature distribution in a growing crystal rod is calculated. Attention is paid to the temperature distribution along the grown crystal and the shape of the crystal-zone interface which influence the crystal quality[62].

In this chapter, the temperature distribution is generally calculated using a non-dimensionalized equation. The calculated results are compared with the experimental results in order to verify the present model. The characteristics and problems of the preparation of the single crystals with high melting points are disscussed. In addition, selecting TiC as a representative example, its temperature distribution is calculated using the modified model. The influence of each parameter on the temperature distribution is examined. Problems of preparing higher quality crystals are discussed.

3-1 Model and calculation

The model under investigation is shown in Fig. 59. The model is set up to be near the real growth conditions of the carbide crystals. The middle part of the rod is heated uniformly along the axial direction by RF heating. Its width is the same as the diameter of the rod. The power is supplied to form a zone with 60% length of the rod diameter. The supplied power is dissipated from the rod surface only by radiation. Both ends of the rod are thermally insulated. The properties of the heated material are independent of temperature and isotropic. The rod

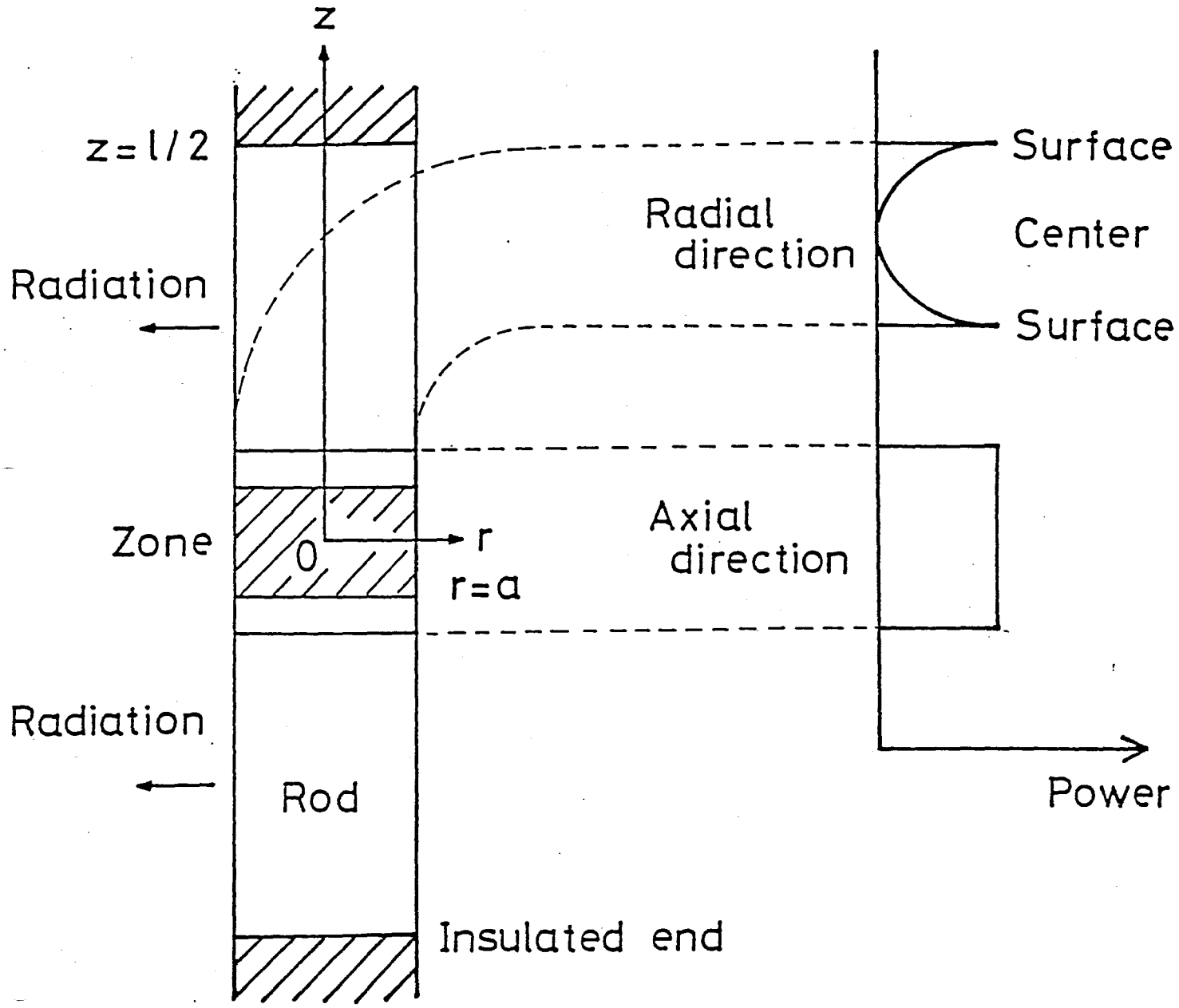

Fig. 59 Floating zone model.

and the molten zone have the same properties. The molten zone has a cylindrical shape. There is no convection in the molten zone. The system is at steady state. No latent heat is generated at the freezing and melting interfaces.

The heating distribution along the radial direction was calculated under the assumption that the rod was put in a homogeneous RF magnetic field, according to ref.[63]. The results are shown in Fig. 60. The heating radial distribution depends on the ratio(δ/a) of the skin depth(δ) to the radius(r=a) of the rod. In the case of a small ratio value, the induced current can be approximated by the equation($I_r/I_a = (a/r)^{0.5} * \exp(-(a-r)/\delta)$). When the ratio value becomes further small, the equation can be approximated by the equation($I_r/I_a = \exp(-(a-r)/\delta)$, which is used in the case of the plane with infinite thickness. In the case of a ratio value larger than 0.7, the induced current linearly decreases from the surface to the central point. No current is induced at the centrer. Fig. 60 also shows the radial distribution in the heating power($(Ir/Ia)^2$).

Under the assumption that the temperature does not change along the azimuth direction, the heat conduction equation in the steady state for cylindrical coordinations can be written as follows[64]:

$$\frac{1}{r}\frac{\partial}{\partial r}\left(r\frac{\partial T}{\partial r}\right) + \frac{\partial^2 T}{\partial Z^2} + \frac{w}{K} = 0 \qquad (1)$$

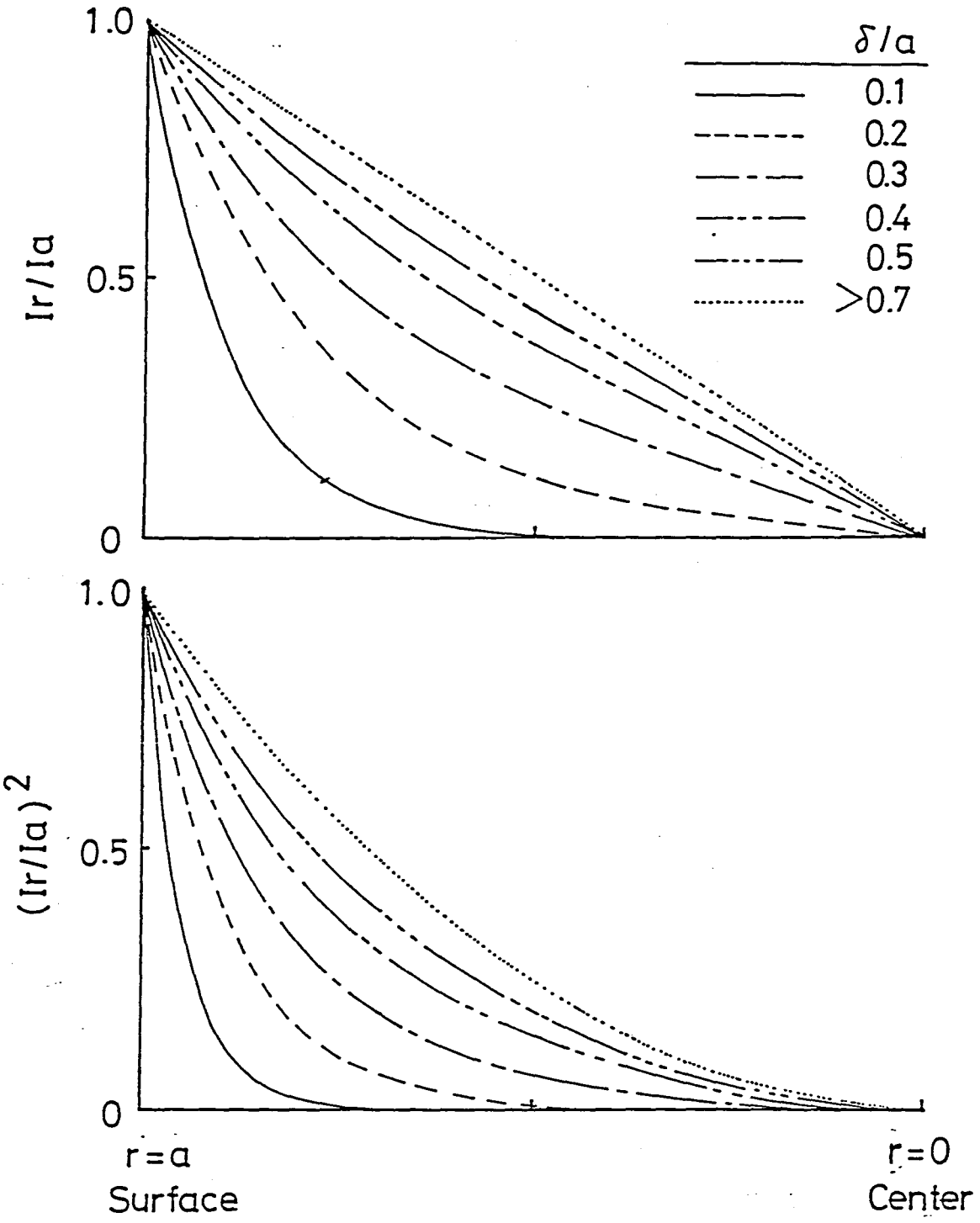

Fig. 60 Induced heating current and power distribution along the radial direction.

where k is the thermal conductivity, and

w is the generated heat per unit time and unit volume. In eq(1), the first term represents axial conduction, and the second term represents radial conduction.

The boundary conditions are: at the axis(r=0, $0 \leq z \leq \ell/2$)

$$\frac{\partial T}{\partial r} = 0, \qquad (2)$$

at the midplane($0 < r < a$, z=0)

$$\frac{\partial T}{\partial Z} = 0, \qquad (3)$$

at the rod surface(r=0, $0 \leq z \leq \ell/2$)

$$-k\frac{\partial T}{\partial r} = e\sigma T^4 \qquad (4)$$

and at the rod end($0 < r < a$, $z = \ell/2$)

$$\frac{\partial T}{\partial Z} = 0, \qquad (5)$$

where e is the emissivity, σ is the Stefan-Boltzmann constant, a is the rod radius and ℓ is the rod length. The heating distribution along the radial direction is supplied, as shown in Fig. 60. The heated width along the axial direction is from z=0 to a. Power required to keep the zone is obtained by integrating the energy dissipated from the surface.

The dimensionless variables are introduced to generally solve the equation: R=r/a, Z=z/a. The non-dimensionalized heat conduction equation in the steady state for cylindrical coordinates can be written as follows:

$$\frac{1}{R}\frac{\partial}{\partial R}\left(R\frac{\partial\theta}{\partial R}\right)+\frac{\partial^2\theta}{\partial Z}+\frac{P}{k\,T_m\,a}=0$$

where R=r/a, Z=z/a, $\theta=T/T_m$ and p is the power(= wa^3). Here, T_m is the melting point. The boundary conditions are: at the axis(R=0, $0 \leq Z \leq L/2$)

$$\frac{\partial\theta}{\partial R}=0,$$

at the midplane($0<R<1$, Z=0),

$$\frac{\partial\theta}{\partial Z}=0,$$

at the rod surface(R=1, $0 \leq Z \leq L/2$),

$$-\frac{\partial\theta}{\partial R}=Bi\cdot\theta^4$$

and at the rod end($0<R<1$, Z=L/2)

$$\frac{\partial\theta}{\partial Z}=0,$$

where L is the dimensionless rod length(ℓ/a) and Bi is the Biot number(= $e\sigma(T_m)^3a/k$), which means the ratio of heat transfer by radiation to transfer by conduction at the rod surface. The heating distribution along the radial direction is also shown in fig.56. The heated width along the axial direction is from Z= 0 to 1.0.

The equation is solved by a relaxation method, as follows. The rod is divided into imaginary blocks of given length. Relatively small steps are used near the interface where the temperature varies considerably. Initial values are given to

each block and the temperature of each block is calculated in turn to adjust the heat balance. This calculation is repeated until the changes in the temperature of all the blocks by calculation are small than 0.5 K or 1.6×10^{-5}.

3-2 Experimental

In order to verify the calculated results, crystals of Mo and TiC, which have the lowest and highest Biot numbers, as seen in Table 32, were prepared by a RF floating zone technique(200 kHz). The experimental procedure to prepare the crystals was described in Chapter 2. Temperature distributions along the crystal rods and the crystal-zone interface shapes were examined. These crystals had to be prepared at 3-5 x 10^5 Pa of helium gas ambient because of suppressing arc discharge between the turns of the work coil and reducing the evaporation from the molten zone. Some heat energies are dissipated away from the rod surface by the ambient gas too. In order to examine the influence of the ambient gas on temeperature distribution, the relationship between the zone temperature(T_z) and the power was measured at 3 x 10^5 Pa of helium gas pressure as described below. Two pieces of the crystal rods with 0.5 cm radius and 4 cm length were mounted at the upper and lower shafts in the furnace. The carbon disk was put between them and the part around the disk was melted to form the molten zone. Next, the temperature at the interface corresponding to the zone temperature(T_z) was measured using a two color pyrometer, which was calibrated up to 2800K and

Table 32 Properties of materials at melting points[36,65]
The rod radius is 0.5 cm. The radio frequency is 200 kHz.

	Mo	W	LaB_6	ZrB_2	TiC	TaC
T_m(K)	2883	3650	2988	3310	3100	3800
k(W/mK)	84	92	29	38	35	70
e	0.28	0.34	0.7	0.7	0.75	0.52
ρ ($10^{-8}\Omega$ m)	81.4	123	210	110	340	195
Bi	0.02	0.05	0.18	0.19	0.18	0.12
δ/a	0.20	0.25	0.33	0.24	0.41	0.31

extrapolated above 2800K. Then the power required to keep the molten zone at temperature(T_z) was obtained from the anode loss.

The interface shape of Mo could not be observed because the molten zone could not be quenched due to a high crystallization velocity. Therefore, the polycrystalline rod with 0.5 cm radius was melted and the initial molten zone, i.e., the zone before the zone pass starts, was observed. The interface of TiC was examined after the second zone pass because the sintered feed rod has a low density in the first zone pass.

The temperature distribution along the rod above the molten zone was measured using the two color pyrometer. Holes(1.5 mm$^{\phi}$x 2 mm) were made in the Mo rod(1 cm$^{\phi}$x 30 cm) in order to lessen the effect of reflection from the wall and the difference between the emissivities at two wave lengthes(λ=0.5 and 0.58 μ). The temperature distribution below the zone was not measured because this part could not be observed directly from the view port due to the existence of the work coil.

3-3 Calculated results and comparison with experimental results

The temperature distribution in the crystal rod is calculated by the heating parameter(δ/a) and the Biot number(Bi) in the model shown in Fig. 59. Table 32 shows the thermal properties of the major refractory materials and their electical resistivity at their melting points[36,65]. When the rod radius is 0.5 cm, Biot numbers are 0.02-0.2. Because of a high thermal

conductivity, metals have lower Biot numbers than the compounds. The heating parameter(δ/a) is 0.2-0.6, when the radio frequency is 200 kHz. Therefore, we calculated the temperature distributions in the cases of Bi=0.01, 0.1, 1.0 and δ/a=0, 0.2, 0.7. The rod length(L) was 160, 80 and 40 in the case of Bi=0.01, 0.1 and 1.0, respectively. These values of length can be regarded as infinite.

3-3-1 Temperature distribution along crystal rod

Fig. 61 shows the temperature distribution at the surface along the growing crystal. The solid line indicates the temperature distribution along a crystal rod heated by the heating parameter of δ/a=0.7, i.e., with deep power penetration(small skin effect). The dashed line indicates the temperature distribution obtained from the one-dimensional model[60]($T(z)=T_m(1+z/\lambda_o)^{-2/3}$, where z is the distance from the crystal-zone interface and $\lambda_o=(5k\pi/9e\sigma T_m^3)^{0.5}$). The temperatures along the rod are slightly higher than those in the one-dimensional model. When the Biot number increased, the difference in the temperature between both models is larger. This result stems from the following two reasons. One is that the part(Z=0.6-1.0) just below the zone is heated in case of the present model, but not in the one-dimensional model. Second is that the temperature difference along the radial direction was considered in the present model. The temperature distribution in the the case of surface heating(δ/a=0) is almost consistent with that in the

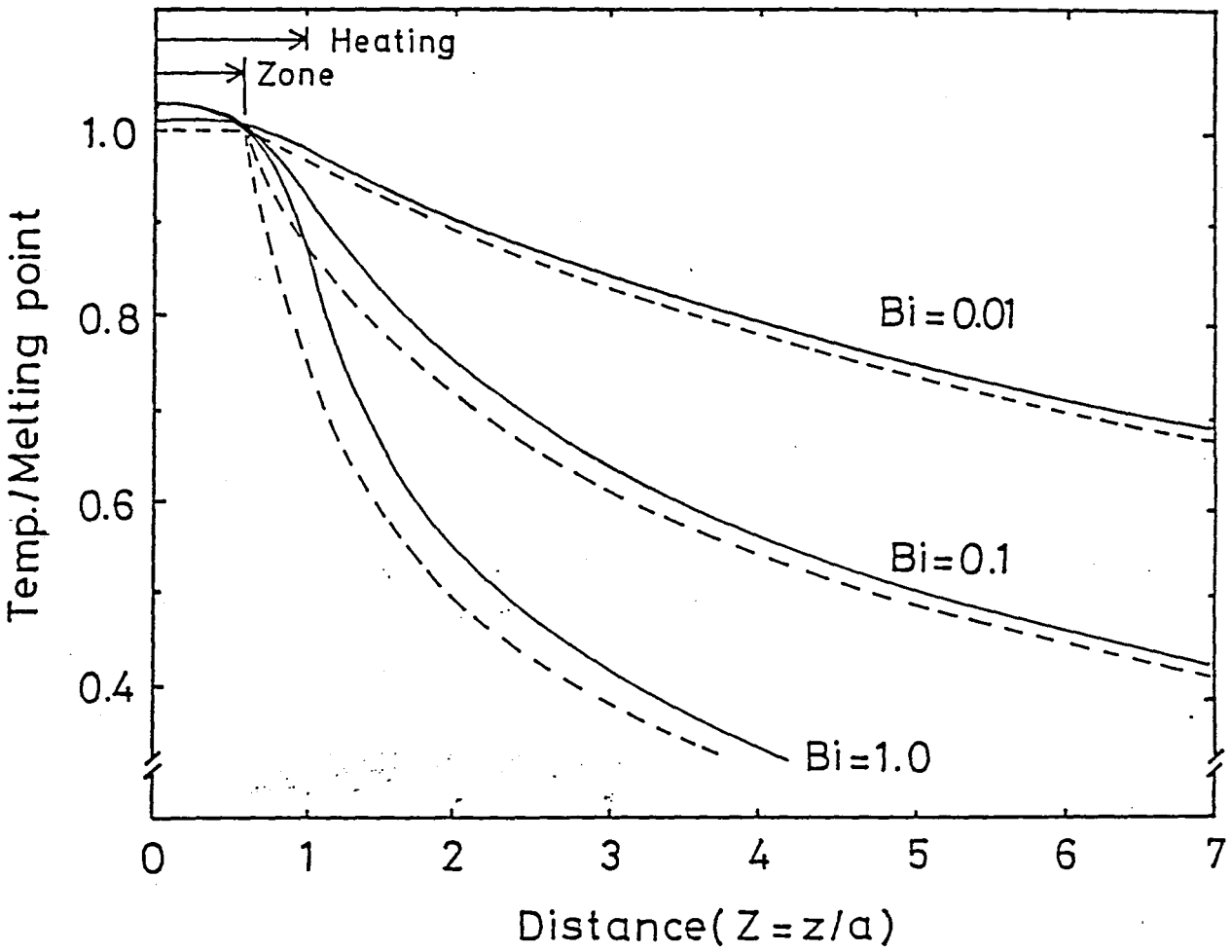

Fig. 61 Temperature distribution at the surface along the grown crystal when the heating parameter(δ/a) is 0.7. The dashed lines show those obtained from the one-dimensional model[60].

one-dimensional model, but the central part of the molten zone is then not melted, as described in ref.[61]. In the case of Bi=0.01(well conducting metals), the temperature gradient is flat. Hence, in the case of preparing the crystal with a limited length, the temperature distribution tends to be influenced by the thermal condition at both ends of the rod[66]. The temperature distribution of refractory metal rods with Biot numbers of 0.02-0.05 is almost similar to this case. Most of the refractory compounds correspond to the case of Bi=0.1. Hence, the crystal rod with melting point of 3100K and 0.5cm radius is prepared at a maximum temperature gradient of about 160K/mm. In the case of Bi=1.0, the temperature gradient close to the molten zone is very steep. The steep temperature gradient affects the quality of the grown crystal and may form cracks in the crystal rod by thermal stress. Hence, the influence of the rod ends on the temperature distribution is only small.

Fig. 62 shows the ratio of the lost power to the supplied power as a function of the distance from the molten zone center. In the case of Bi=0.01, 12% of the supplied power is lost from the zone surface. Two thirds of the power are lost until the distance of Z=7. Ninety per cent is lost until Z=20. In the case of Bi=1.0, it is found that 50% of the supplied power is lost already from the zone surface. The power lost until a distance of Z=2 is already higher than 90%. Most of the hesting energy is lost from the crystal region near the molten zone because the energy loss by radiation is proportional to the

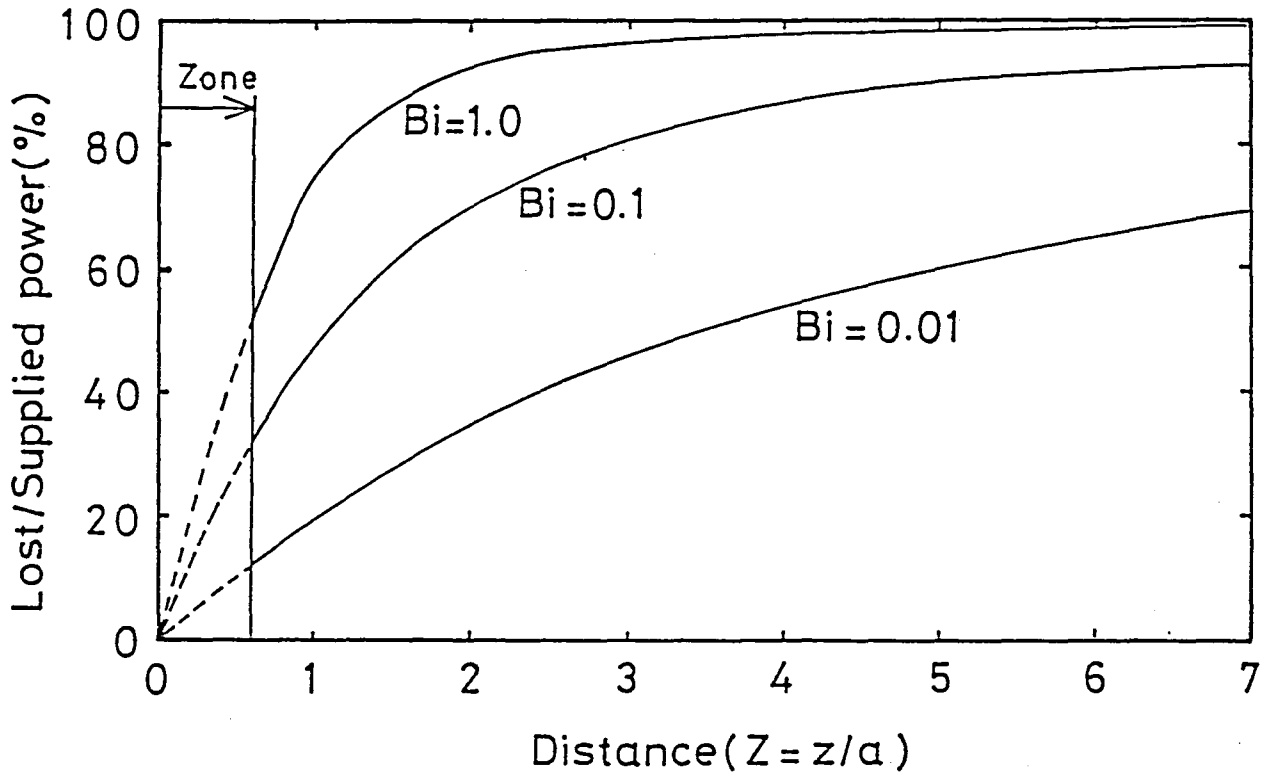

Fig. 62 Ratio of lost power to supplied power as a function of distance from zone-center.

fourth power of temperature(T^4).

3-3-2 Shape of crystal-zone interface

Fig. 63 shows the solid-liquid interface shapes of the crystal with various Biot numbers(Bi=0.01, 0.1 and 1.0) for three different heating parameters(δ/a=0, 0.2 and 0.7). The shaded portion is the molten zone. The isotherms are drawn at intervals of θ=0.0322, corresponding to 100K if the interface temperature is 3100K.

In the case of surface heating(δ/a=0), the interface shape is always convex toward the molten zone because the surface temperature is highest. The crystal with low Biot number has a relatively low convex interface. When the Biot number becomes larger, the interface shape becomes more convex. In the RF heating cases of δ/a=0.2 and 0.7, the interface shape is undulated or concave toward the molten zone. The reason is that despite the surface is heated most, it is cooler than the less heated adjacent interior because of the radiation from the surface. In the case of Bi=0.01, the temperature gradient is small and the interface shape is nearly flat. When the Biot number becomes larger, the surface is cooled more by radiation. Only when both the Biot number and the heating parameter are large, the interface shape is concave.

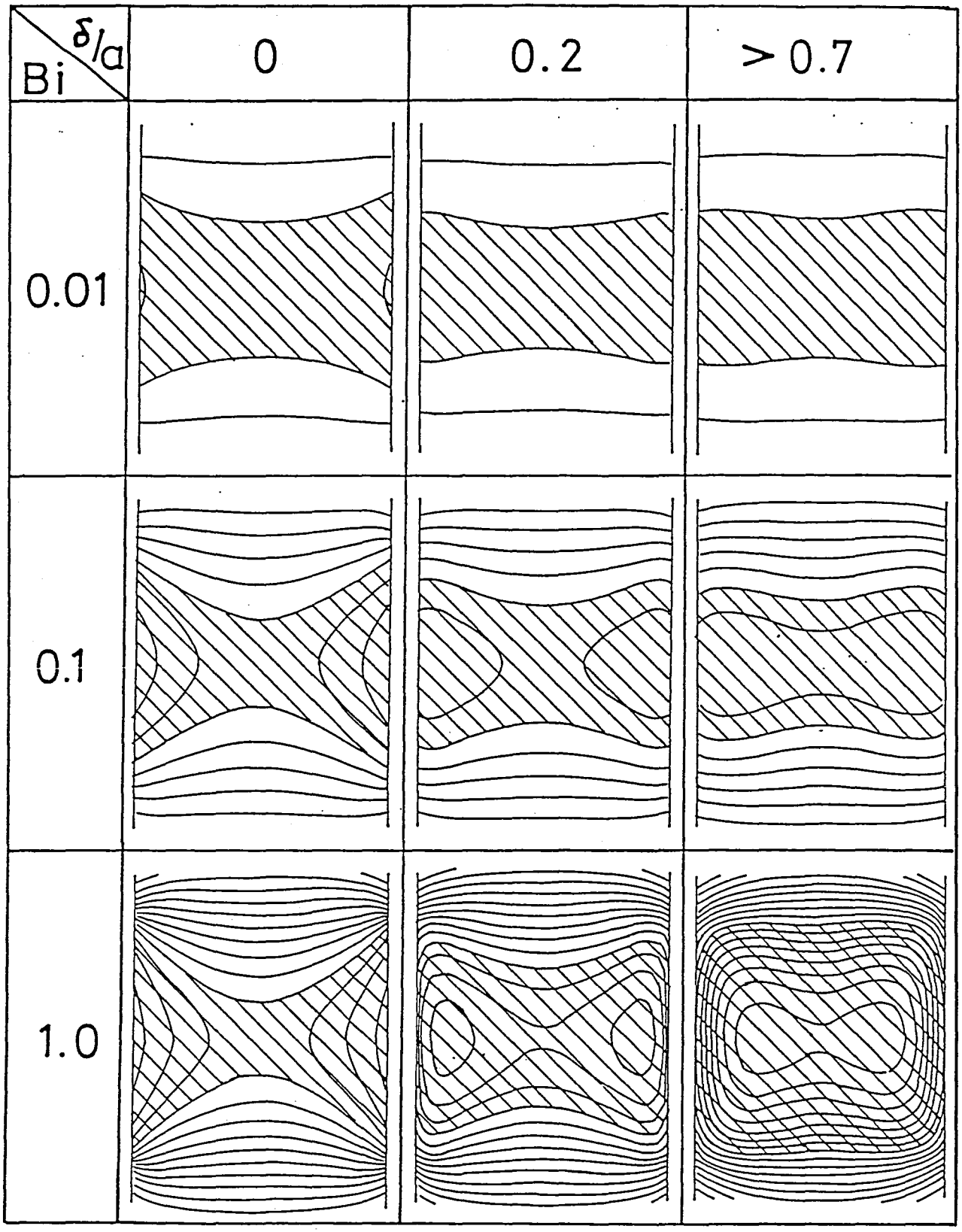

Fig. 63 Shape of crystal-zone interfaces. The shaded portion is the zone. Isotherms are drawn at intervals of θ=0.0322.

3-3-3 Comparison between the experimental and calculated results

Figs. 64 and 68 show the temperature distributions of the Mo and TiC rods along the growth direction. The calculated results agree with the experimental results. Figs. 65 and 66 show the calculated temperature distributions and the cross sections of Mo and TiC rods. Each interface shape agrees well with the calculated result. Hence, the presented model well explains the temperature distribution in the high temperature part of the growing crystal rod.

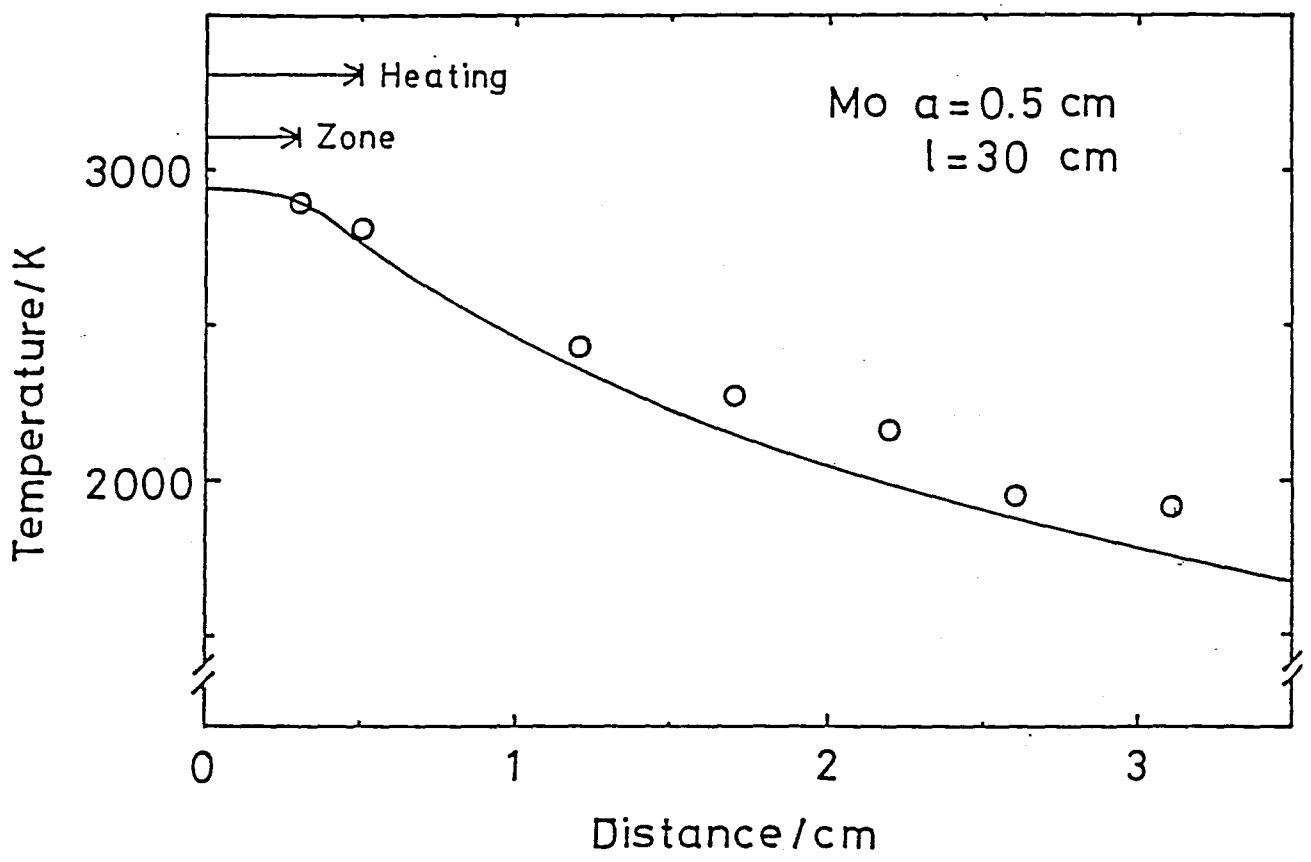

Fig. 64 Temperature distribution along Mo rod. Solid line and circles(O) indicate calculated and measured values, respectively.

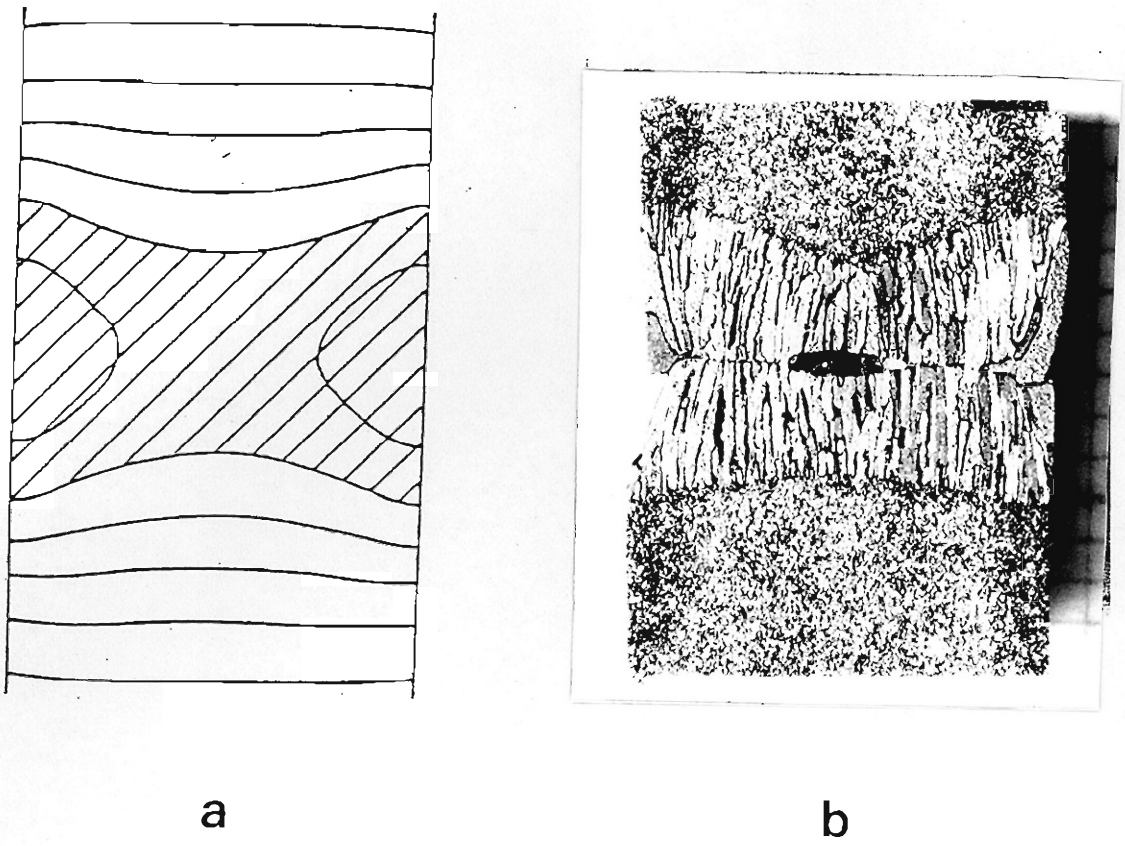

Fig. 65 (a) Calculated temperature distribution of Mo rod. The temperature of interface is 2883 K. Isotherms are drawn at intervals of 100 K. (b) Photograph of the longitudinal cross section of the nitial molten zone of Mo rod.

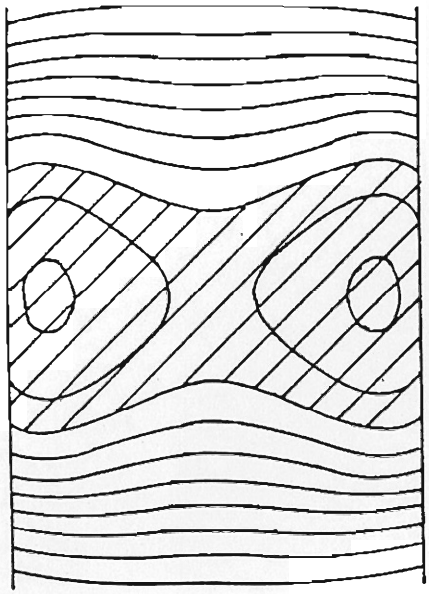

Fig. 66 (a) Calculated temperature distribution of TiC rod. The temperature of interface is 3100K. Isotherms are drawn at intervals of 100K. (b) Photograph of the longitudinal cross section of the molten zone of TiC crystal rod. The part below the zone is the crystal.

3-4 Temperature distribution in a growing TiC crystal rod

The properties of $TiC_{0.96}$ crystal at the melting point are listed in Table 32. The reasons why these values were adapted are described below. The $TiC_{0.96}$ crystal, which has the least carbon defect, is prepared at about 3100K by a RF heating(200 kHz). The thermal conductivity(k) and electrical resistivity(ρ) at the melting point is obtained to be 35 $W m^{-1} K^{-1}$ and $3.4 \times 10^{-6} \Omega cm$, respectively, by the extrapolation from the present measuremental results up to 1300K. These values are reasonable, comparing with the data described in refs.[36] and [65]. The emissivity(e) is adapted to be 0.75 from ref.[36]. These properties are assumed to be independent of the temperature because these properties does not change so much at the high temperature region. Rod radius(a) and zone length(l_z) are 0.5 cm and 0.6cm, respectively, because the size of grown crystal rod generally has the radius with 0.4-0.5cm and the molten zone length with 0.5-0.6cm. The heated length(l_h) is assumed to be 1.0cm because the work coil thickness is about 0.8cm. The temperature(T_{shield}) of the radiation shield, which is the inside wall of the chamber, is estimated to be 350K because the ambient helium gas pressure increases by 15-17% during a zone pass. Therefore, the boundary condition(4) is presented to be

$$-k \frac{\partial T}{\partial r} = e\sigma (T^4 - T_{shield}^4).$$

The latent heat at both interfaces is neglected because the temperature gradient is steep. Using these materials constants,

the temperature distribution is calculated using the equation(1). Table 33 listed the conditions used for numerical calculation. The influence of each parameter on the temperature distribution is examined.

3-4-1 Relationship between zone temperature and heating power

The relationship between zone temperature(T_z) and power(p) required to keep the molten zone had been calculated analytically using a one-dimensional model[62]. The relationship between T_z and P is $p=2.4\pi a e\sigma (T_z)^4(\lambda_o+a)$ where $=(5ka/(9e\sigma(T_z)^3)^{0.5}$. In the case when the heat is lost from only the zone($\lambda_o << a$), only the latter term contributes to the power, which is proportional to T_z^4, because the temperature gradient along the rod is very steep. On the other hand, in the case when the heat is mainly lost from the rod surface($\lambda_o >> a$), only the former term contributes to the power, which is proportional to $(T_z)^{2.5}$. Therefore, the power is proportional to $(T_z)^{2.5-4}$.

The TiC crystal must be prepared at 3-5 x 10^5 Pa of the ambient helium gas pressure condition, as described in Chapter 2. The influence of helium gas pressure on power was examined. Fig. 67(a) and (b) show the both calculated results on the zone temperature-power relationship and the experimental data, respectively. In the calculated results, the power required to keep the molten zone at the temperature(T_z) is proportional to $(T_z)^{3.1}$. The result is consistent with that obtained from the

Table 33 Conditions used for numerical calculation

Frequency	50, (200), 2000	kHz
Radius(a)	0.25, (0.5), 1.0	cm
Temperature of radiation shield(T_{shield})	0, (350), 2000	K
Heated length(l_h)	0.6·a, (2·a), 4·a	cm
Zone length(l_z)	1.2·a	cm
Rod length(l)	40·a	cm

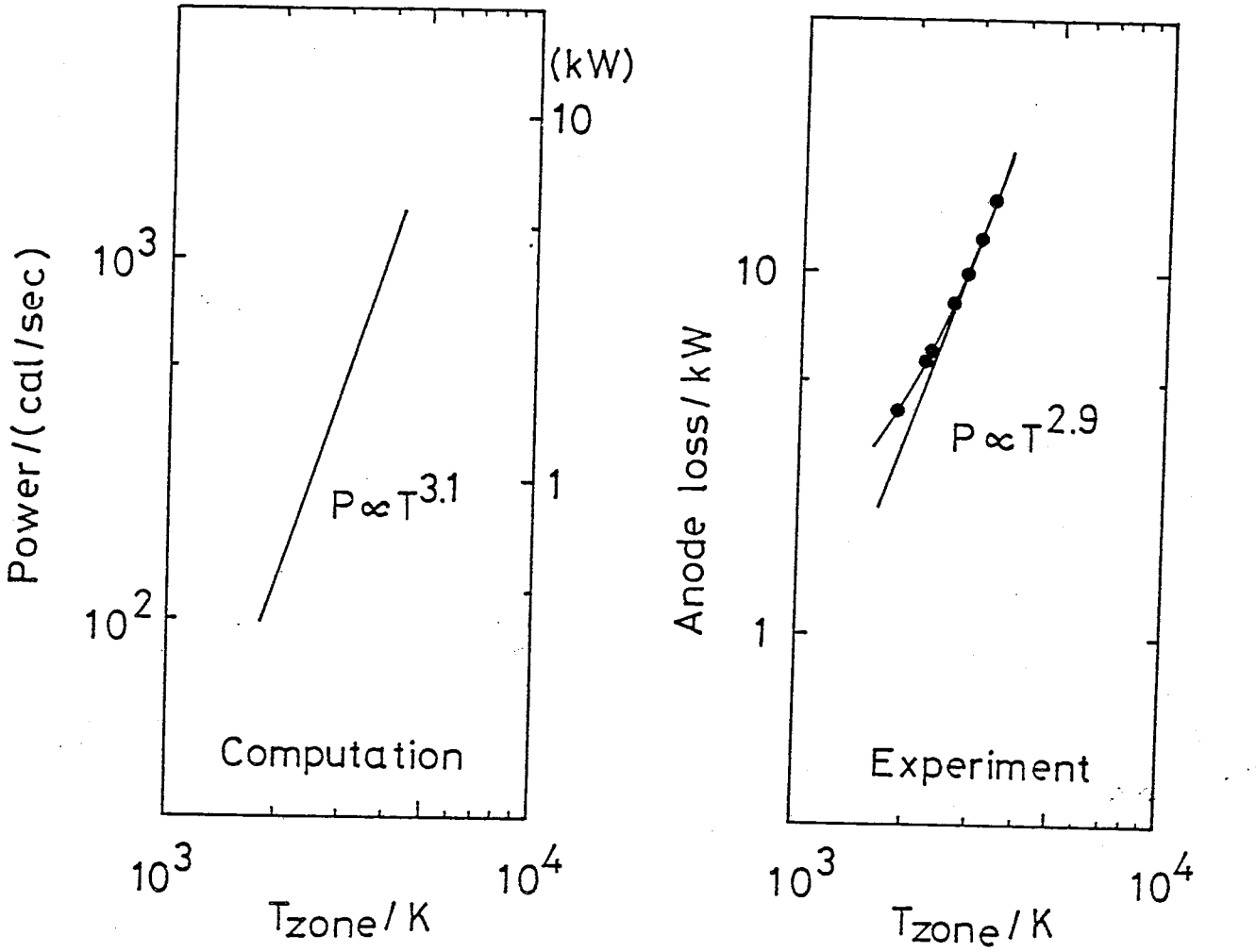

Fig. 67 Relationship between the zone temperature and the heating power. The zone length is regarded as 1.2 (radius) at the surface.

one-dimensional model[60]. On the other hand, in the present experimental results, the power is proportional to $(T_z)^{2.9}$ at temperature higher than 2500K. The calculated result is almost consistent with the experimental one. However, at lower temperature than 2500K, the power does not change according to the $(T_z)^{2.9}$ rule. This fact indicates that the heat loss due to the ambient gas can not be neglected at the lower temperature than 2500K. However, when the zone temperature is higher than 2500K, most of the supplied power is found to be lost as a radiation energy. This consideration was supported by the experimental results shown in Fig. 48. Therefore, the helium gas hardly influences the temperature distribution at the high temperature part because the radiation energy is mainly lost from the high temperature part.

As seen in Fig. 67, it is found that about 12% of the anode loss of an oscillator tube is consumed for keeping the molten zone because the $TiC_{0.96}$ crystal is prepared at 3100K.

Furthermore, the relationship between the power and the crystal radius(a) was calculated, when the zone length at the surface was 60% of the rod diameter. The power required to keep the molten zone is proportional to $a^{1.7}$ in the range of a=0.1 to 1.5cm. This result is also consistent with that calculated from the one-dimensional model.

3-4-2 Temperature distribution along growth direction

It is well-known that the temperature gradient infuluences

the quality of the crystal. It was pointed out that the large temperature gradient along the crystal rod forms the labyrinth defect structure(three dimentional network defect structure) in the KCl crystal prepared by a CZ technique[67,68]. The defect structure which was similar to the labyrinth structure was observed as shown in Fig. 54.

Fig. 68 shows both the calculated temperature distribution at the surface along the growth direction and the experimental data(o). As seen in this figure, the calculated result agreed with the experimental data. The temperature gradient becomes maximum at the part(z=0.8) just below the zone. Its values is about 200 K/mm, which is too steep to grow the high quality crystal. Therefore, the temperature gradient at the part from the zone to 1cm distance, which is above 2000K, must be decreased by using an after-heater.

Further, Fig. 68 shows the ratio of lost power(from the midplane to the distance) to supplied power. Thirty five per cent of the supplied power is lost from the zone surface. The power lost until the distance of z=2 cm is higher than 90%. Therefore, most of the supplied power is found to be lost from the part near the zone because the energy loss due to radiation is proportional to the temperature of the fourth power(T^4). This fact indicates that the power required to keep the molten zone is hardly influenced by the thermal conditions at the rod ends during a zone pass. That is to say, the heat loss hardly changes during a zone pass as far as the growth temperature(the

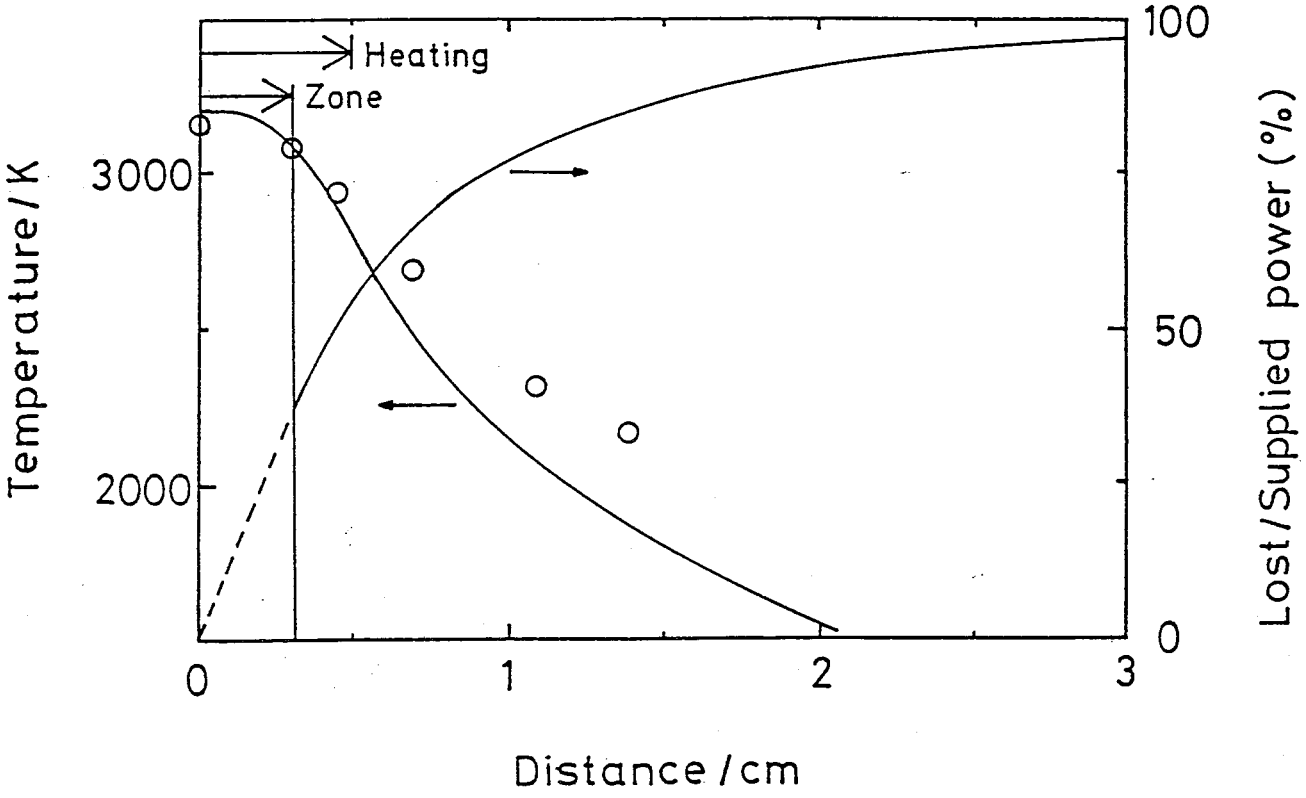

Fig. 68 Temperature distribution of TiC rod at surface along growth direction and ratio of lost power to supplied power as a function of the distance from zone-center when temperature of radiation shield is 350K. Circle(o) indicates the measured temperature of the rod.

zone composition) does not change. Actually, when the TiC crystal was prepared by a modified zone leveling method, the heating power hardly needed to be controlled during a zone pass as already described in hapter 2.

3-4-3 Shape of crystal-zone interface

It is expected that the interface shape depends on both the temperature and compositional distributions along the radial direction near the interface. The chemical composition of TiC crystal rod hardly changed along the radial direction within the limits of error as already described in Chapter 2. This fact suggested that the interface shape is determined by the temperature distribution.

Fig. 66(a) shows the temperature distribution at the molten zone and the just grown crystal of $TiC_{0.96}$. The shaded portion is the molten zone. The temperature at the interface is 3100K. The isotherms are drawn at intervals of 100K. Fig. 66(b) shows the longitudinal cross section of the $TiC_{0.96}$ crystal rod. The calculated result agrees well with the crystal-zone interface shape. This result suggests that the heat is lost mainly by radiation at the high temperature part. It is found that the convection in the molten zone does not influence the temperature distribution because TiC has a relatively high thermal conductivity.

The shape of the interface is convex at the middle part and concave at both ends. The surface temperature is decreased by

radiation though the surface is most heated, as shown in Fig. 60. This causes the single crystal to be surrounded by the polycrystalline rim with about 1 mm thickness because the grains grow normal to the interface as already described in chapter 2.

The heat which dissipates through the interface is estimated to be about 75 cal/sec from the data of thermal conductivity(35 $W m^{-1} K^{-1}$), the average temperature gradient(1130 deg/cm) at the interface and the cross section($0.5^2 \pi cm^2$). On the other hand, the latent heat at the interface is about 0.84 J/sec because the crystal is prepared at a growth rate of about 2 g/h(0.5 cm/h) and the freezing heat of TiC is 1390 J/g[36]. Therefore, it is reasonable for the latent heat to be negligible in the present model.

From the above results, this model was found to be valid. Therefore, the influence of each parameter on the temperature distribution are examined below.

3-4-4 Effect due to radio frequency

The effect of the radio frequency on the interface shape was examined, as shown in Fig. 69. The frequency is related to the heating distribution, as shown in Fig. 70. When the frequency is 50 kHz, which deepestly supplies the power to the molten zone, the position with the maximum temperature along the radial direction near the interface moves slightly to the inner part, compared with that of 200 kHz. Therefore, the polycrystalline rim becomes a little more thick. In the case of 2 MHz, the

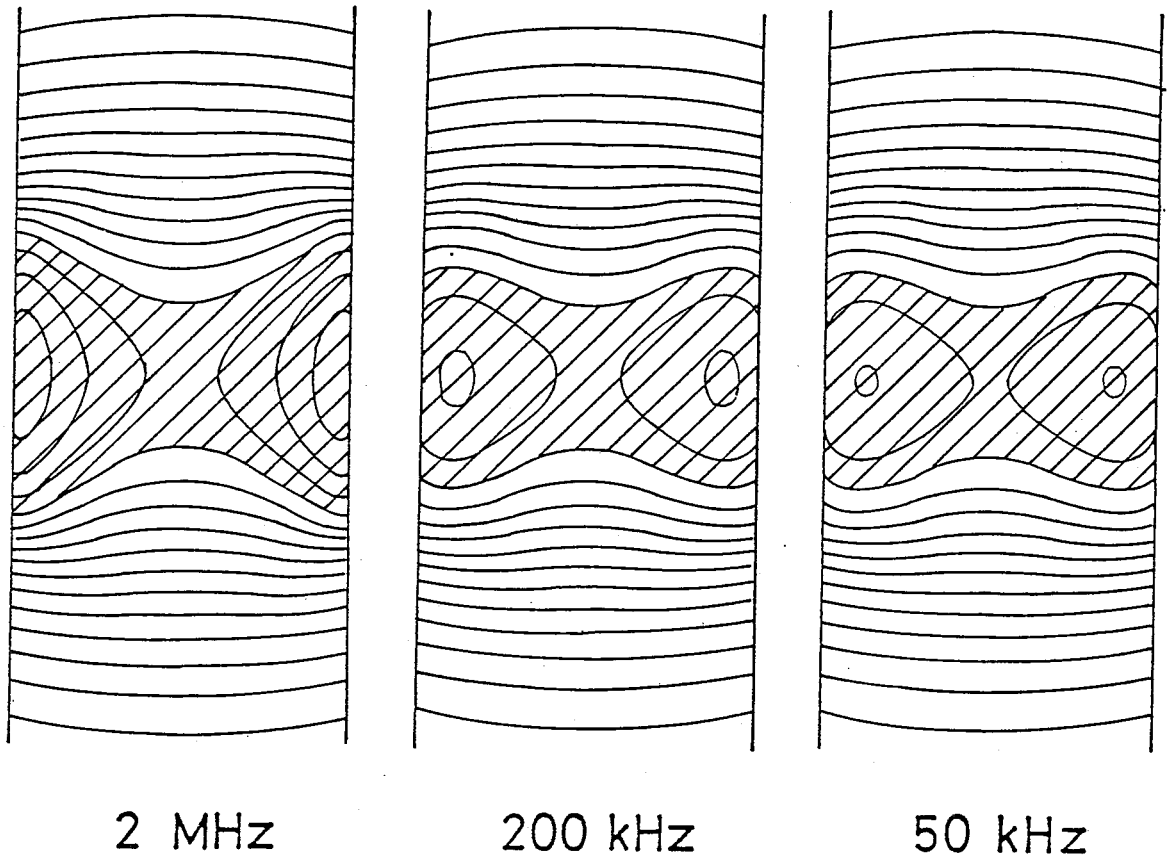

Fig. 69 Dependence of the temperature distribution on the radio frequency in TiC rods. The rod radius is 0.5 cm.

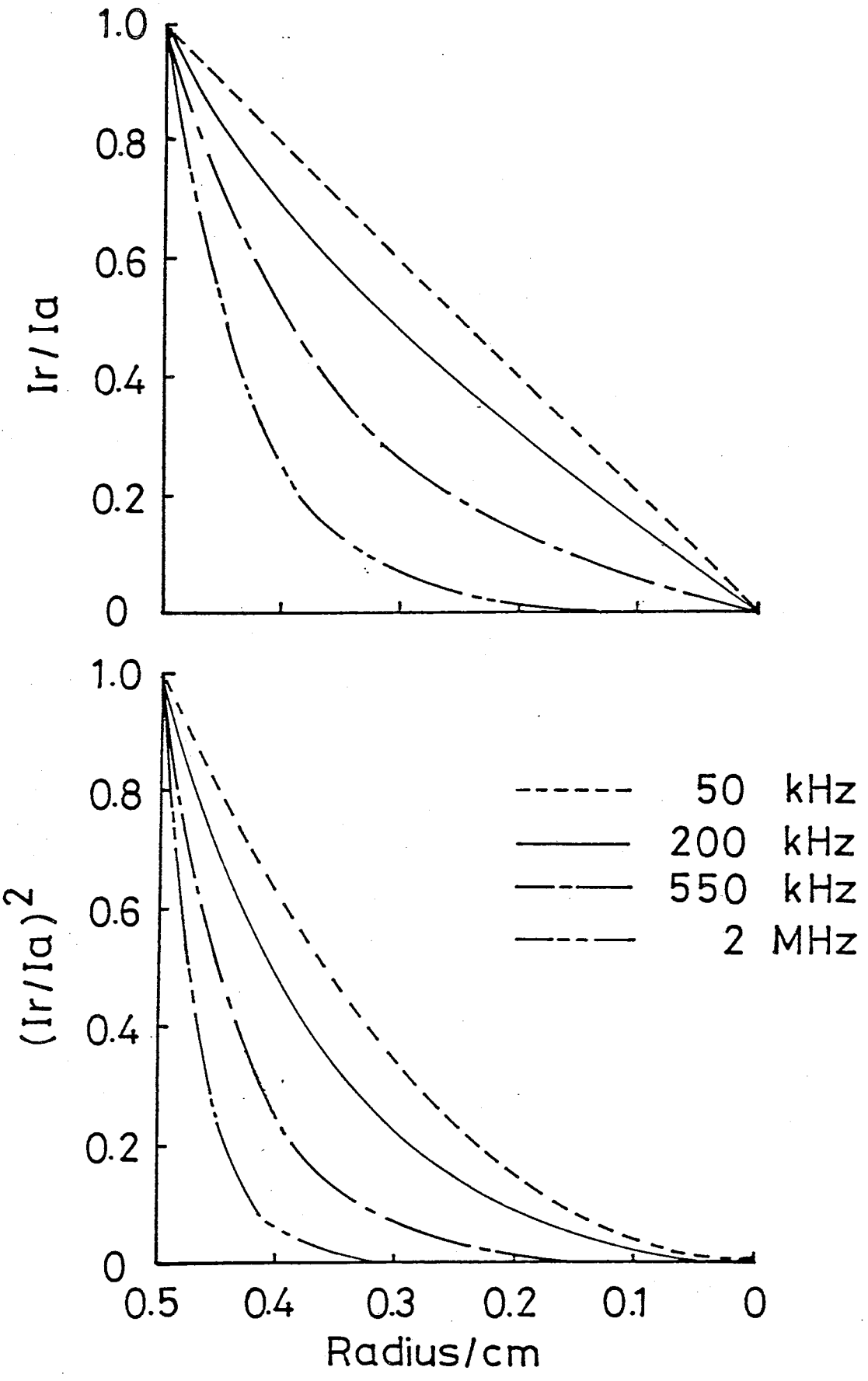

Fig. 70 Induced heating current and power distribution in TiC rod along the radial direction.

interface shape becomes convex to the molten zone. The polycrystalline rim is not formed around the crystal rod. However, the differece in the temperature between the central and surface parts near the interface becomes large. The crystal quality may become bad because the thermal stress is introduced to the just grown crystal. Many subgrains(less than 3 degree deviation) would be introduced in the crystal rod.

Therefore, the above results show that 200 kHz is the appropriate frequency in the case of preparing TiC crystal rod with 0.5 cm radius.

3-4-5 Size effect

The temperature distributions in the rods with 0.25, 0.5 and 1.0 cm radii were calculated in the case of heating due to 200 kHz. The size effect is related to the Biot number and the heating parameter. The results are shown in Fig. 71. The radial heating distributions are shown in Fig. 72. The dash-dotted line indicates the temperature distribution obtained from the approximate equation. It is found that this approximate equation can be used in the case of low heating parameter(δ/a). The dashed line is calculated from the equation which is used in the case of a plane. In the case of a=0.25 cm, the power is supplied to the inner part, compared with the case of a=0.5 cm. The interface shape becomes more flat. This fact indicates that the small radius of rod is advantageous for the preparation of the high quality crystals. However, it should be noted that the

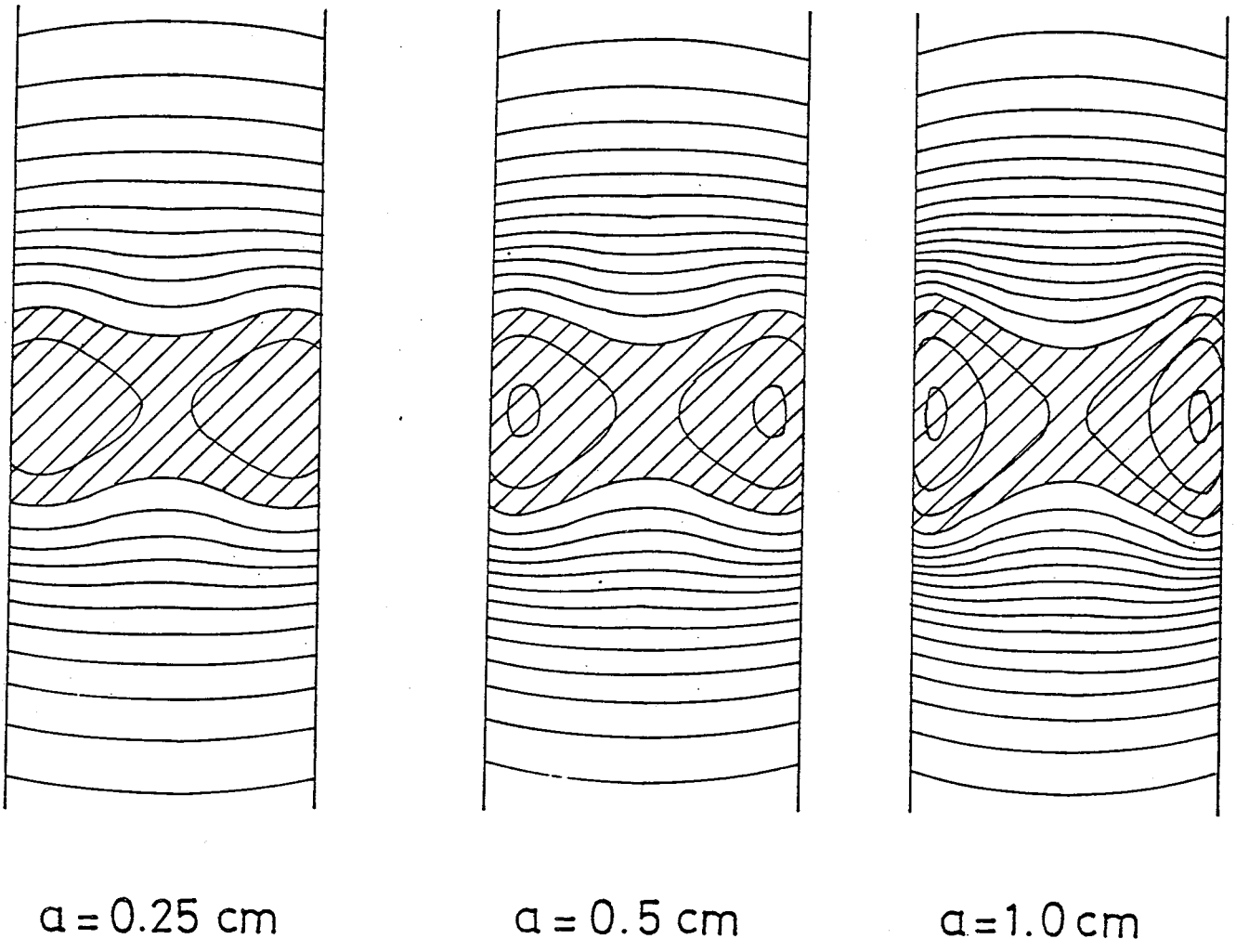

Fig. 71 Dependence of the temperature distribution on the crystal radius of TiC rod. The radio frequency is 200 kHz.

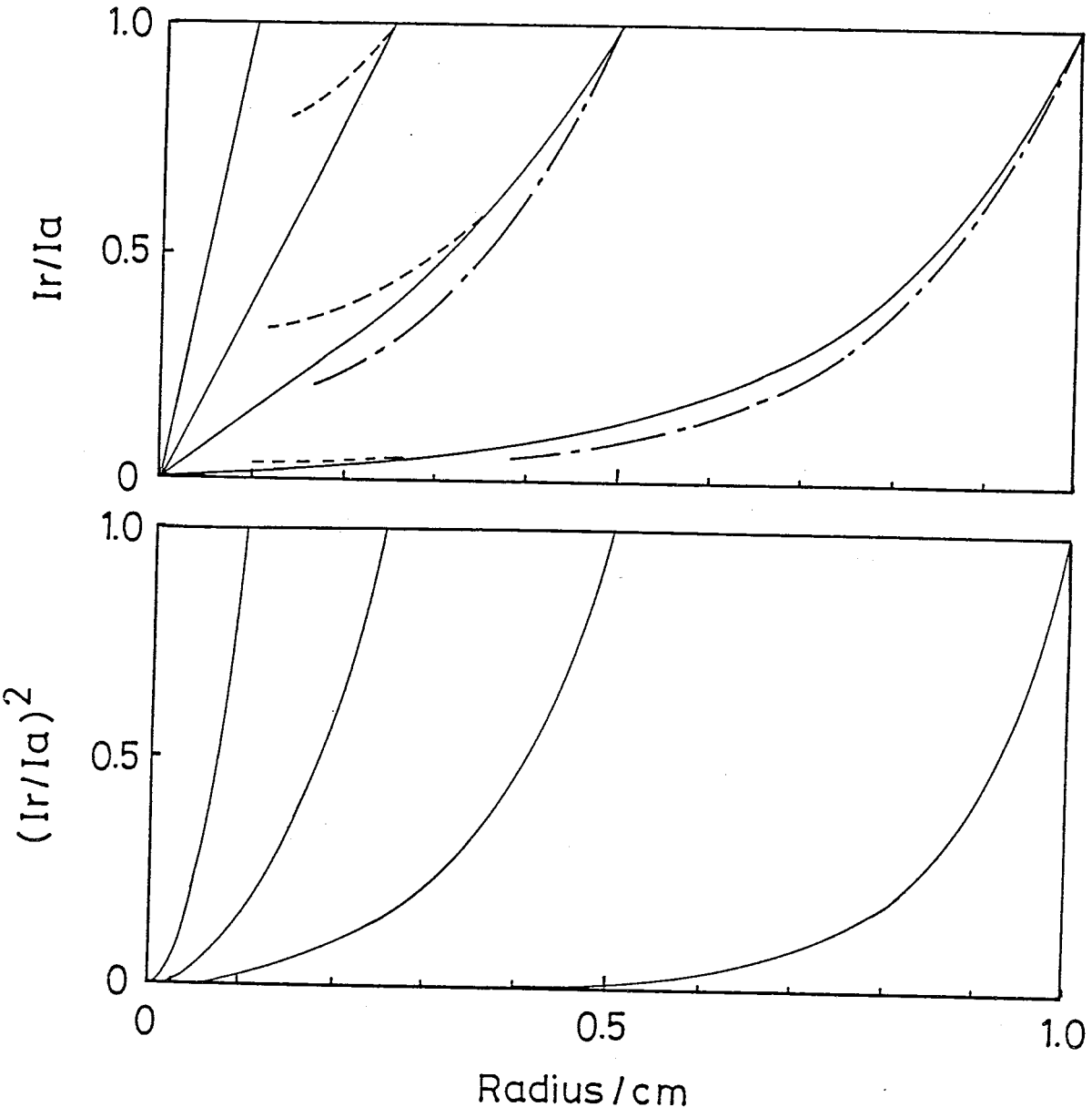

Fig. 72 Induced heating current and power distribution of TiC rod along the radial direction. The dashed line is obtained from an approximate equation. The dash-dotted line indicates that obtained from the equation in the case of a plane with infinite thickness.

temperature gradient along the growth direction becomes steep. As the radius becomes large, the interface shape becomes more convex to the molten zone. Therefore, it is difficult to prepare a high quality crystal with large radius.

The interface shape is concave at the position of 0.5-1.1 mm from the surface. Therefore, the crystal rods with 0.25-1.0 cm radii always have polycrystalline rims with about 1 mm thickness, as far as the 200 kHz is used.

3-4-6) Effect of radiation shield

The temperature distributions in case when the temperature (T_{shield}) of the radiation shield are 0 and 2000K, were compared with those in case when T_{shield}=350K. The temperature distributions for T_{shield}=0 and 350K, are the same at the high temperature part. The temperature of 350K is too low to influence the temperature distribuiton.

Fig. 73(a) shows the temperature distribution at the surface along the growth direction in case when T_{shield} is 2000K. The temperature of the grown crystal is asymptotic to 2000K, as the zone advances. However, the temperature gradient just below the interface, which is maximum, is not so small as expected, compared with that for the case of T_{shield}=350K, because the energy loss due to radiation is proportional to the difference of temperature to the fourth power, $(T^4 - (T_{shield})^4)$, between crystal surface and radiation shield.

The temperature distribution at T_{shield}=2000K is shown in

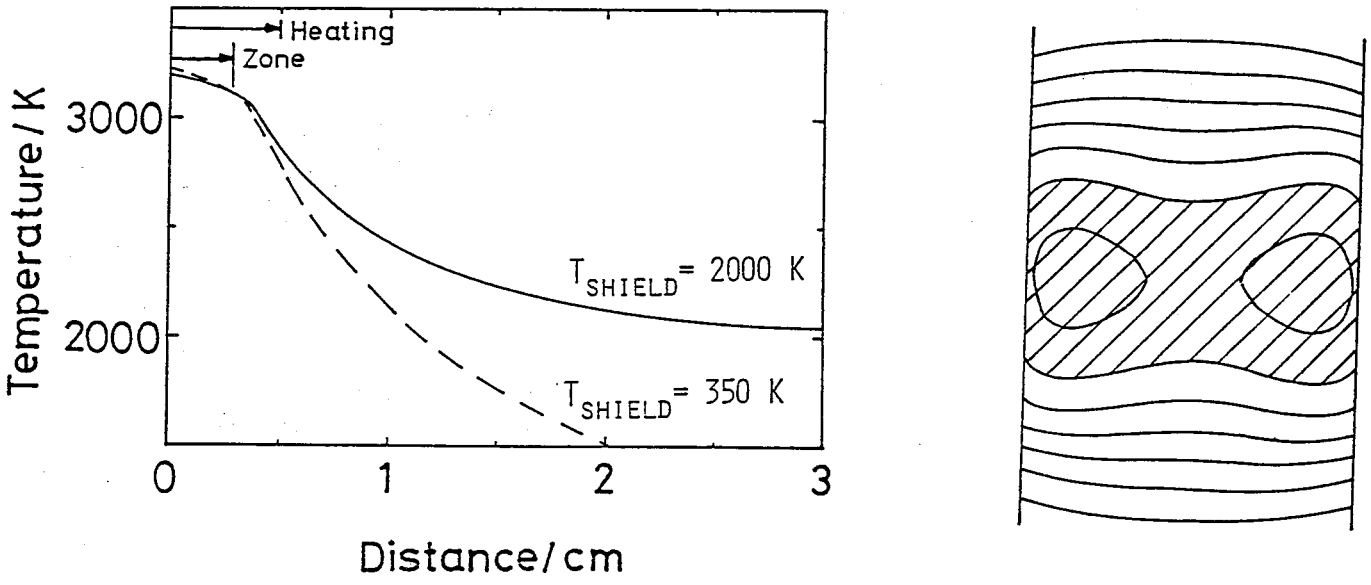

Fig. 73 (a) Temperature distribution at the surface of TiC rod along the growth direction. (b) Temperature distribution in case when the temperature of the radiation shield(T_{shield}) is 2000K.

Fig. 73(b). The molten zone is heated more uniformly, compared with the result obtained in the case(Fig. 66) when T_{shield}=350K. However, the temperature of 2000K is not enough to raise the surface temperature at the interface. Therefore, the crystal have a polycrystalline rim.

Therefore, in order to decrease the temperature gradient and to exclude the polycrystalline rim, the temperature of radiation shield shoud be made close to the molten zone temperature.

3-4-7 Effect of heated width

Fig. 74 shows the temperature distribution along the rods, when the heated width are 30%, 100% and 200% of the rod diameter and the zone with 60% of the rod diameter is formed. When the heated width is narrow(l_h=0.3 cm), the middle part of the rod must be heated up to 3900 C. Therefore, more heating power is needed, compared with the result obtained in the case of l_h=1.0cm, as shown in Fig. 75. When the wide part is heated(l_h=2.0 cm), the temperature distribution along the just grown crystal rod is gentle. This is advantageous to prepare the high quality crystal, but it is difficult to pass a zone stably because the zone length changes much due to a small temperature fluctuation. Fig. 76 shows the interface shapes. In the case of l_h=0.3 cm, the interface shape becomes concave because this part is not heated(only cooling). In the case of l_h=2.0 cm, the part around the zone is heated homogeneously. The interface shape is concave because the temperature gradient along the growth

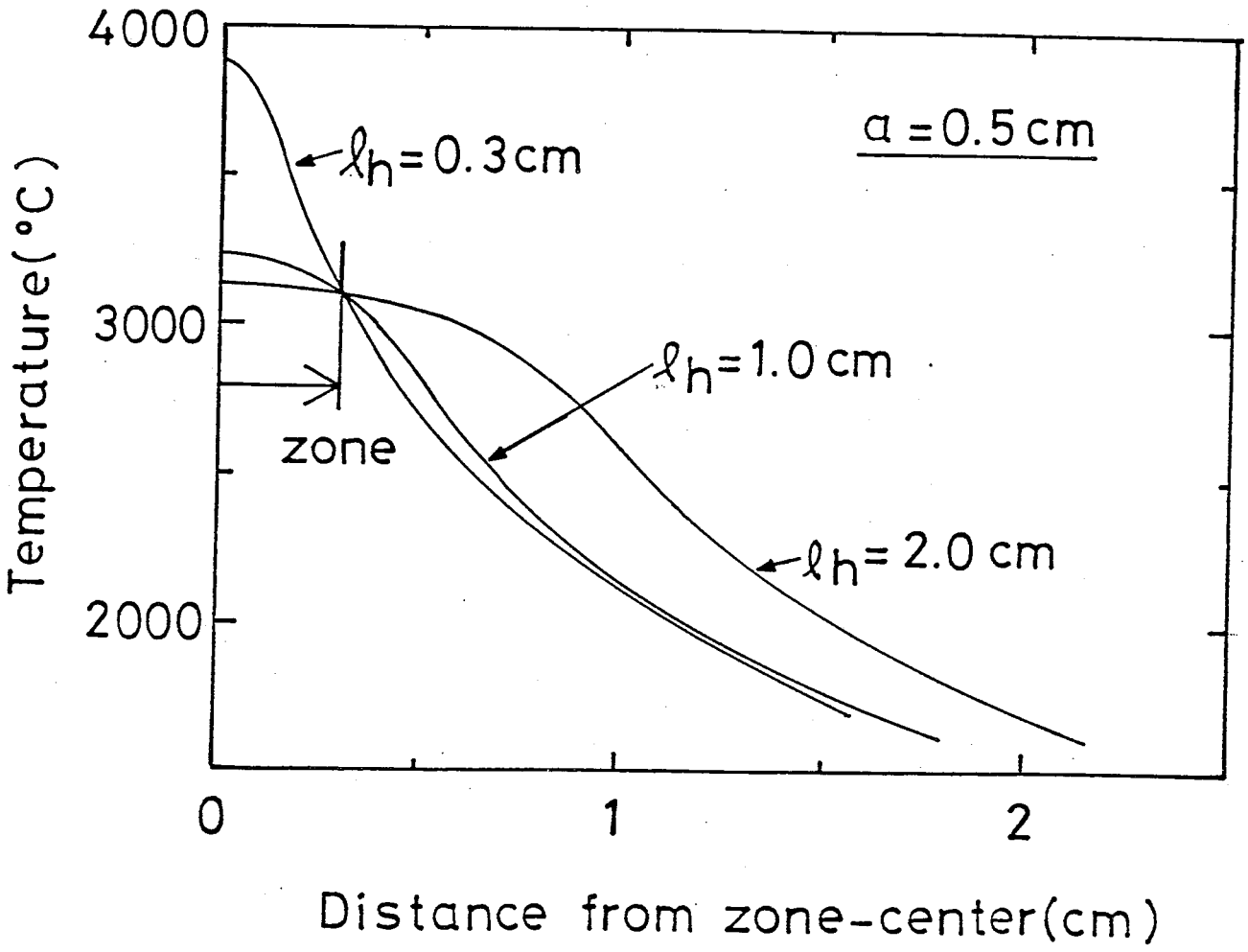

Fig. 74 Temperature distribution along the crystal rod of TiC in the cases of l_h=2.0, 1.0 and 0.3 cm.

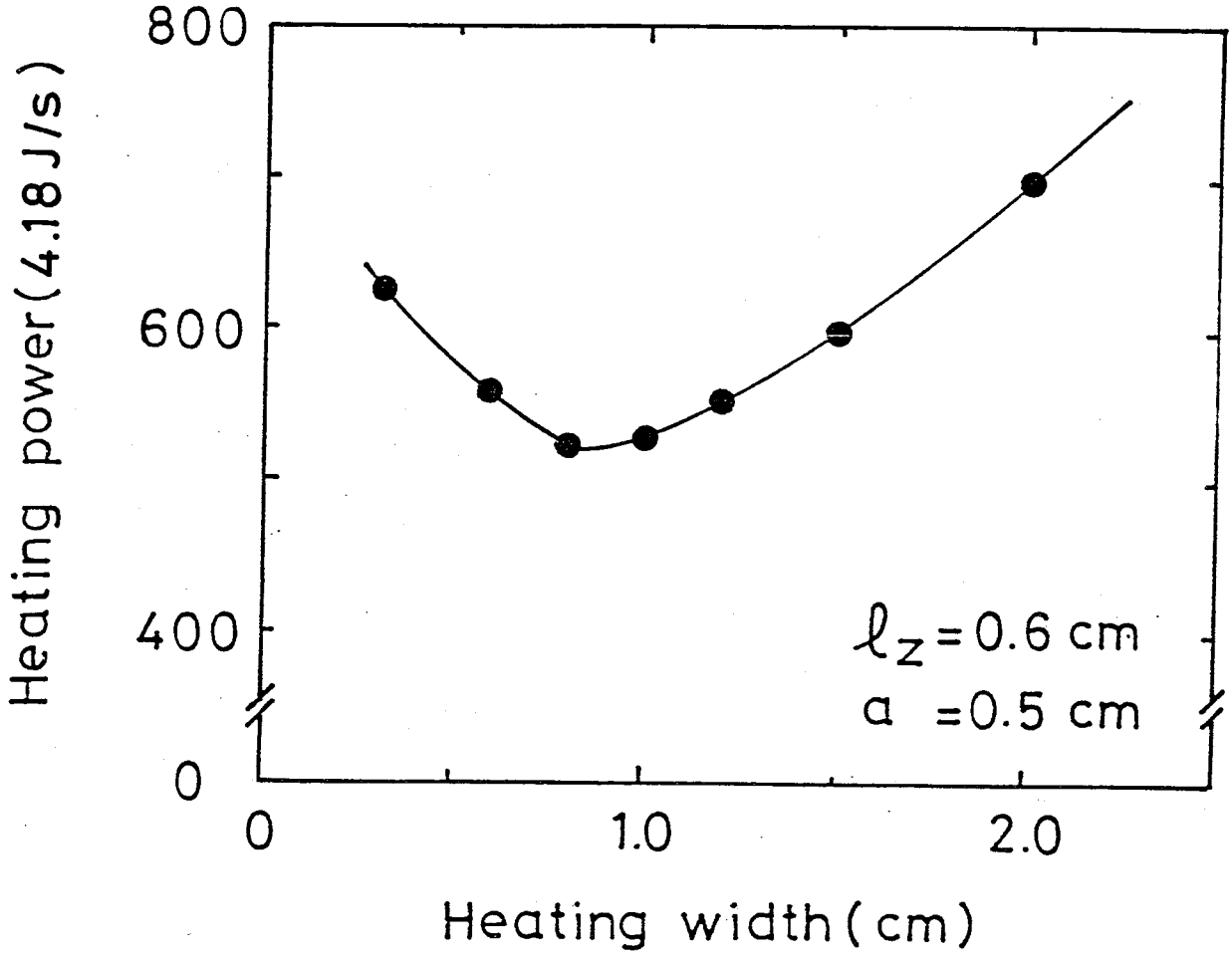

Fig. 75 Relationship between the heated width and the power of TiC rod.

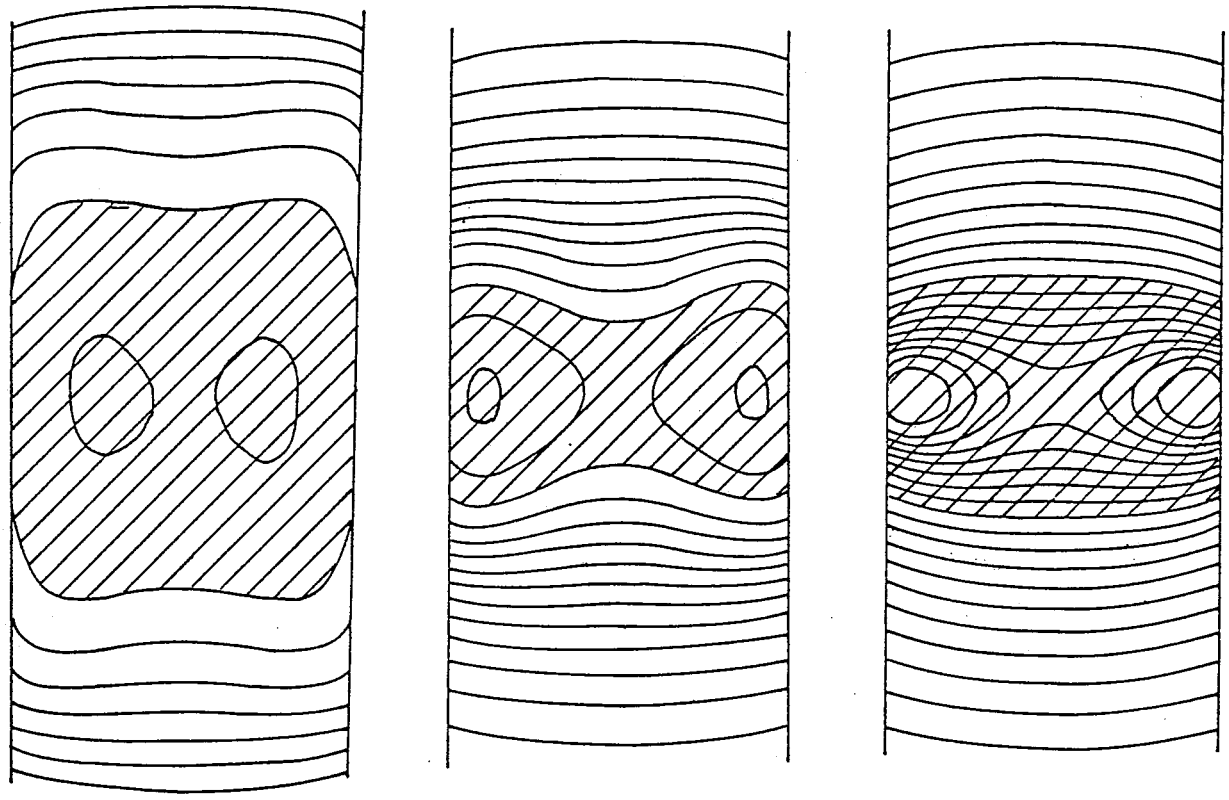

Fig. 76 Temperature distributions in TiC rod in the cases of l_h=2.0, 1.0 and 0.3 cm.

direction is small at the interface. The reason is as follows. The power supplied to the zone is small because the heat which dissipates through the interface is small. Therefore, the temperature distribution in the zone strongly reflects the cooling mode, and the interface shape becomes concave. This fact suggests that the interface shape tends to become concave, when the temperature gradient just below the zone is decreased. Anyhow, when the interface is concave, the single crystal of TiC can not be prepared. Therefore, a radiation shield is better as an after-heater than a RF heating due to the work coil design.

3-5 Discussion and conclusion

The temperature distribution in the crystal rod is determined by the heating parameter(δ/a) and Biot number(Bi). In the case of low Biot number, the temperature gradient is small. The interface shape is nearly flat regardless of the value of the heating parameter. This is advantageous for the preparation of high quality crystal. However, in the case of low Biot number due to small radius, it should be noted that the temperature gradient along the growth direction gets large, as seen in Fig. 61. Therefore, the quality of the crystal with small radius is not always good. It was reported[55] that from the results of preparation of KCl crystal whose quality is easily influenced by thermal stress, the dislocation density was unchanged in the range of the diameter from 14 to 1.5 mm because the crystal with small radius was prepared under the large

temperature gradient. In the case of large Biot number, the temperature gradient is steep. The temperature distribution is strongly affected by the manners of heating and cooling. Therefore, the appropriate heating parameter(δ/a) must be selected in order to make the interface shape slightly convex in the centrer.

When the crystal with 0.5 cm radius is prepared by RF heating, the interface shape always becomes wavy or nearly flat because the Biot number is less than 0.2. The concave interface does not exist in the experimental results described in Chapter 2, although it is observed in the preparation of YAG crystals by a floating zone technique using an infrared radiation convergence type heater[69].

Convection in the zone can be observed during a zone pass. However, it is concluded that the convection does not influence the temperature distribution from the experimental results shown in Figs 65 and 66. The reason is that materials, such as Mo and TiC, have relatively high thermal conductivities.

Generally, the molten zone is not cylindrical, but the middle part is necked-in. In the case of RF heating, the interface shape tends to be more convex to the zone because the RF coupling decreases toward in the middle part of the zone. This phenomenon was observed in the present experiments. In the case when only surface of the zone was heated, for example, by electron bombardment, the interface shape becomes flatter than the convex shape obtained from the calculation because the heated

middle surface of the zone approaches the central part of the convex interface, compared with the results obtained in the case of the imaginary cylindrical zone.

The crystals with high melting points must be prepared at several atmospheres of the ambient gas, such as He and Ar, in order to suppress an arc discharge and to reduce evaporation. The surface of the growing crystal is then cooled by the ambient gas as well as by radiation. However, in the high temperature region, most of the supplied power is lost as radiation energy. Therefore, the presented model, in which the crystal is prepared in vacuum, can be applied to all the cases of the preparation of crystals with high melting points.

In order to prepare the higher quality crystal with 0.5 cm radius using 200 kHz, the following points were clearified by the present author. The heated width is the same as the diameter of the rod. The zone length at the surface is about 60 % of the diameter. The temperature gradient at the just grown crystal must be made small by an after-heater. As for the after-heater, a radiation shield is better than a RF heating due to the work coil design. Therefore, higher quality crystals will be prepared by the method shown in Fig. 77.

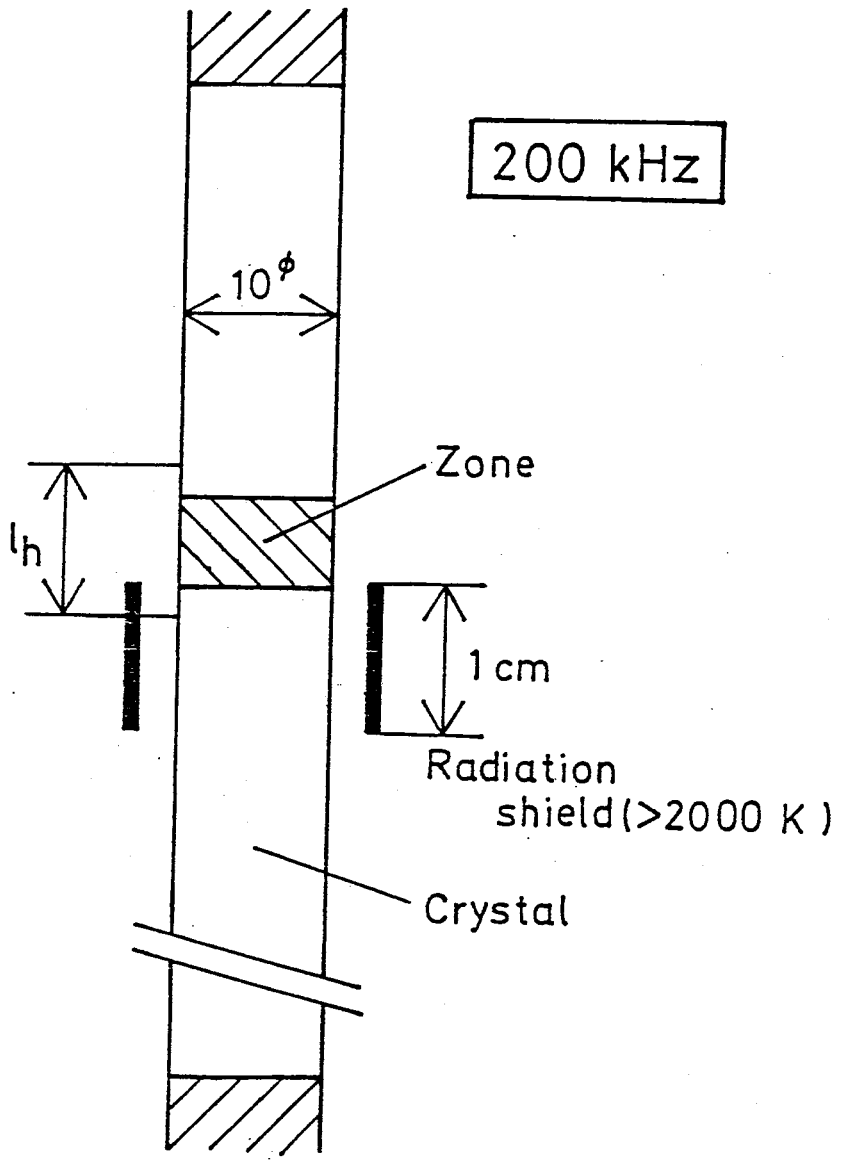

Fig. 77 Preparation of high quality crystals with high melting point.

4. CRYSTAL GROWTH OF OTHER MATERIALS WITH HIGH MELTING POINTS

The materials which are considered in the present paper have melting points above 2500 °C and metallic electrical conductivities. There are about fifty materials with high melting points above 2500 °C[12,70,71], as shown in Fig. 78: the IVa-VIa group carbides, the di-, tetra- and hexa-borides, the IVa-Va group nitrides, refractory metals and so on. The IVa-VIa monocarbides have the highest melting points among these materials. Among them, $TaC_{0.9}$ has the highest melting point(3983 °C)[12]. All of the compounds, except WC, coexist with a liquidus phase in the phase diagram. Therefore, it is expected that single crystals can be principally prepared by a floating zone technique. Many of these crystals were tried to be prepared by a floating zone technique[10,11,72-76].

There are mainly two kinds of heating method in the floating zone technique; electron bombardment and RF induction heatings. The electron bombardment, which is used to prepare the metal crystals[4,35], has a high heating efficiency, but must be used in vacuum($< 10^{-2}$ Pa). The bombardment is a surface heating, but the interface shape does not become too convex because the metals have low Biot numbers, that is, high thermal conductivities. In addition, the preferential evaporation does not occur because a metal is an element. These are the reasons why an electron bombardment is suitable for preparing the metal crystals. If

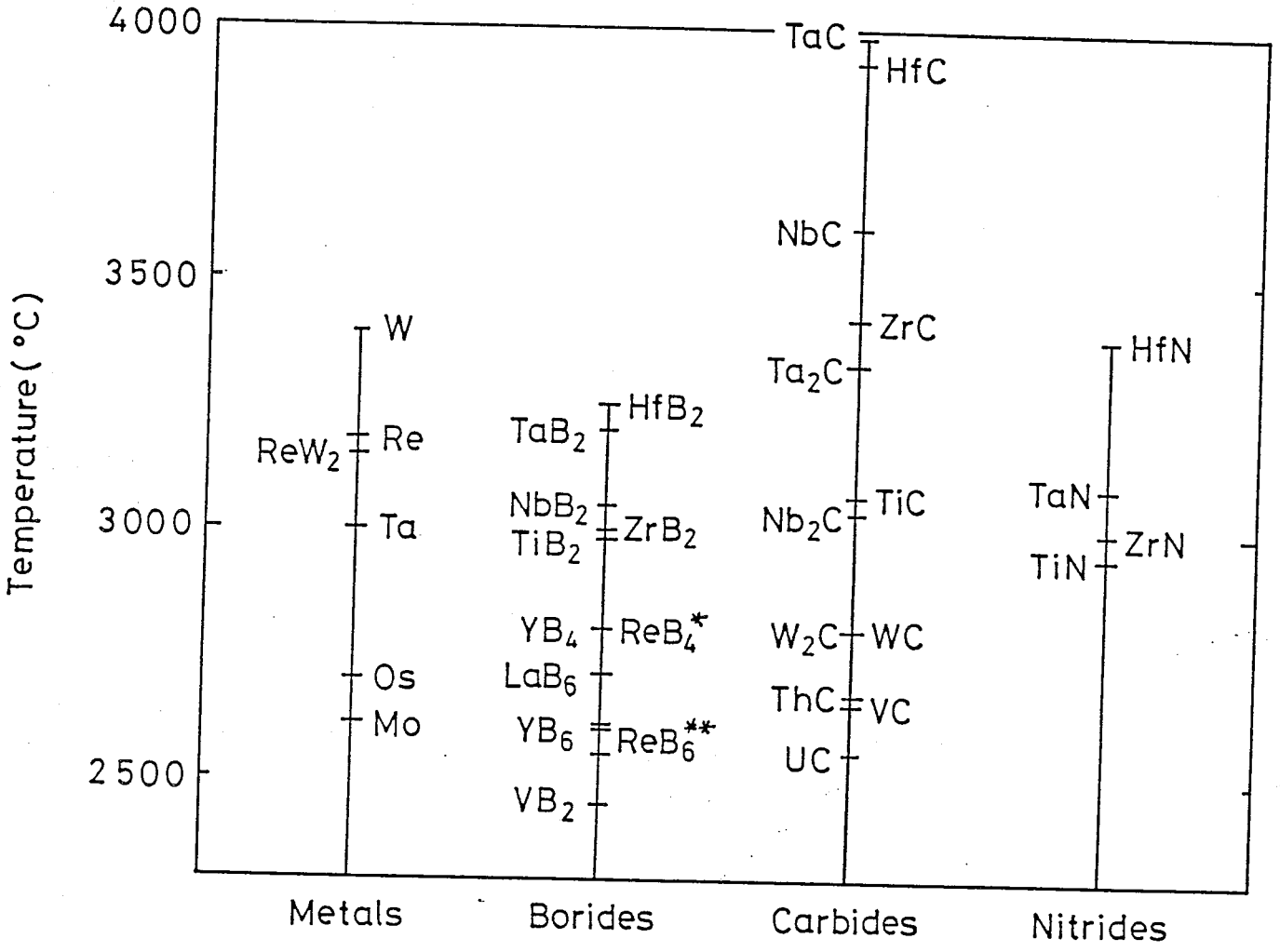

Fig. 78 Melting points of refractory materials: Re*=Dy, Ho, Er, Tm, Yb, and Lu: Re**=La, Ce, Pr, Nd, Pm, Sm, Eu and Gd.

this heating method is applied to preparing the single crystals of compound, it is difficult to prepare the high quality crystal because of the too convex interface and preferential evaporation. Therefore, the crystals of refractory compounds are not prepared by this method. On the other hand, in the case of RF heating, not only the surface but also the interior of the sample are heated. By selecting the radio frequency, the control of heating distribution along the radial direction of the sample rod is easy, and the interface shape can be controlled. This is advantageous for preparation of high quality crystals of compounds. In addition, the evaporation can be reduced because crystals can be prepared under the high pressure of the ambient gas. Therefore, the RF heating is the best method to prepare the crystals of the refractory compounds.

In the case of preparation of refractory compound crystals by a RF induction heating, three matters must be mainly considered; heating power, arc discharge and evaporation. The power required to keep the molten zone depends on melting point of compound, crystal radius, zone length, emissivity and thermal conductivity. In order to melt $TaC_{0.90}$ rod with 0.5 cm radius, which has the highest melting point(3983°C), the power is estimated to be 5.8 kW from the calculation. The efficiency of RF heating is 12%, as described in Chapter 3. Therefore, a RF generator with 50 kW(= 5.8/0.12) in maximum output is needed to prepare the crystals of all the refractory materials. As for a frequency of a RF generator, about 200 kHz is appropriate for

preparation of the compound crystals, as described in Chapter 3. Actually, when an initial molten zone is formed, the most power is consumpted. Therefore, it is also important to prepare a feed sintered rod with high density, as described in Chapter 2.

The power required to keep the molten zone is proportional to about three power of the zone temperature($T_z^{\ 3}$) in the case of the refractory compounds, as described in Chapter 3. The difference of 100K in the growth temperature above 3000K corresponds to that of about 10% in the heating power. Therefore, the higher the growth temperature is, the more difficult it is to prepare the crystals because of mainly arc discharge. In the case of preparation of HfC and TaC crystals, the growth temperature could be decreased by about 500K by applying a modified zone leveling method, compared with the results obtained using a usual floating zone method. This is a reason why these crystals were first prepared in the present study.

The arc discharge occurs depending on a prepared crystal, a kind of an ambient gas, its pressure and so on. The boride crystals were prepared under an ambient gas of Ar[11,73]. However, the carbide crystals can not be prepared stably under an Ar gas condition because a small arc discharge often occured. Therefore, a helium gas, which has the highest ionization potential, was used as an ambient gas. The discharge is caused by the evaporation products which grow as dendrites under high electric field. Therefore, in the case of preparation of a

crystal under violent evaporation, the pressure of about 10^6 Pa of He gas is needed in order to suppress the arc discharge perfectly.

Evaporation strongly influences the chemical composition and volume of the zone because the zone volume is small. Therefore, the desired crystal can not be often obtained. There are two kinds of evaporation: vaporization and preferential evaporation. The former does not cause a severe problem so much as the latter because the zone composition does not change so much. Only the countermeasure against the evaporation product is needed. It was reported that the single crystals of CaO(T_m=2600°C)[77], CaS(T_m=2444°C)[77], Li_2O(T_m=1500°C)[78], which have high vapor pressures at their melting points, were prepared by a floating zone using an infrared convergence type heater. In the case of RF floating zone method, the crystal with high vapor pressure can be prepared using a work coil with large inside diameter under the conditions of high growth rate and high ambient gas pressure. However, the more the evaporation product is, the more difficult it is to prepare crystals. The latter(preferential evaporation) is not solved perfectly yet because evaporation itself must be decreased. In the preparation of carbide crystal, the problem was almost solved by controlling the chemical composition of the feed rod and the growth conditions such as the growth rate and the pressure of helium gas. However, TiC and ZrC crystals with carbon poor composition could not be prepared because of preferential eveporation of the metal. The vapor pressure of the

metal can be estimated to be several torrs at the growth temperature condition[20]. On the other hand, when the crystals of NbC, TaC and HfC are prepared in the carbon rich compositional region, carbon violently evaporates from the molten zone. The vapor pressure of carbon, as an element, is several 10^4 Pa at the growth temperature[36]. It is expected that carbon partial pressure is the same level of the vapor pressure of the metal, such as Ti and Zr, in the carbon poor compositional region. However, single crystals of NbC, TaC and HfC could be prepared because the evaporated carbon, which adhered to the coil as a dendrites, is remelted back to the molten zone when the evaporation product are contacted with the zone. Therefore, the quantity of the lost carbon due to evaporation is small substaintially. This is a reason why the TaC and HfC crystals with carbon rich compositions were prepared in the present study.

In the case of another materials, preferential evaporation causes the trouble when the growth temperature is high. For example, it was reported[73] that TaB_2 and NbB_2 crystals, which has the highest melting points among the borides, could not be prepared due to preferential evaporation of boron. However, the crystal of ZrB_2, which has slightly lower melting point than TaB_2 and NbB_2, was prepared[74]. The partial pressure of boron at growth temperature is not measured, but boron, as an element, is estimated to have 10^3-10^4 Pa of vapor pressure[70]. The partial pressure can be thought to be several 10^2 Pa, which is at the

same order as that of the metal in the preparation of TiC and ZrC crystals with carbon poor composition, because the constituent element has lower vapor pressure than the element. Therefore, when the difference in vapor pressures between the constitutent elements are higher than 10^2 Pa, it is difficult to prepare the single crystals. In order to prepare these crystals, the evaporation rate must be decreased to less than one tenth. Therefore, there are two ways: one is that the growth rate must be increased by higher than one order, that is, higher than 20 cm/h. However, this high growth rate can not be expected to supply a high quality crystal[33]. Second one is to increase the pressure of the ambient gas. The evaporation rate is proportional to $P^{-(3/4)}$, as described in Chapter 2. Therefore, in order to decrease the evaporation rate to less than one tenth, the pressure must be increased more than 20 times, that is, higher than 20 MPa. It is very difficult to prepare crystals with high melting points under such high pressure condition. Consequently, a preferential evaporation can be prevented to some extent by improving the growth conditions. From the present experimental results shown in Fig. 19, it is found that 10^6 Pa of an ambient gas pressure decreases to one-fifth of evaporation rate, compared with the results obtained in the case of an atmospheric pressure. However, at higher than 10^6 Pa, the effect is small because 10 MPa of helium gas pressure is needed to decrease further to one-fifth. Therefore, if the compositional change due to preferential evaporation can be prevented, the

crystal can be prepared under a lower pressure than 2×10^6 Pa of an ambient gas in most cases.

A modified zone leveling method is developed in the process of preparation of the carbide crystals with wide non-stoichometric compositional range. This method can be also applied to that of a crystal with stoichiometric composition, and has the following merits. The zone composition is kept constant during a zone pass in spite of a preferential evaporation from a zone. Therefore, the growth temperature is kept constant and a zone pass can be stabilized. Further, the crystal can be prepared at a lower temperature(a little above the eutectic temperature) by approaching the zone composition to the eutectic composition as already described in the cases of TaC and HfC crystal preparation.

As for the impurity refining, most of impurities are refined by evaporation because of the high growth temperature. In order to prepare the high purity crystals, the starting materials which do not contain impurities with low vapor pressures must be selected.

In order to prepare single crystal rods, it is important to control the interface shape to be a little convex toward the zone. When the crystal with 0.5 cm radius is prepared by a RF floating zone technique, the interface shape is always convex toward the zone at the central part, as described in Chapter 3. Therefore, the single crystal can be always obtained from the central part as far as the zone is stably passed and the zone

composition is kept to be the desired chemical composition. If the single crystal can not be prepared in spite of a stable zone pass, the crystal radius should be small.

The single crystal prepared in this way will be several mm in size and have the etch pit density of $10^{6-7}/cm^2$, depending on the growth temperature.

As further problems, there are preparation of the nitride crystals(TiN, NbN and so on) and preparation of the crystals with microscopically high quality.

The nitrides have very high vapor pressure of nitrogen at their melting points. Nitrogen is lost as a gas from the sample. Therefore, it is difficult to obtain the nitride crystal with the desired phase and/or chemical composition. The nitride crystals were tried to be prepared at the high nitrogen gas pressure but the large crystal could not be obtained yet[72,76]. To prepare the nitride crystals is a task worth challenging.

In order to prepare high quality crystals, seeding and necking techniques, which are used in the preparation of the semiconductor crystals, such as Si and GaAs, are well-known. However, it is difficult to neck down the crystal because the zone shape is determined by the shape of work coil, as descrbed in Chaper 2. Therefore, many subgrains which are introduced into the crystal at the seeding process can not be excluded. The obtained crystal is the same as prepared without a seed crystal. Furthermore, even though the necking can be done, there is a problem to be solved. Since the crystal is prepared at a steep

temperature gradient, the three dimensional nextwork defect structure is introduced during a zone pass. After now, it is necesarry to develope the heating way how the necking process can be carried out, and to improve the growth conditions not to introduce the defect structure during a zone pass.

5. SUMMARY

(1) The single crystals of the IVa and Va group transition metal carbides have been prepared by a floating zone technique. In order to prepare high quality crystals, the technique to maintain a molten zone stable at the high temperature(>3000°C) has been established(Section 2-2).

(2) A modified zone leveling method has been developed and the crystals with homogeneous desired chemical compositions have been prepared(Section 2-3 and 2-4) In this method, the molten zone is kept constant during a zone pass. Therefore, the zone can be passed at a constant temperature, and a zone pass is stabilized. This method can be also applied to measurement of evaporation from a zone, i.e., the composition of the evaporation product from a molten material, the evaporation rate and so on, as shown in section 2-5.

(3) Impurity refining has been examined. Oxygen and nitrogen impurity content in the crystal depend on those in the feed rod. Therefore, in order to prepare a feed rod with low oxygen and nitrogen content, sintering has been carried out under high vacuum condition using a rotary pump with high evacuation rate and a diffusion pump. On the other hand, metal impurities are refined depending on the vapor pressures because of high growth temperature. Therefore, selecting starting materials which hardly contain impurities with low vapor pressures, such as W and Mo, the high purity crystals have been prepared.

(4) The relationship among the chemical composition, lattice

constant and density has been examined. It was confirmed that a nonstoichiometry comes from only carbon defect.

(5) From the observation of crystal rods, the shape of the crystal-zone interface was found to be important to prepare high quality crystals because the crystals grow normal to the interface. Therefore, the crystal rods of the IVa carbides, which have high Biot numbers, are surrounded by polycrystalline rims because the surface part is cooled by radiation. On the other hand, the crystals of the Va carbides, such as NbC and TaC, have no rims because they have low Biot numbers(high thermal conductivity and low emissivity, compared with the IVa carbides).

(6) The etch pattern of each crystal has been observed. The defects form a three-dimensional net work structure, which is a lablynth structure. The crystals have been found to be prepared under too steep temperature gradient to prepare a dislocation free crystal. The etch pit densities are 10^{6-7} /cm^2 depending on the growth temperature.

(7) The carbide crystals must be prepared at an ambient gas of high pressure(less than 1 MPa). Therefore, the effects of helium pressure on the heating power, evaporation rate and crystal quality were examined, using a modified zone leveling method. It has been found that He gas does not influence the heating power so much, but does evaporation rate($P^{-0.75}$) and the crystal quality.

(8) Temperature distribution in a growing crystal rod is important to prepare high quality crystals. Therefore, the

temperature distribution was calculated. The calculated results agreed well with the experimental results. The temperature distribution was determined by a heating parameter(δ/a) and Biot number(Bi). The growth conditions such as radio frequency and heating width were inspected. The RF heating has been found to be the best method because the interior of the sample is heated. It has been found that the temperature gradient at the part just below the zone(about 1 cm) should be small to prepare higher quality crystals. The method by which a high quality crystal can be prepared has been proposed.

ACKNOWLEDGEMENTS

The author would like to express his sincere thanks to Prof. M. Koizumi, Osaka University, for his encouragement throughout this work and critical reading of this thesis, and prof. M. Shimada, Tohoku University, for his kind advices in the preparation of this thesis. This research was condcted at National Institute for Research in Inorganic Materials. He wishs to thank Prof. S. Kawai, Osaka University, and Drs. Y. Ishizawa and T. Tanaka for their continuous encouragements and valuable insights. He is also indebted to Drs. A. Hara and Y. Doi, Sumitomo Electric Industries Ltd., for the chemical analyses of carbon, oxygen and nitrogen, and to Mr. S. Honma for his advices in the measurements of X-ray topography.

References

[1] P.H.Keck and M.J.E.Golay, Phy.Rev.,89(1953)1297.

[2] J.A.Belk, J.Less-common Metals, 1(1959)50

[3] H.W.Schader, Trans.Met.Soc. AIME, 218(1960)649

[4] B.R.Pamplin, Crystal growth(Pergamon Press, Oxford, 1975).

[5] R.W.Johnson, J.Appl.Phys. 34(1963)352.

[6] W.Precht and G.E.Hollox, J.Crystal Growth, 3,4(1968)818.

[7] J.S.Haggerty, D.W.Lee and J.F.Wenckus, Tech.Report- AFML-TR-68-228(Air Force Materials Laboratory, Ohio, 1968).

[8] J.Billinghuam, P.S.Bell and M.H.Lewis, J.Crystal Growth 13/14(1972)693.

[9] Y.Kumashiro, A.Itoh and S.Misawa, J.Less-Common Metals, 32(1973)21.

[10] A.N.Christensen, J.Crystal Growth 33(1976)99.

[11] T.Tanaka, E.Bannai, S.Kawaii and T.Yamane, J.Crystal Growth 30(1975)193.

[12] L.E.Toth, Transition Metal Carbides and Nitrides(Academic Press, New York, 1971).

[13] H.Adachi, K.Fujii,S.Zaima, Y.Shibata, C.Oshima, S.Otani and Y.Ishizawa, Appl.Phys.Lett.43(702)1983.

[14] M.Ono, H.Hogo, H.Shimizu and H.Murakami, in: Proc. 27th Intern.Field Emission Symp.,Tokyo,1980,p353.

[15] C.Oshima, T.Tanaka, M.Aono, R.Nishitani, S.Kawai and F.Yajima, Appl.Phys.Lett, 35(1979)822.

[16] H.Tanaka, K.Saiki, S.Otani A.Koma and S.Tanaka, J.Nucl.Mater.116(1983)317.

[17] M.Mohri, K.Watanabe and T.Yamashina, J.Nucl.Mater., 75(1978)7.

[18] C.M.Braganza, G.M.McCracken and S.K.Erents, in:Plasma-Wall Interactions(Proc.Intern.Symp.Julich,1976) p.257.

[19] D.Dew-Hughes and R.Jones, Appl.Phys.Lett.36(1980)856.

[20] E.K.Storms, The Refractory Carbides(Academic Press, New York, 1967).

[21] W.S.Williams, Progress in Solid State Chemistry (Pergamon Press, Oxford, 1972).

[22] A.Henjered, L.Kjellsson, H-O.Andren and H.Norden, Scripta Metallurgica 15(1981)1023.

[23] Z.Wokulski and K.Wokulska, J.Crystal Growth, 62(1983)439.

[24] M.Futamoto, I.Yuito, U.Kawabe, O.Nishikawa, Y.Tsunashima and Y.Hara, Surface Science 120(1982)90.

[25] V.S.Sinel'Nikova and V.N.Gurin, Hi.Tem-Hi.Press 7(1975)507.

[26] T.Takahashi, K.Sugiyama and H.Itoh, J.Electochem.Soc. 117(1970)541.

[27] D.J.Rowcliffe and W.J.Warren, J.Mater.Sci. 5(1970)345, and, ibid.,6(1971)207.

[28] A.P.Gerk and J.J.Gilman, J.Appl.Pyys. 39(1968)4497.

[29] R.M.Leonhardt and L.Peichl, J.Crystal Growth 54(1981)223.

[30] L.R.Fleischer and J.M.Tobin, J.Crystal Growth, 8(1971)235

[31] L.R.Fleischer and J.M.Tobin, J.Crystal Growth, 8(1971)243

[32] F.Yajima, T.Tanaka, E.Bannai and S.Kawaii, J.Crystal Growth 47(1979)493.

[33] M.E.Packer and M.J.Murray, J.Crystal Growth 16(1972)240.

[34] S.Otani, S.Honma, T.Tanaka and Y.Ishizawa, J.Crystal Growth 61(1983)1.

[35] W.G.Pfann, Zone Melting, 2nd ed. (Wiley, New York, 1966).

[36] R.B.Kotelinikov, S.N.Bashlykov, Z.G.Galiakbarov and A.I.Kashtanov, Special Refractory Metals and Compounds (Metallurgia, Moscow, 1969)(in Russian).

[37] W.S.Willams and R.D.Schaal, J.Appl.Phys. 33(1962)955.

[38] S.Otani, T.Tanaka and A.Hara, J.Crystal Growth 51(1981)164.

[39] S.Otani and T.Tanaka, J.Crystal Growth, 51(1981)381.

[40] K.Kumashiro, E.Sakuma, Y.Kimura, H.Ihara and S.Misawa, J.Crystal Growth 52(1981)597.

[41] Y.Hou, S.Otani, T.Tanaka and Y.Ishizawa, J.Crystal Growth, (to published).

[42] L.M.Adelsburg and L.H.Cadoff, J.Am.Ceram.Soc. 51(1968)213.

[43] E.Rudy, S.Windisch and L.E.Brukl, Planseeber Pulvermet. 16(1968)3

[44] C.H.de Novion, R.Lorenzell and P.Costa, C.R.Acad.Sci.Paris 263(1966)775.

[45] J.D.Venables, D.Kahn and R.G.Lye, Phil.Mag. 18(1968)177.

[46] K.Hiraga, Phil.Mag. 28(1973)1301.

[47] J.Billinguam, P.S.Bell and M.H.Lewis, Acta.Cryst. A28(1972)602.

[48] Y.Kumashiro, E.Sakuma, Y.Kimura, H.Ihara and S.Misawa, J.Crystal Growth 53(1981)597.

[49] S.Otani, T.Tanaka and Y.Ishizawa, J.Crystal Growth 62(1983)211.

[50] C.P.Kempter, E.K.Storms and R.J.Fries, J.Chem.Phys 33(1960)1873.

[51] S.Otani, T.Tanaka and Y.Ishizawa, J.Crystal Growth 55(1981)431.

[52] S.Otani and T.Tanaka, J.Less-Common Metals, 82(1981)63.

[53] Y.Kumashiro, Y.Nagai, H.Kato, E.Sakuma, K.Watanabe and S.Misawa, J.Mater. Sci.,16(1981)2930.

[54] A.L.Bowman, J.Phys.Chem., 65(1961)1596.

[55] G.A.Sobakar and S.V.Tsivinsky, Izv.AN SSSR, ser.fiz. 36(1972)580, cited by T.Inoue and H.Komatsu(Kristall und Technik 14(1979)1511)

[56] B.M.Klein, D.A.Papaconstantopoulos and L.L.Boyer, Phys.Rev.B, 22(1980) 1946.

[57] W.S.Williams, Progress in Solid State Chemistry, vol.6,(Pergamon Press, 1972)57.

[58] L.W.Shacklette and W.S.Williams, Phys.Rev.B, 7(1973)5041.

[59] W.S.Williams, Phys.Rev., 135(1964) A505.

[60] D.K.Donald, Rev.Sci.Instr.32(1961)811.

[61] N.Kobayashi, J.Crystal Growth 43(1978)417.

[62] S.Otani, T.Tanaka and Y.Ishizawa, J.Crystal Growth 66(1984).

[63] S.Nakamura, Induction heating(Kohsei Press, Tokyo, 1970)(in Japanese)

[64] H.S.Carslaw and I.C.Jaeger, Conduction of Heat in Solids 2nd ed.(Clarendon, Oxford,1959).

[65] Y.S.Touloukian, Ed., Thermophysical Properties of Matter(Prenum, New York,1970).

[66] V.H.Kuo and W.R.Wilcox, J.Crystal Growth 12(1972)191

[67] L.G.Eidel'man, Sov.Phsics-Doklady 13(1968)378.

[68] T.Inoue and H.Komatsu, Kristall u. Technik 13(1978)K31

[69] K.Kitamura, S.Kimura and K.Watanabe, J.Crystal Growth 57(1982)475.

[70] Handbook of Chemistry and Physics, 55th ed.(CRC Press, Boca Raton, FL, 1975).

[71] V.I.Matkovich, ED., Boron and Refractory Borides(Springer-Verlag, 1977).

[72] Y.Kumashiro, E.Sakuma, Y.Kimura, H.Ihara and S.Misawa, J.Less-Common Metals, 75(1980)187.>

[73] K.Nakano, K.Nakamura, Y.Kumashiro and E.Sakuma, J.Crystal Growth 52(1981)602.

[74] T.Tanaka, R.Nishitani, C.Oshima and E.Bannai and S.Kawai, J.Appl.Phys.,51(1980)3877.

[75] T.Tanaka, E.Bannai and S.Kawai, Ceramics, 11(1976)1083.

[76] B.Scheerer, J.Crystal Growth 44(1980)61.

[77] Y.Kaneko, K.Morimeto and T.Koda, OYOBUTSURI, 50(1981)289.

[78] I.Shindo, S.Kimura, K.Noda, T.Kurasawa and S.Nasu, J.Nucl.Mater.,79(1979)418.